

# **Control of Generalized Physical Systems for Real-World Haptics**

September 2014

A thesis submitted in partial fulfillment of the requirements for the degree of  
Doctor of Philosophy in Engineering



**Keio University**

Graduate School of Science and Technology  
School of Integrated Design Engineering

Morimitsu, Hidetaka

# Acknowledgements

This dissertation is the summary of my research from April 2009 to September 2014 as the member of Katsura laboratory in Keio University. Five years and a half have passed since I entered the Katsura laboratory, the Faculty of Science and Technology, Keio University. With full of kind people and under good environments, I was able to focus on my research work. Moreover, I was able to obtain valuable experiences. Without the helps from people and environments, I did not think I could manage the research activities.

First of all, I would like to express my appreciation to my supervisor Associate Professor Dr. Seiichiro Katsura in Keio University. His insightful teaching and comments always supported and kept motivating my research work. I greatly feel grateful to the members of my Ph. D. dissertation committee, Professor Dr. Kouhei Ohnishi in Keio University, Professor Dr. Hideo Saito in Keio University, and Associate Professor Dr. Yoshihiro Taguchi in Keio University.

I would like to show my gratitude to the Professors who gave precious comments at the research meetings. I sincerely would like to express my appreciation to Professor Dr. Kouhei Ohnishi in Keio University, Professor Dr. Toshiyuki Murakami in Keio University, Professor Dr. Hiroaki Nishi in Keio University, Associate Professor Dr. Takahiro Yakoh in Keio University, and Associate Professor Dr. Seiichiro Katsura in Keio University.

During my course, I had the experience to study in University of California, Berkeley. I would like to show my gratitude to the “International Collaborative Research of Perception and Expression Media for Development of Medical Access Space,” the one of the programs of “Strategic Young Researcher Overseas Visits Program for Accelerating Brain Circulation,” for providing me the great opportunity. I feel grateful to Professor Dr. Masayoshi Tomizuka in University of California, Berkeley. He supported my life in California and gave valuable comments to my research.

As my career of research activities, the Japan Society for the Promotion of Science (JSPS) has provided me the financial support. I would like to show my gratitude to the organization. I feel grateful for the Global COE Program “High-Level Global Cooperation for Leading-Edge Platform on Access Space (C12)” for financially helping me. In addition, I would like to show my appreciation to Strategic Information and Communications R&D Promotion Programme (SCOPE) and Ministry of Education,

Culture, Sports, Science and Technology, Grant-in-Aid for Scientific Research for Young Scientists (A), for supporting my research.

I would like to express my gratitude to my family for supporting me. Their dedicated assistance really helped my life.

Lastly, I would like to express my appreciation again for all people who supported my research activities.

September, 2014  
Hidetaka Morimitsu

# Contents

<b>Acknowledgements</b>	<b>i</b>
<b>Table of Contents</b>	<b>ii</b>
<b>List of Figures</b>	<b>vi</b>
<b>List of Tables</b>	<b>xi</b>
<b>1 Introduction</b>	<b>1</b>
1.1 Background of This Dissertation . . . . .	1
1.1.1 Recognition of Remote Environment via Transmission of Audiovisual Information	1
1.1.2 Real-world Haptics for Kinesthetic Sensation and Motion Control . . . . .	2
1.1.3 Technologies on Thermal Haptics . . . . .	5
1.2 Motivation of This Dissertation . . . . .	7
1.3 Chapter Organization of This Paper . . . . .	9
<b>2 Robust Control of Across Variable Flow</b>	<b>12</b>
2.1 Introduction . . . . .	12
2.2 Generalized Physical Variables . . . . .	13
2.2.1 Analogies Between Different Kinds of Physical Systems . . . . .	13
2.2.2 Across and Through Variables . . . . .	17
2.3 Generalized Form of Control Device . . . . .	18
2.4 Robust Control of Across Variable Flow . . . . .	20
2.5 Case of Thermodynamic Systems . . . . .	22
2.6 Generalized Control Conductance and Control Systems . . . . .	23
2.6.1 Generalized Control Conductance . . . . .	23
2.6.2 Control System of Across Variable . . . . .	24
2.6.3 Control System of Through Variable . . . . .	25
2.7 Control of Multi-Degree-of-Freedom System . . . . .	26

2.8	Experiments on Across Variable Control . . . . .	27
2.8.1	Overview of Experiments (Across Variable Control) . . . . .	27
2.8.2	Results of Experiments (Across Variable Control) . . . . .	29
2.9	Experiments on Through Variable Control . . . . .	32
2.9.1	Overview of Experiments (Through Variable Control) . . . . .	32
2.9.2	Results of Experiments (Through Variable Control) . . . . .	33
2.10	Summary of Chapter 2 . . . . .	35
<b>3</b>	<b>Bilateral Control Based on Across Variable Flow for Reproduction of Physical Power Interaction</b>	<b>36</b>
3.1	Introduction . . . . .	36
3.2	Reproduction of Generalized Power Interaction . . . . .	37
3.3	Generalized Reproduction of Bilateral Power Flow . . . . .	38
3.3.1	AVF-based 4ch Control System . . . . .	38
3.3.2	Comparative Methods . . . . .	39
3.4	Analyses Based on Generalized Intermediate Impedance . . . . .	40
3.4.1	Hybrid Parameters of Control Systems . . . . .	40
3.4.2	Symmetric Property and Hybrid Parameters . . . . .	41
3.4.3	Generalized Intermediate Impedance . . . . .	43
3.5	Analyses Based on Bond Graphs . . . . .	47
3.5.1	Lyapunov-based Analyses Using Bond Graph . . . . .	47
3.5.2	Bond Graph of AVF-based 4ch Bilateral Control . . . . .	47
3.5.3	Bond Graph of Reflection-based Bilateral Control . . . . .	49
3.6	Analyses Based on Pole Placements . . . . .	51
3.7	Common-Mode Control of Entropy Flows . . . . .	53
3.8	Experiments of Bilateral Control . . . . .	54
3.8.1	Overview of Experiments (Bilateral Control) . . . . .	54
3.8.2	Results of Experiments (Bilateral Control) . . . . .	56
3.8.3	Results of Experiments (Generalized Intermediate Impedances) . . . . .	59
3.8.4	Results of Experiments (Comparison with Reflection-based Control) . . . . .	64
3.9	Summary of Chapter 3 . . . . .	66
<b>4</b>	<b>Performance Enhancement of Bilateral Control under Communication Delay</b>	<b>67</b>
4.1	Introduction . . . . .	67
4.2	Bilateral Control under Time Delay . . . . .	68
4.3	Phase-lag Compensation and Stability . . . . .	69

4.3.1	Analyses on Use of Phase-lag Compensator Based on Bond Graph . . . . .	69
4.3.2	Analyses on Phase-lag Compensator Based on Differential Modal Space . . . . .	72
4.4	Design of Through Variable Compensator . . . . .	74
4.4.1	Through Variable Compensator for Sub-optimal Tracking . . . . .	74
4.4.2	Modification of Through Variable Compensator . . . . .	75
4.4.3	Determination of Gain $k$ . . . . .	79
4.5	Simulations of Using Phase-lag Compensator . . . . .	79
4.6	Experiments of Using Compensator for Through Variable Control . . . . .	82
4.6.1	Overview of Experiments (Compensator for Through Variable Control) . . . . .	82
4.6.2	Results of Experiments (Compensator for Through Variable Control) . . . . .	84
4.7	Experiments of Comparison Using Hybrid Parameters . . . . .	86
4.7.1	Overview of Experiments (Comparison Using Hybrid Parameters) . . . . .	86
4.7.2	Results of Experiments (Comparison Using Hybrid Parameters) . . . . .	88
4.8	Summary of Chapter 4 . . . . .	91
<b>5</b>	<b>Bilateral Control Between Systems with Different Control Performances</b>	<b>92</b>
5.1	Introduction . . . . .	92
5.2	Bilateral Control Between Different Control Performances . . . . .	94
5.3	Analyses on Modal Space of Bilateral Control Between Different Bandwidths . . . . .	96
5.4	Construction of Compensator for Interference Terms . . . . .	97
5.5	Discussions on the Effectiveness of Using the Compensator . . . . .	100
5.6	Experiments of Bilateral Control with Different Bandwidths . . . . .	101
5.6.1	Overview of Experiments (Bilateral Control with Different Bandwidths) . . . . .	101
5.6.2	Results of Experiments (Bilateral Control with Different Bandwidths) . . . . .	103
5.7	Summary of Chapter 5 . . . . .	105
<b>6</b>	<b>Bandwidth Improvement of Thermal Haptic Display for Mixed Rendering of Mechanical and Thermal Sensations</b>	<b>106</b>
6.1	Introduction . . . . .	106
6.2	Modeling of Thermoelectric Device . . . . .	107
6.2.1	Structure and Coordinates of Thermoelectric Device . . . . .	107
6.2.2	Transfer Functions of Electrode and Ceramic Plate Part . . . . .	109
6.2.3	Block Diagram of Peltier Device . . . . .	110
6.3	Heat Inflow Observer . . . . .	111
6.3.1	Construction of Heat Inflow Observer . . . . .	111
6.3.2	Approximation of Heat Inflow Observer . . . . .	112

6.4	Modification of the Output of Heat Flow Sensor . . . . .	114
6.5	Identification of Thermal Contact Resistance . . . . .	116
6.6	Experiments of Observer-based Heat Inflow Estimation . . . . .	116
6.6.1	Overview of Experiments (Heat Inflow Estimation) . . . . .	117
6.6.2	Results of Experiments (Output Modification of Heat Flow Sensor) . . . . .	119
6.6.3	Results of Experiments (Estimation of Heat Inflow) . . . . .	120
6.6.4	Results of Experiments (Observer-based Control of Heat Inflow) . . . . .	121
6.7	Experiments of Observer-based Thermal Bilateral Control . . . . .	122
6.7.1	Overview of Experiments (Observer-based Thermal Bilateral Control) . . . . .	122
6.7.2	Results of Experiments (Observer-based Thermal Bilateral Control) . . . . .	123
6.8	Experiments of Mixed Rendering of Mechanical and Thermal Sensations . . . . .	124
6.8.1	Overview of Experiments (Mixed Rendering of Mechanical and Thermal Sensations) . . . . .	124
6.8.2	Results of Experiments (Mixed Rendering of Mechanical and Thermal Sensations)	125
6.9	Summary of Chapter 6 . . . . .	127
<b>7</b>	<b>Conclusions</b>	<b>128</b>
	<b>References</b>	<b>134</b>
	<b>Achievements</b>	<b>143</b>

# List of Figures

1-1	Transmission flow of audiovisual information. . . . .	2
1-2	Kinesthetic bilateral control. . . . .	3
1-3	Thermal interaction between operator and device. . . . .	5
1-4	The motivation of this dissertation. . . . .	8
1-5	Chapter organization of this dissertation. . . . .	10
2-1	Distributed parameter model of each physical system. (a) Mechanical system (wave equation). (b) Electrical system (telegraphic equation). (c) Thermal system (thermal diffusion equation). . . . .	13
2-2	Elements in each physical system based on mobility analogy. . . . .	17
2-3	Generalized control device described by using bond graph. . . . .	18
2-4	Generalized control device described by using block diagram. . . . .	19
2-5	Robust control of AVF based on observer of disturbance through variable. . . . .	20
2-6	Bond graph of robust control of AVF. . . . .	21
2-7	Approximated bond diagram of perfect AVF control. . . . .	21
2-8	Estimation of disturbance heat flow. . . . .	23
2-9	Bond graph of across variable control. . . . .	25
2-10	Bond graph of through variable control. . . . .	25
2-11	Examples of multi-degree-of-freedom system. . . . .	26
2-12	Experimental setup of across variable control (mechanical system). . . . .	28
2-13	Experimental setup of across variable control (thermal system). . . . .	28
2-14	Experimental results of across variable control (mechanical system). . . . .	30
2-15	Experimental results of across variable control (thermal system). . . . .	30
2-16	Experimental results of across variable control (mechanical system and without disturbance observer). . . . .	31
2-17	Experimental results of across variable control (thermal system and without disturbance observer). . . . .	31
2-18	Experimental setup of through variable control (mechanical system). . . . .	32



2-19	Aluminum block used for through variable control of thermal system. . . . .	32
2-20	Experimental results of through variable control (mechanical system). . . . .	33
2-21	Experimental results of through variable control (thermal system). . . . .	33
3-1	Schematic of bilateral control for reproduction of power interaction. . . . .	37
3-2	Block diagram of the AVF-based 4ch control system. . . . .	39
3-3	Generalized intermediate impedance in power transmission. . . . .	43
3-4	Impedances in the case of across variable-based bilateral control. . . . .	45
3-5	Impedances in the case of through variable-based bilateral control. . . . .	45
3-6	Impedances in the case of AVF-based bilateral control ( $C_e$ is changed). . . . .	46
3-7	Impedances in the case of AVF-based bilateral control ( $C_i$ is changed). . . . .	46
3-8	Bond graph of AVF-based 4ch control. . . . .	48
3-9	Approximated bond graph for stability analysis of AVF-based 4ch control. . . . .	48
3-10	Bond graph of reflection-based control. . . . .	50
3-11	Approximated bond graph for stability analysis of reflection-based control. . . . .	50
3-12	Pole movements of AVF-based 4ch control system. . . . .	52
3-13	Pole movements of reflection-based control system. . . . .	52
3-14	Entropy flow in thermal bilateral control. . . . .	53
3-15	Experimental setup of bilateral control (mechanical system). . . . .	54
3-16	Experimental setup of bilateral control (thermal system). . . . .	54
3-17	External environments used for thermal bilateral control. . . . .	54
3-18	Experimental results of across variable-based bilateral control (mechanical system). (a) Velocity responses. (b) Force responses. . . . .	56
3-19	Experimental results of through variable-based bilateral control (mechanical system). (a) Velocity responses. (b) Force responses. . . . .	56
3-20	Experimental results of AVF-based 4ch bilateral control (mechanical system). (a) Velocity responses. (b) Force responses. . . . .	57
3-21	Comparison of velocity and force responses. (a) Velocity responses. (b) Force responses. . . . .	57
3-22	Experimental results of across variable-based bilateral control (thermal system). (a) Temperature responses. (b) Heat flow responses. . . . .	58
3-23	Experimental results of through variable-based bilateral control (thermal system). (a) Temperature responses. (b) Heat flow responses. . . . .	58
3-24	Experimental results of AVF-based 4ch bilateral control (thermal system). (a) Temperature responses. (b) Heat flow responses. . . . .	59
3-25	Comparison of temperature responses. . . . .	59
3-26	Intermediate impedance of across variable-based bilateral control (mechanical case). . . . .	60

3-27	Intermediate impedance of through variable-based bilateral control (mechanical case). . . . .	60
3-28	Intermediate impedance of AVF-based bilateral control (mechanical case, $C_e$ is changed). . . . .	61
3-29	Intermediate impedance of AVF-based bilateral control (mechanical case, $C_i$ is changed). . . . .	61
3-30	Intermediate impedance of across variable-based bilateral control (thermal case). . . . .	62
3-31	Intermediate impedance of through variable-based bilateral control (thermal case). . . . .	62
3-32	Intermediate impedance of AVF-based bilateral control (thermal case, $C_e$ is changed). . . . .	63
3-33	Intermediate impedance of AVF-based bilateral control (thermal case, $C_i$ is changed). . . . .	63
3-34	Experimental results of AVF-based bilateral control (mechanical system, contact with aluminum block). (a) Velocity responses. (b) Force responses. . . . .	64
3-35	Experimental results of reflection-based bilateral control (mechanical system, contact with aluminum block). (a) Velocity responses. (b) Force responses. . . . .	64
3-36	Experimental results of AVF-based bilateral control (thermal system, contact with cooled aluminum block). (a) Temperature responses. (b) Heat flow responses. . . . .	65
3-37	Experimental results of reflection-based bilateral control (thermal system, contact with cooled aluminum block). (a) Temperature responses. (b) Heat flow responses. . . . .	65
4-1	AVF-based 4ch bilateral control under time delay. . . . .	69
4-2	Bilateral control with phase-lag compensator under time delay. . . . .	70
4-3	Block diagram of differential modal space under time delay. . . . .	72
4-4	Gain diagram of $1 + e^{-Ts}C_{cp}$ . . . . .	73
4-5	Gain diagram of $C_{cpi}$ (the case of $C_e = 30.0, T = 0.1, C_{cpe} = (0.5s + 10.0)/(s + 10.0)$ ). . . . .	75
4-6	Gain diagram of $C_{cpi}$ (The case of $C_e = 30.0, C_i = 1.0, T = 0.1, C_{cpe} = (0.5s + 10.0)/(s + 10.0)$ ). . . . .	76
4-7	Idea of modifying the compensator $C_{cpi}$ . . . . .	76
4-8	Implementation of $C_{cpi}$ . . . . .	77
4-9	Gain diagrams of hybrid parameters with different gain $k$ (changed from 0.0 with increment of 0.2). . . . .	78
4-10	Simulation results of bilateral control without phase-lag compensation (free operation). (a) Position responses. (b) Force responses. . . . .	80
4-11	Simulation results of bilateral control with phase-lag compensation (free operation). (a) Position responses. (b) Force responses. . . . .	80
4-12	Simulation results of bilateral control without phase-lag compensation (contact motion). (a) Position responses. (b) Force responses. . . . .	81
4-13	Simulation results of bilateral control with phase-lag compensation (contact motion). (a) Position responses. (b) Force responses. . . . .	81
4-14	Experimental setup for checking the compensator in through variable control. . . . .	82

4-15	Schematic illustration of 2-link manipulator. . . . .	82
4-16	Experimental results of bilateral control under time delay (without compensator). (a) Position responses in $X$ direction. (b) Position responses in $Y$ direction. (c) Force responses in $X$ direction. (d) Force responses in $Y$ direction. . . . .	84
4-17	Experimental results of bilateral control under time delay (with compensator). (a) Position responses in $X$ direction. (b) Position responses in $Y$ direction. (c) Force responses in $X$ direction. (d) Force responses in $Y$ direction. . . . .	85
4-18	Values of compensator gain $k$ . (a) $k$ for control in $X$ direction. (b) $k$ for control in $Y$ direction. . . . .	86
4-19	Experimental setup used for comparing with other compensation methods. . . . .	87
4-20	Experimental results of measuring hybrid parameters. (a) Results of measuring $H_{12}$ and $H'_{12}$ . (b) Results of measuring $H_{21}$ and $H'_{21}$ . . . . .	89
4-21	Experimental results of measuring symmetric ratios. (a) Symmetric ratio $R_{12}$ . (b) Symmetric ratio $R_{21}$ . . . . .	90
5-1	AVF control of haptic device that has imperfect transmission characteristics. . . . .	93
5-2	Equivalent block diagram of the AVF control. . . . .	94
5-3	AVF-based 4ch bilateral control with different control performances. . . . .	95
5-4	Differential modal space of the bilateral control. . . . .	96
5-5	Common modal space of the bilateral control. . . . .	97
5-6	Disturbance observer constructed in common modal space. . . . .	98
5-7	Compensation for the disturbance in common modal space. . . . .	99
5-8	Equivalent block diagram of common modal space. . . . .	100
5-9	Experimental setup of bilateral control (different bandwidths, mechanical system). . . . .	101
5-10	Experimental setup of bilateral control (different bandwidths, thermal system). . . . .	101
5-11	Experimental results of system with different control performances (mechanical control, without compensation). (a) Velocity responses. (b) Force responses. . . . .	103
5-12	Experimental results of system with different control performances (mechanical control, proposed system). (a) Velocity responses. (b) Force responses. . . . .	103
5-13	Experimental results of system with different control performances (thermal control, without compensation). (a) Temperature responses. (b) Heat flow responses. . . . .	104
5-14	Experimental results of system with different control performances (thermal control, proposed system). (a) Temperature responses. (b) Heat flow responses. . . . .	104
6-1	Structure of Peltier device. . . . .	107

6-2	Coordinates of each part of the device. (a) Coordinate of electrode part. (b) Coordinate of ceramic plate part. . . . .	108
6-3	Block diagram of heat transfer in Peltier device. . . . .	111
6-4	Block diagram of the heat inflow observer. . . . .	112
6-5	Approximated block diagram of Peltier device. . . . .	113
6-6	Heat inflow observer based on approximated model. . . . .	113
6-7	Coordinate of thermal sensor. . . . .	114
6-8	Block diagram for identifying thermal contact resistance. . . . .	116
6-9	Experimental setup for heat inflow estimation. . . . .	117
6-10	Schematic representation of experimental setup (estimation of heat inflow). . . . .	117
6-11	Schematic representation of experimental setup (modification of output of heat flow sensor). . . . .	118
6-12	Experimental results (0.1 Hz). (a) Temperature responses. (b) Heat flow responses. . . .	119
6-13	Heat flow responses (contact). . . . .	120
6-14	Estimation results of heat inflow. . . . .	120
6-15	Results of heat inflow control (reference: 1.0 W). . . . .	121
6-16	Experimental setup for observer-based thermal bilateral control. . . . .	122
6-17	Experimental results of thermal bilateral control (use of heat inflow observer). (a) Temperature responses (the case without using the observer). (b) Heat inflow responses (the case without using the observer). (c) Temperature responses (the case with using the observer). (d) Heat inflow observer (the case with using the observer). . . . .	123
6-18	Experimental setup for mixed rendering of mechanical and thermal sensations. . . . .	124
6-19	Operation example of the mixed rendering system of mechanical and thermal sensations. . . . .	125
6-20	Experimental results of mixed rendering of mechanical and thermal sensations. (a) Responses of across variables (with the heat flow sensor). (b) Responses of across variables (with the observer). (c) Responses of through variables (with the heat flow sensor). (d) Responses of through variables (with the observer). . . . .	126

# List of Tables

2.1	Across and through variables based on mobility analogy. . . . .	17
2.2	Parameter values for experiments (mechanical system). . . . .	29
2.3	Parameter values for experiments (thermal system). . . . .	29
3.1	Control objectives for each physical system. . . . .	38
3.2	Parameter values for plotting gain diagrams. . . . .	44
3.3	Parameter values for plotting pole movements. . . . .	51
3.4	Parameter values for bilateral control (mechanical system). . . . .	55
3.5	Parameter values for bilateral control (thermal system). . . . .	55
4.1	Parameter values used for simulations. . . . .	79
4.2	Parameter values used for experiments of controlling 2-link manipulators. . . . .	83
4.3	Parameter values used for comparative methods. . . . .	87
5.1	Parameter values for bilateral control with different control performances (mechanical system). . . . .	102
5.2	Parameter values for bilateral control with different control performances (thermal system). . . . .	102
6.1	Parameter values used for identification. . . . .	118
6.2	Measured gains from electrical current to surface temperature. . . . .	121
6.3	Parameter values for bilateral control (observer-based thermal bilateral control). . . . .	122
6.4	Parameter values for bilateral control (mixed rendering of mechanical and thermal sensations). . . . .	125

# Chapter 1

## Introduction

---

In Chapter 1, the background, motivation and chapter organization of this dissertation are described. For explaining the former two parts, the related studies are introduced.

### 1.1 Background of This Dissertation

#### 1.1.1 Recognition of Remote Environment via Transmission of Audiovisual Information

Recognition of environment is important and essential factor for human beings. The obtainment of physical information on things and external environment is enabled by the functions of sensory organs. Based on the information, humans decide their actions and live in this world.

One of the challenging themes in engineering has been the extension of the recognition functions so that those work beyond the spatial constraints. In old days, humans had no means to sense the information on remote environment. The only ways they could utilize were letter and hearing from other people and to deduce the state of remote environment by making full use of such text and linguistic information. The telephone invented by Alexander Graham Bell was a innovation in a sense that humans obtained the mean to hear the sound at remote place. This function is brought by transforming the acoustic wave into electrical signal, transmitting and reproducing those by electro-acoustic transducer. Television developed by the utilization of electro-optical instruments was also the remarkable invention, and it can show the vision of remote place. Fig. 1-1 shows the transmission flow of audiovisual information. The physical phenomena occurring at remote place are dealt by transducers, and the transformed signals are communicated: combination of the “transformation of energy configurations” and “handling the

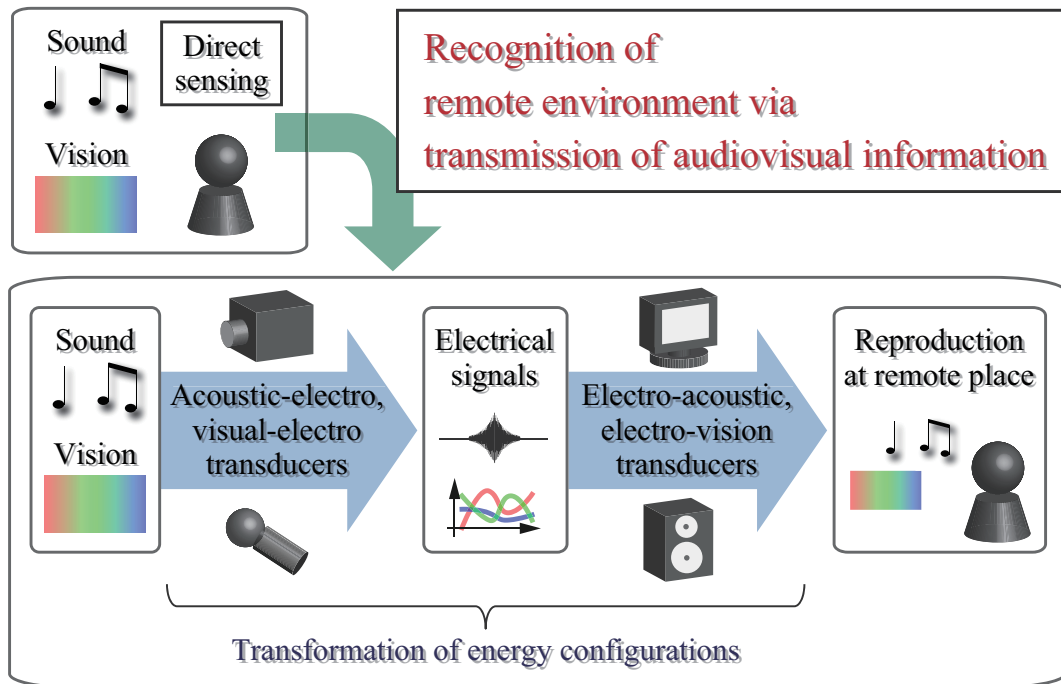


Fig. 1-1: Transmission flow of audiovisual information.

transformed signals” realized the functions. As well as the real-time transmission, this idea can be applied to the preservation of the audiovisual information. Concretely speaking, sound and video recorders were developed. These gave humans the way to sense the information beyond not only spatial but also temporal constraints: they are able to hear and see the sound and vision anytime and anywhere.

With the development of the network technologies, the information is widely utilized as represented by the applications such as broadcasting, multimedia devices and videophones. The systems and technologies are now imperative for current life of humans.

### 1.1.2 Real-world Haptics for Kinesthetic Sensation and Motion Control

Following to audiovisual information, the engineered handling of haptic sensation has recently been researched. The word “hapt” is from a greek word meaning “touch,” and rendering the information is expected to contribute for enhancing the reality in recognizing the environment. The academic field that treats the rendering of the information is called haptics. Up to now, enormous amount of researches have been reported. The first system of transmission and reproduction of haptic information was developed by Goertz [1]. It consists of master and slave systems, and the slave device was designed to follow the

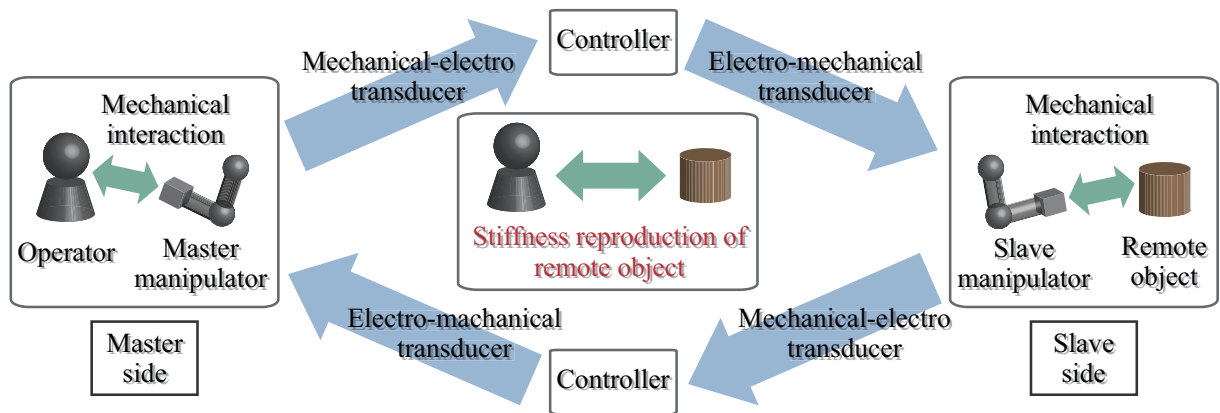


Fig. 1-2: Kinesthetic bilateral control.

movement of the master system. The motivation of this study was to develop the system for manipulation in nuclear plants, and the system enabled the operators stay away from dangerous place by having the slave system act the kinesthetic interaction as an remote agent. The system was mechanically made at first, and later the system that employs electrical devices was developed [2].

As represented by the word “five senses,” there also exist the sensory information that can be used for communication such as sense of smell and taste, other than the haptic sensation. However, the feature that discriminates the haptic sensation from the other type of information is that it is stimulated on the basis of bilateral interaction between human and environment. It is represented by the famous physical law called action-reaction law: human touches environment and environment touches human. The law indicates the necessity of bidirectional structure in handling the transmission of haptic information. Based on this, bilateral control was invented [3–7]. The schematic illustration is shown in Fig. 1-2. Here, the transduction of mechanical and electrical power is done bidirectionally. The final goal of the system is to control the master and slave manipulators to synchronize mechanically.

The configuration of control system has always been the problem in the field of bilateral control. In earlier stage, synchronization of workspace velocities of end effectors was set as the control objectives. Based on this, velocity-based bilateral control system was proposed [8, 9]. The other type of control systems is force-based one, and this system focuses on rendering the force generated at slave side for master operator [10]. This one is called as force-based bilateral control method. One of the famous types of bilateral control is force-reflecting type scheme, in which force control is conducted at the master side whereas position control is implemented at the slave side [11–16]. This type is widely utilized as the effective control scheme. In addition to the pure rendering of remote object, the idea was applied for



micro manipulation and macro-micro bilateral control was proposed [17–19].

As noted above, the function that the bilateral control system should realize is to render the stiffness of remote object. Lawrence defined the “transparency” of the rendering from inspiration by 2-port circuit [20], and it enabled the performance analyses on bilateral control schemes. In [20], 4ch bilateral control scheme was also proposed. Similar idea was also proposed by Hannaford [21,22]. Another topic existing in the research field is the stabilization of the system operation under time delay [23]. Since the structure of control system should take the bilateral form, the feedback of signal is needed. As known in the control theory, the time delay generated by communication between master and slave systems in the feedback loop easily deteriorates the stability of system. For addressing the problem, there exist researches that treat  $H_\infty$  and  $\mu$ -synthesis theories [24, 25]. Gunter proposed wave variable for tele-manipulation, and realized the stabilization of the system under communication delay [26–28]. The passivity is the most famous method for addressing the problem [29–32]. The idea of the method is similar to that of wave variable, and it can ensure the system stability by considering the dissipation of energy at communication block.

As well as the researches on the tele-manipulation, the technologies on motion control of robotic systems have been developing. The refined control of robotic motion and interaction between robot and environment are actively researched. Following to the pure position and force control of robotic manipulator, impedance control was invented [33,34]. In an idea called control stiffness [35], the control system has intermediate characteristics between position and force control. As for the robust control of motor, Ohnishi proposed the disturbance observer that can estimate and compensate for the disturbance torque [35–39]. With the use of the observer, acceleration control system was developed, and it was found that the robust control of acceleration is the fundamental factor for realizing any tasks of motion control such as controlling position, force and virtual impedance [40]. In [41], the acceleration control realized by using sliding mode controller was proposed by Savanovic. Raibert developed the theories on hybrid control; the combination of force and position control [42]. Then, Sakaino extended of the theory on hybrid control and proposed oblique coordinate control [43]. In the method, task Jacobian and mass matrices are derived in oblique coordinate and advanced motion control is realized.

Recently, the integration of technologies on bilateral control and motion control yielded novel types of systems. Matsumoto proposed the 4ch bilateral control based on the acceleration control [44]. Iida proposed operability and reproducibility [45] based on hybrid parameters, and found that the system was the strong candidate for realizing the high transparency of bilateral control. The system is called

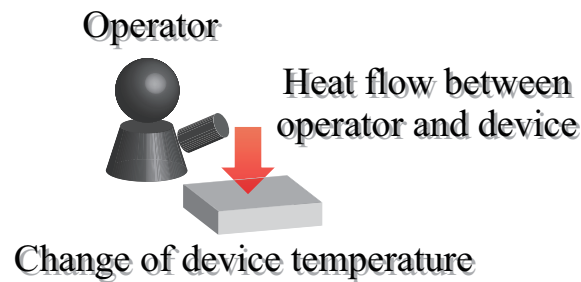


Fig. 1-3: Thermal interaction between operator and device.

ABC in abbreviation, and along with the development of the system, the academic field called real-world haptics emerged [46]. The real-world haptics is one of the fields of haptics, and it focuses on the rendering of haptic sensation induced by the contact with the object that exists in real. In that sense, the tele-manipulation based on bilateral control is included as one of the topics in the field. Among the many kinds of control schemes, the ABC is often treated as the unit system in the researches of real-world haptics. There exist researches in which acceleration control is utilized for macro-micro bilateral control [47, 48]. Katsura extended framework of bilateral control into multiple systems and proposed multilateral control system [49]. The scheme is effective for broadcasting haptic information, and cooperative tele-operation is researched [50–52]. As for the preservation of haptic information, Yokokura proposed motion-copying system [53, 54] in which position and force information is stored while bilateral control is conducted. The system is highly capable of reproducing the kinesthetic motion of operator. Then, disturbance observer was utilized also for the stabilization under communication delay, and Natori proposed communication disturbance observer that can compensate for the adverse effect by the delay as the disturbance [55–58]. With the passivity-based approach, the observer is thought as the effective method for delay compensation.

### 1.1.3 Technologies on Thermal Haptics

So far the kinesthetic rendering of remote environment has been introduced. Since the real-world haptics is developed under the history of tele-manipulation using the bilateral control of manipulators, the academic field mainly treated the kinesthetic sensation. However, the sensation does not cover the all range of haptic sensation. The haptic sensation consists of several elemental sensations: kinesthetic, surface and thermal sensations [63, 64]. As well as the kinesthetic rendering, thermal haptics which is a research field on providing thermal sensation has been developing. In thermal haptics, thermal devices

are utilized for rendering thermal sensation [59–62]. Fig. 1-3 depicts the thermal interaction using a thermal device. According to the temperature difference between the operator and the device, heat flows into/out of the device. Then, the device changes its temperature on the basis of the heat flow and thermal energy generated interior of the device. By the heat flow and device temperature, the operator feels the thermal sensation.

In the field of thermal haptics, Peltier device is often employed. It is a thermoelectric device that facilitates the heat flow based on the Peltier effect [65]: heat flow is generated when two different metals or semiconductors are joined and electrical power is applied. The device has relatively fast response characteristics and can be driven easily by DC-power source, and it is utilized for many kinds of applications such as cooling computer components, heat pump for mini-sized refrigerator, etc [66–68]. In [69], the use of the device for bio-microfluidic platform is introduced. From same reasons, the device is thought to be applicable for haptic devices [70].

In the past, temperature control of the device was mainly focused. The temperature variation in contacting with material is recorded, and the device temperature is controlled to mimic the contact. In contacting with the objects, the thermal properties of human finger are important [71, 72]. On this perspective, the model of human finger is derived and included in the controller design in some researches. On the other hand, heat flow is also considered as the important physical variable and the history of heat flow in contact is reproduced in [73]. These are not real-time transmission of thermal sensation and include the virtual reality as one of the targets. In [74], the thermoelectric device was mounted on the manipulator with stage, and kinesthetic and thermal sensations are simultaneously rendered as the application of virtual reality. Some researchers challenged implementing the device with vibrotactile actuators for supplementing the surface sensation [75, 76]. Then, a medical simulator that renders both mechanical and thermal property of virtual object was developed in [77]. The development of small-sized thermal rendering device was reported in [78].

Along with the researches on providing thermal sensation, thermal control itself is also handled as the research topic. The Peltier device is known to have nonlinear characteristics such as Joule heat. For the control with long time constant, PID control of the device is sufficient. However, in utilizing the device for thermal haptics, the bandwidth of the thermal system should be set as wide as possible, and the nonlinear terms should be taken into account for designing controller for realizing precise thermal rendering. As the examples of the studies on controlling the Peltier device, operator-based control theory has been applied for controlling the device in [79]. As the robust control system, the heat disturbance

observer is constructed for compensating for the disturbance factors in thermal control [80,81]. The use of sliding-mode controller for robust temperature control was presented in [82].

There also exist the studies on real-time transmission of information on thermal sensation. Tachi proposed the concept of Telexistence and implemented the function of thermal rendering [83]. In the developed system, the temperature of remote robotic hand is measured and temperature of the device was regulated to be same as that of the robotic hand [84]. In the similar way, Caldwell combined thermal device, vibrotactile actuator, pressuring instrument, camera and microphone in order to have the operator feel immersed in remote environment. In these systems the thermal device does not exist in remote side, and the rendering is done only in one direction. The number of researches on thermal bilateral control is fewer than the kinesthetic cases; however, there are some research reports [85]. The idea of thermal bilateral control was introduced in [86]. In [86], several types of couplings between master and slave thermal devices (temperature and temperature, heat flow and temperature, etc) were tested. Moreover, the bilateral control with prediction of finger temperature was presented [87]. The thermal bilateral control with scaling was proposed in [88].

## **1.2 Motivation of This Dissertation**

The kinesthetic and thermal controls, as well as the technologies on rendering of those information, are treated in different ways. From the viewpoint of the application of haptic rendering systems, the appropriate structure of the system can be different; the unilateral transmission of measured thermal states and controlling the thermal haptic device can be enough as the remote thermal display, whereas the bilateral structure as well as the short time period of control and high resolution of sensors is required for remote communication of kinesthetic sensation, since the bandwidth of kinesthetic sensation is much higher than that of thermal sensation. Although the requirements for rendering the respective sensations are different, from the viewpoint of physical phenomena, the contact of human with the environment can be comprehended as the exchange of physical powers between them; not only the mechanical power but also the thermal one flows from one side to the other side. Like a handshake in which the contacted materials can change those temperatures according to the heat flow between them, there are cases in which the mutual interactions of thermal powers cannot be neglected in thermal rendering; in these cases, both the temperature and heat flow should be controlled in bilateral direction for rendering the thermal properties of the remote objects. As for this mutual interaction, it is able to say that the real-world haptics

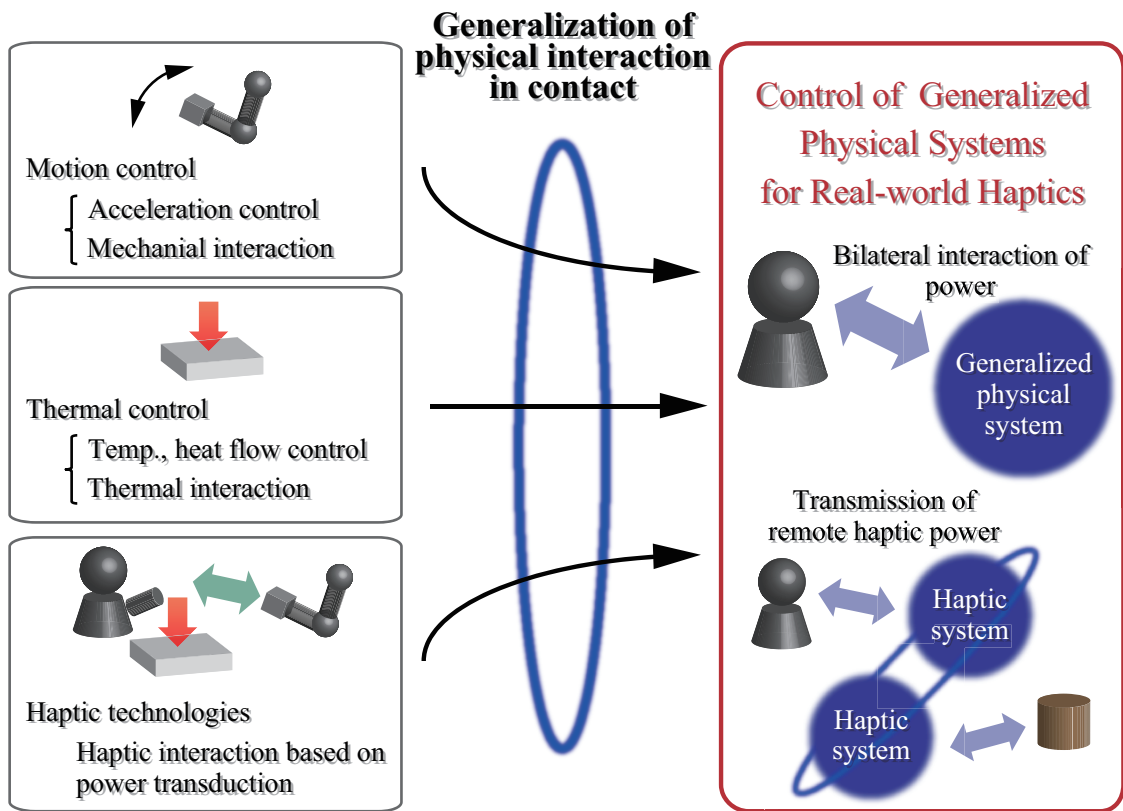


Fig. 1-4: The motivation of this dissertation.

mainly treated the kinesthetic sensation, whereas the bilateral rendering of thermal sensation has a short history and methodologies for the control have not been established yet.

The motivation of this dissertation is to generalize the framework of reproducing the physical phenomena that are occurring at the contact; the bilateral exchanges of physical powers are handled in unified way. The motivation of the study is illustrated in Fig. 1-4. For the generalization, this study considers the integration of motion control, thermal control and haptic technologies. By deriving the framework of mutual reproduction, it is expected that the modality as well as the quality of communication is increased. Moreover, the mixed rendering of mechanical and thermal sensations becomes possible under the concept of generalized physical powers. This kind of system is only realized by considering the bilateral control system in unified manner. Realizing the feature that enables the interaction of different kinds of physical powers is also the important theme in this dissertation, and it can lead to the invention of the novel haptic applications.

The one of the most famous representation methods of the generalized systems' dynamics is bond

graph [89–91]. It was proposed by Paynter, and physical variables are categorized into two parts: the effort and flow [92]. For example, mechanical force and electrical voltage are treated as effort whereas the velocity and current are categorized as flow. The multiplication of effort and flow has a unit of power, and then the unified elements for energy storing and dissipation are defined. The bond graph connects the elements by arrows, and effort and flow are allocated so that the arrows in graph can represent the power flow. Meanwhile, Firestone focused on the allocation topology of elements, and defined the across and through variables [93]. The former one is the difference of potential across the element, and through variable is defined to be the physical quantity that goes through the element. For instance, the voltage difference across the electrical resistance corresponds to the across variable, and electrical current flowing through it is treated as through variable. This type of definition enables the consistent analogy of different physical systems in a sense that the series and parallel connections of elements are maintained. The concept of these analogical theories is extended to include also the thermal system, which involves the generation of entropy in irreversible process. For example, Thoma proposed RS-element so that the contradictions in power flow of bond graph don't occur [94].

In present control engineering, block diagram and state-space equations are preferred. Here, analyses in frequency domain and more mathematical calculation with less consideration on physical meaning are conducted. Currently the bond graph is less employed than these methods; however, the graph has advantage that it can explicitly represent the flow of physical power. Even the gains in controller can be interpreted as the source or elements to handle the power flows [95]. The aim of this dissertation is to treat the bilateral power reproduction in unified way for real-world haptics, and the theory of bond graph that can handle the power flows becomes the key factor for this endeavor. In future industry, developing systems for embodying physical properties of objects in mutual direction can involve a lot of different types of physical phenomena, not only mechanical and thermal fields. The concept in this dissertation for unification of bidirectional rendering will play an important role for that field.

### **1.3 Chapter Organization of This Paper**

Fig. 1-5 shows the chapter organization of this dissertation. First, the robust motion control and thermal control are generalized by the control of across variable flow in Chapter 2. The system with the controller is utilized as the unit for the bilateral control. Then, the bilateral control based on the across variable flow is constructed in Chapter 3. The Chapters 2 and 3 mainly focus on the theory expansion of

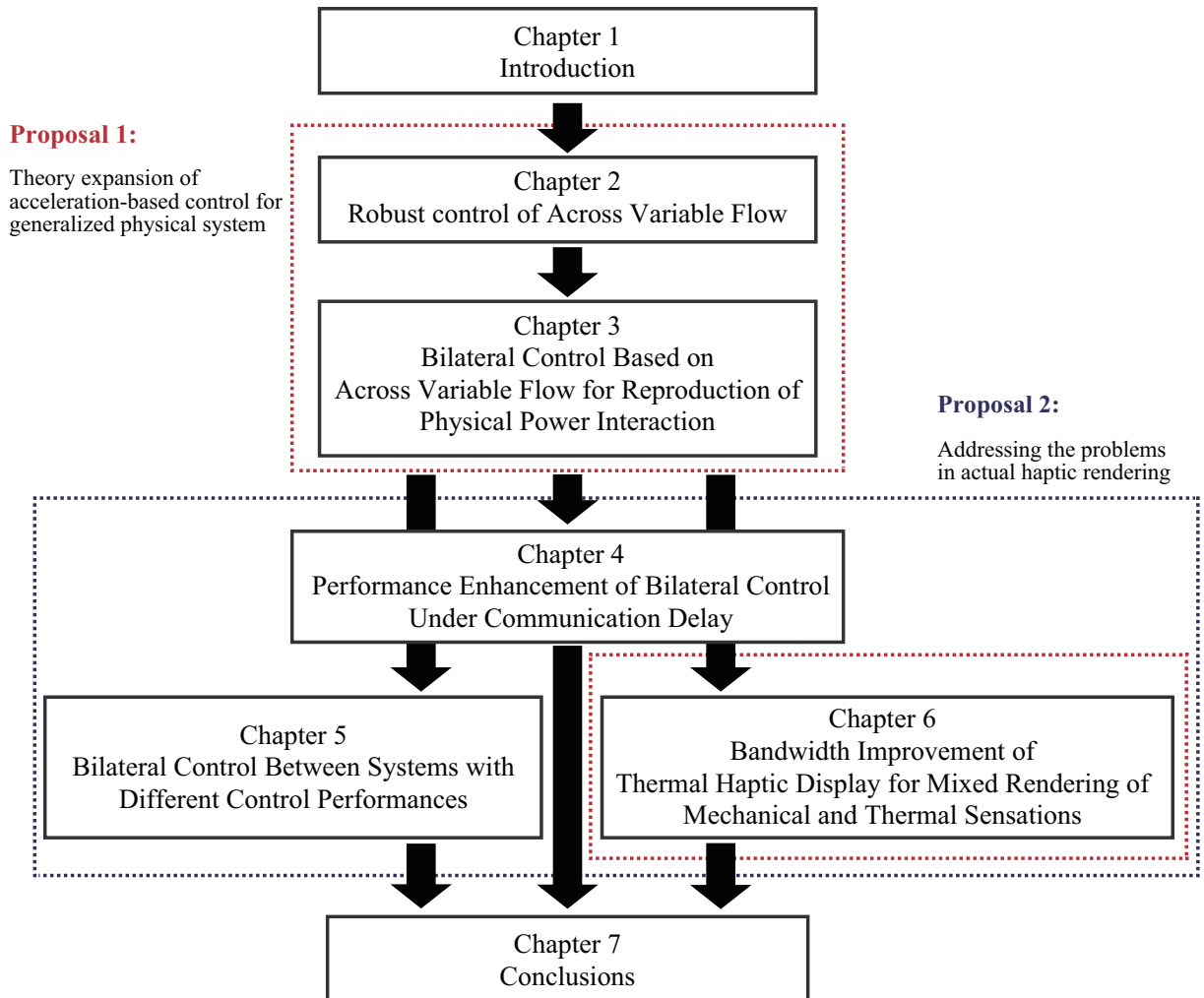


Fig. 1-5: Chapter organization of this dissertation.

acceleration-based control [35,44] for generalized physical systems.

After the expansion of the framework, this dissertation treats the problems existing in actual bilateral control. One of the major problems for applying the control is communication delays between master and slave systems. The delays easily deteriorate the performance and stability of the systems [23]. Therefore in Chapter 4, filters for recovering the performances under the delay are proposed [96]. Then in Chapter 5, compensation for bilateral control with different control performances is treated [97]. In the practical situation, there can be the cases in which the master and slave systems employ the devices with different control bandwidths, and the topic is handled in the chapter. Chapter 6 focuses on the thermal haptic device, and proposes a heat inflow observer [98]. The observer enables the omitting of the heat

flow sensor, and it is expected to enhance the response characteristics of thermal system. For testing the effectiveness of the developed observer, observer-based thermal bilateral control and the mixed rendering is demonstrated in the chapter. The mixed rendering can only be realized by considering the generalized physical powers, and the experiment is not only conducted for testing the observer but also for showing the possibilities of novel kinds of haptic applications.

Through Chapters 2 and 3, the framework of bilateral control design is constructed. On the other hand, the Chapters 4, 5 and 6 address the problems in actual bilateral control. Therefore, this dissertation covers the wide range of themes including the abstraction of theories and practical implementation. Finally in Chapter 7, this dissertation is summarized by some conclusion remarks.



## Chapter 2

# Robust Control of Across Variable Flow

---

### 2.1 Introduction

In this chapter, robust control of across variable flow (AVF) that will be used as the fundamental unit for bilateral reproduction of power transmission is introduced. The across variable is one of the generalized physical variables, and using it enables the unified handling of different kinds of physical systems. The AVF is the changing rate of across variable, and the perfect control of AVF corresponds to an normalization of capacitive element of generalized device. By the normalization, the controller design becomes free from the disturbance terms and actual amount of the device capacitance. Moreover, this dissertation defines generalized control conductance that corresponds to the control stiffness [35] in the field of motion control. Systems should realize the wide range of the index values in order to handle the various kinds of control tasks. In accordance with the index, control systems of across and through variables with the utilization of AVF controller are introduced. The constructed systems will have the large potential to be applied for the bilateral control.

The contents of this chapter are as follows. Section 2.2 introduces the across and through variables, which are the one kind of the generalized physical variables. In this section, the explanations on some generalized elements that form the dynamics of physical objects are included. Section 2.3 shows the generalized form of control device using the variables and elements. Then, the robust control of AVF based on the observer of disturbance through variable is constructed in Section 2.4. The case of thermodynamic systems that need special treatments is explained in Section 2.5. In Section 2.6, generalized control conductance is defined. Then, the control systems of across and through variables are constructed with the

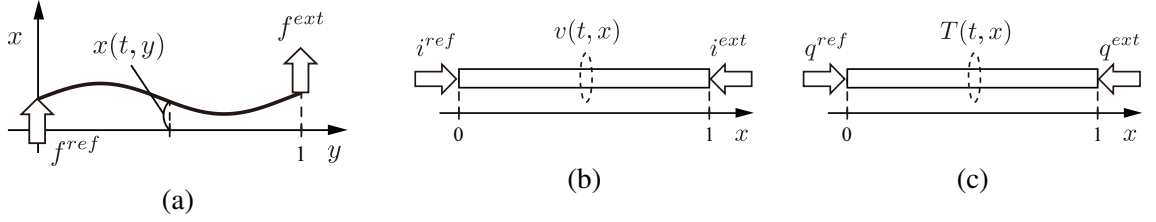


Fig. 2-1: Distributed parameter model of each physical system. (a) Mechanical system (wave equation). (b) Electrical system (telegraphic equation). (c) Thermal system (thermal diffusion equation).

use of the AVF controller, and relation between the systems and the defined index is discussed. In Section 2.7, control of multi-degree-of-freedom system is briefly explained. The experimental examples are shown in Sections 2.8 and 2.9. Finally, this chapter is concluded in Section 2.10.

## 2.2 Generalized Physical Variables

Things are surrounded by many kinds of physical phenomena: mechanical, electrical, magnetic, thermal and so on. For example, electrical field moves an electron in the field, and thermal energy is transferred from high temperature area to low temperature one. As represented by an electrical motor, the engineers have been developing the effective combination of the phenomena in order to realize certain tasks and functions [92], and a lot of devices, instruments and systems have been invented. For discussing the systems in unified approach, variables in generalized physical systems are introduced in this section.

### 2.2.1 Analogies Between Different Kinds of Physical Systems

As the preliminary for deriving the generalized physical systems, governing equations for mechanical, electrical and thermal systems are firstly considered, respectively. This dissertation handles one dimensional physical phenomena, and models of the systems are shown in Fig. 2-1. Here,  $x$ ,  $f$ ,  $v$ ,  $i$ ,  $T$  and  $q$  denote position, force, voltage, current, temperature and heat flow, respectively. Then, the superscripts  $ref$  and  $ext$  represent the reference and external value, respectively. In modeling, the materials are set to have unit length. Then mechanical, electrical and thermal systems are modeled by wave equation, telegraphic equation and thermal diffusion equation, respectively. The governing equations for each physical system are described below

$$\frac{\partial^2 x(t, y)}{\partial t^2} = \frac{K}{M} \frac{\partial^2 x(t, y)}{\partial y^2} \quad (2.1)$$

$$\frac{\partial^2 v(t, x)}{\partial t^2} = \frac{1}{LC} \frac{\partial^2 v(t, x)}{\partial x^2} \quad (2.2)$$

$$\frac{\partial T(t, x)}{\partial t} = \frac{\lambda}{\rho c} \frac{\partial^2 T(t, x)}{\partial x^2}, \quad (2.3)$$

where  $K$ ,  $M$ ,  $L$ ,  $C$ ,  $\lambda$ ,  $\rho$ ,  $c$  stiffness, mass, inductance, capacitance, heat conductivity, density and specific heat capacity, respectively. Note that these physical properties are described in the form of density of the material. Then, the resistance elements are neglected in the telegraphic equation.

Next, the initial and boundary conditions for the equations are set as follows:

[Wave equation]

$$x(0, y) = 0 \quad (2.4)$$

$$\frac{\partial x(0, y)}{\partial t} = 0 \quad (2.5)$$

$$K \frac{\partial x(t, 0)}{\partial y} = -f^{ref}(t) \quad (2.6)$$

$$K \frac{\partial x(t, 1)}{\partial y} = f^{ext}(t) \quad (2.7)$$

[Telegraphic equation]

$$v(0, v) = 0 \quad (2.8)$$

$$\frac{\partial v(0, x)}{\partial t} = 0 \quad (2.9)$$

$$\frac{1}{L} \frac{\partial v(t, 0)}{\partial x} = -\frac{di^{ref}(t)}{dt} \quad (2.10)$$

$$\frac{1}{L} \frac{\partial v(t, 1)}{\partial x} = \frac{di^{ext}(t)}{dt} \quad (2.11)$$

[Thermal diffusion equation]

$$T(0, x) = 0 \quad (2.12)$$

$$\lambda \frac{\partial T(t, 0)}{\partial x} = -q^{ref}(t) \quad (2.13)$$

$$\lambda \frac{\partial T(t, 1)}{\partial x} = q^{ext}(t). \quad (2.14)$$

By applying the Laplace transformation for temporal and spatial domains [99], followings are obtained

$$\frac{M}{K} s^2 x(s, p) = p^2 x(s, p) - px(s, 0) - \frac{\partial x(s, 0)}{\partial y} \quad (2.15)$$

$$LCs^2 v(s, p) = p^2 v(s, p) - pv(s, 0) - \frac{\partial v(s, 0)}{\partial x} \quad (2.16)$$

$$\frac{\rho c}{\lambda} sT(s, p) = p^2 T(s, p) - pT(s, 0) - \frac{\partial T(s, 0)}{\partial x}, \quad (2.17)$$

where  $s$  and  $p$  are Laplace operator for spatial and temporal domain, respectively. By the conditions described above and inversed Laplace transformation, the transfer functions of each physical system are consequently derived as

$$x(s, y) = \frac{1}{K\sqrt{\frac{M}{K}}s} \frac{\cosh\left(s\sqrt{\frac{M}{K}}(1-y)\right)}{\sinh\left(s\sqrt{\frac{M}{K}}\right)} f^{ref}(s) + \frac{1}{K\sqrt{\frac{M}{K}}s} \frac{\cosh\left(s\sqrt{\frac{M}{K}}y\right)}{\sinh\left(s\sqrt{\frac{M}{K}}\right)} f^{ext}(s) \quad (2.18)$$

$$v(s, x) = \frac{L}{\sqrt{LC}s} \frac{\cosh\left(s\sqrt{LC}(1-x)\right)}{\sinh\left(s\sqrt{LC}\right)} s i^{ref}(s) + \frac{L}{\sqrt{LC}s} \frac{\cosh\left(s\sqrt{LC}x\right)}{\sinh\left(s\sqrt{LC}\right)} s i^{ext}(s) \quad (2.19)$$

$$T(s, x) = \frac{1}{\sqrt{\lambda\rho c}s} \frac{\cosh\left(\sqrt{\frac{\rho c}{\lambda}}s(1-x)\right)}{\sinh\left(\sqrt{\frac{\rho c}{\lambda}}s\right)} q^{ref}(s) + \frac{1}{\sqrt{\lambda\rho c}s} \frac{\cosh\left(\sqrt{\frac{\rho c}{\lambda}}sx\right)}{\sinh\left(\sqrt{\frac{\rho c}{\lambda}}s\right)} q^{ext}(s). \quad (2.20)$$

In the transfer functions above, the hyperbolic functions are included. Since it is difficult to handle those in the current form, approximating the transfer function is considered. The hyperbolic function can be expanded as

$$\begin{aligned} \sinh(k) &= k \left(1 + \frac{1}{\pi^2}k^2\right) \left(1 + \frac{1}{4\pi^2}k^2\right) \dots \\ &= k \prod_{n=1}^{\infty} \left(1 + \frac{k^2}{\pi^2}\right) \end{aligned} \quad (2.21)$$

$$\begin{aligned} \cosh(k) &= 1.0 \left(1 + \frac{4}{\pi^2}k^2\right) \left(1 + \frac{4}{9\pi^2}k^2\right) \dots \\ &= \prod_{n=1}^{\infty} \left(1 + \frac{k^2}{(n - \frac{1}{2})^2\pi^2}\right). \end{aligned} \quad (2.22)$$

Therefore, the first order approximations become

$$\sinh(k) \simeq k \quad (2.23)$$

$$\cosh(k) \simeq 1.0. \quad (2.24)$$

Applying these to the transfer functions and by substituting  $x = 1$  or  $y = 1$  (the terminal part of the

material), the dynamic equations of each physical system are obtained as

$$\dot{x}(s) = \frac{1}{Ms}(f^{ref}(s) + f^{ext}(s)) \quad (2.25)$$

$$v(s) = \frac{1}{Cs}(i^{ref}(s) + i^{ext}(s)) \quad (2.26)$$

$$T(s) = \frac{1}{\rho cs}(q^{ref}(s) + q^{ext}(s)). \quad (2.27)$$

The derived equations have similar form; the relation between the input and output is described by the first order differential equation. This is the basis of using the analogies between different kinds of systems.

In deriving the dynamic equations, some approximations of the models and equations were applied. Followings are the summary of the assumptions made in this dissertation and possible differences between the physical systems in actual implementation:

- As shown in Fig. 2-1, one dimensional physical phenomena are treated in this dissertation.
- Moreover, the physical properties such as mass and thermal conductivity are constant and uniform in the material.
- Related to the two points above, this dissertation assumes that the device is the conservative system. For instance, it is expected that the heat conduction between the lateral side of the device and the surrounding environment occurs in addition to the one-dimensional heat transfer; however, this factor is considered to be small and neglected. Moreover, this dissertation treats the solid device, and the factors such as the phase transition are also neglected.
- The expanded terms of hyperbolic functions are related to the zeros and poles (roots of numerator and denominator polynomials) of the transfer functions. Since the locations of the roots of the terms are determined by the physical properties of each system, the validity of the approximation depends on the properties.
- Related to above, the bandwidth of the model that is valid for describing the system operation is different among the physical systems. For example, thermal device has the narrow bandwidth whereas the electrical motor has wider one. For the simplicity of the discussion, it is assumed that the approximated model is valid for all frequency range in Chapter 2 and 3, whereas the influence of the difference between the simplified model and actual one on the haptic communication is considered in Chapter 5.

Table 2.1: Across and through variables based on mobility analogy.

Variables	Mechanical system	Electrical system	Thermal system
Across variable	Velocity $V$	Voltage $V$	Temperature $T$
Through variable	Force $F$	Current $I$	Entropy flow $\dot{S}$

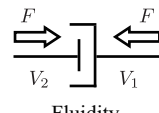
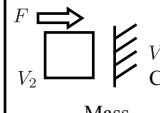
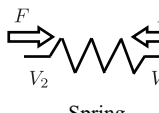
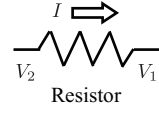
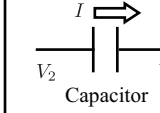
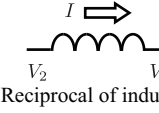
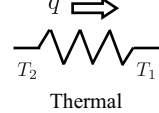
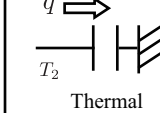
Physical systems	R element $e = \alpha i$	C element $e = \frac{1}{\beta} \int i dt$	I element $i = \gamma \int e dt$
Mechanical system	 Fluidity	 Mass	 Spring
Electrical system	 Resistor	 Capacitor	 Reciprocal of inductor
Thermal system (in pseudo bond graph)	 Thermal resistance	 Thermal capacitance	None

Fig. 2-2: Elements in each physical system based on mobility analogy.

- The simplest approximation of the hyperbolic function is equivalent to that the system is treated as the single-lumped parameter model.

## 2.2.2 Across and Through Variables

The variables can be divided into two kinds: across and through variables [93]. As the electrical current flows through resistance according to the voltage difference across the element, the general physical phenomena can be comprehended in analogical way as that a quantity goes through an element following the difference of potential quantity across the element. The analogy is called as mobility analogy, and the former and the latter quantities are defined as through and across variables, respectively. The across and through variables can be defined as the duality of physical systems, and the analogies of dynamic equations observed in previous part can be comprehended by these variables.

The variables for each kind of physical systems are shown in Table. 2.1. From here, across and through variables will be represented by  $e$  and  $i$ , respectively. As the other type of uniform expressions,

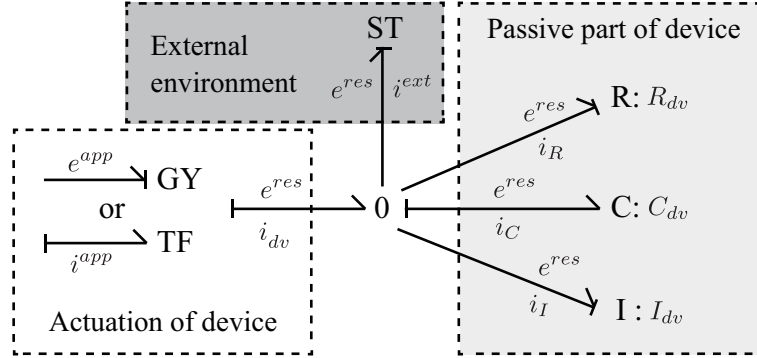


Fig. 2-3: Generalized control device described by using bond graph.

there are effort and flow variables. The reason why the across and through variables are employed is that the topologies of element connections are preserved; series and parallel connections become common for all systems. Fig. 2-2 shows elements defined for each physical system. There are three kinds of elements defined in the analogy: resistive (R), capacitive (C) and inertia (I) elements [92]. Each element relates the across and through variables as

$$\text{R element : } e = \alpha i \quad (2.28)$$

$$\text{C element : } e = \frac{1}{\beta} \int i dt \quad (2.29)$$

$$\text{I element : } i = \gamma \int e dt, \quad (2.30)$$

where  $\alpha$ ,  $\beta$  and  $\gamma$  denote the amount of each element. By using the variables and elements mentioned above, all the kinds of physical systems can be treated in unified approach.

In Fig. 2-2, pseudo bond graph is considered in thermal system. Moreover, (2.27) is different from the rule shown in Table. 2.1; heat flow is employed instead of entropy flow [100]. To be precise, the irreversible process of thermal phenomena should take the generation of entropy into account. For addressing this point, RS element [94] is defined as the supplemental one, whereas this chapter only introduces thermal resistance and capacitance for simplification. The difference of using real and pseudo bond graphs in actual thermal control is discussed in Section 2.5.

## 2.3 Generalized Form of Control Device

Next, control device which will be used for constructing haptic system is unified using the generalized variables and elements. Fig. 2-3 shows the generalized form of control device described by using bond

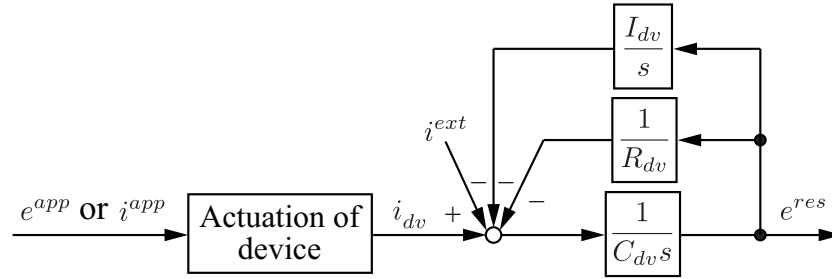


Fig. 2-4: Generalized control device described by using block diagram.

graph. Here,  $R$ ,  $C$  and  $I$  denote resistive, capacitive and inertia element, respectively. The superscripts  $app$ ,  $res$  and  $ext$  mean applied, response and external value, respectively. Then, subscript  $dv$ ,  $R$ ,  $C$  and  $I$  represent device, resistive, capacitive and inertia element, respectively. The capacitive element is used for describing (2.25), (2.26) and (2.27), and the other elements are employed to represent the modeling error of the physical systems. Bond graph is useful for representing the power flow inside of the system. The arrow in the graph represents the flow of physical power; alongside the arrow the across and through variables (in general effort and flow variables are used, whereas across and through variables are employed in this dissertation) are located, and the multiplication of variables yields the unit of power.

The operation of the device can be divided into three parts: actuation of device, interaction with external environment and passive part of the device. The first part represents the generation of reference power  $e^{res} i_{dv}$ . The part corresponds to torque generation by electrical motor, heat flow generated by Peltier device, etc. Here, the reference input ( $e^{app}$  and  $i^{app}$ ) can be both across and through variables; however, in general those finally become input of through variable by using transformer or gyrator. For example, servo amplifier of motor generates force reference (corresponding to  $i_{dv}$ ) based on current reference ( $i^{app}$ ). Then, by the interaction with the external environment, another through variable  $i^{ext}$  is generated. Finally, subtracted power input goes into the passive elements of the device. As a result, the response of across variable  $e^{res}$  (for example, velocity and temperature responses) is determined. Note that there can be cases that only some of the elements are enough, like that the  $R_{dv}$  and  $C_{dv}$  are enough for describing the movement of electrical motor.

The translation of the bond graph as the form of block diagram is shown in Fig. 2-4. In Fig. 2-4,  $s$  denotes Laplace operator. Here, “actuation of device” denotes generation of through variable  $i_{dv}$  e.g. torque coefficient of motor  $K_t$  and Peltier coefficient  $\Pi$  of thermoelectric device. Using the diagram, robust control system of AVF is constructed.



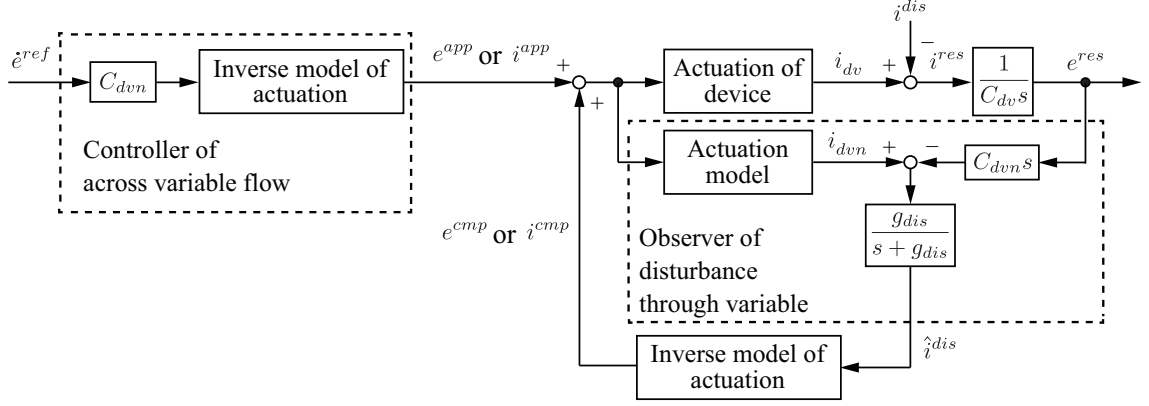


Fig. 2-5: Robust control of AVF based on observer of disturbance through variable.

## 2.4 Robust Control of Across Variable Flow

As shown in Figs. 2-3 and 2-4, the through variable generated by the interaction between the device and external environment (represented by  $i^{ext}$ ) can effect on the response of the device. In addition to that, there exist dissipation and leakage of injected energy by R and I elements, and these also change the response of across variable. Realizing the system that is robust against these terms is essential for simplifying and clarifying the strategy of control design.

Addressing the above problems, this study constructs robust AVF control system based on observer of disturbance through variable as shown in Fig. 2-5. Here,  $g$  denotes cut-off frequency of low-pass filter, and superscripts  $ref$ ,  $cmp$  and  $\hat{\cdot}$  mean reference, compensation and estimated values, respectively. Then, the subscripts  $n$  and  $dis$  represent nominal value and disturbance observer, respectively. In the control system, command of application ( $e^{app}$  or  $i^{app}$ ) is generated based on the reference of across variable flow  $\dot{e}^{ref}$ , nominal value of C element  $C_{dvn}$  and inverse model of device actuation. The disturbance observer estimates the amount of disturbance through variable  $i^{dis}$  by comparing the  $i_{dvn}$  with consequent through variable  $i^{res}$  that brought the response of the device. Here, the disturbance through variable is defined as

$$i^{dis} = i^{ext} + \frac{1}{R_{dv}} e^{res} + I_{dv} \frac{1}{s} e^{res}. \quad (2.31)$$

Supposing that  $C_{dvn} = C_{dv}$  and actuation model is perfectly identified, the disturbance through variable is estimated by the observer as

$$\hat{i}^{dis} = \frac{g_{dis}}{s + g_{dis}} i^{dis}. \quad (2.32)$$

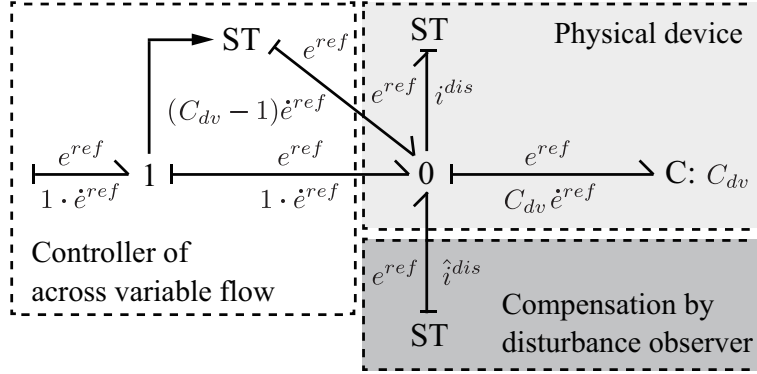


Fig. 2-6: Bond graph of robust control of AVF.

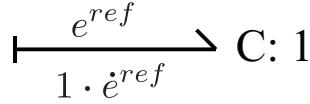


Fig. 2-7: Approximated bond diagram of perfect AVF control.

The low-pass filter is for reducing the noise amplification by differentiating the response  $e^{res}$ . Note that even when there exist identification errors, the observer estimates those as one of the disturbance terms and compensation is possible. By adding the  $e^{cmp}$  or  $i^{cmp}$  as the compensation, the system enhances its robustness against the disturbance through variable. With the use of the compensation, the transfer function from disturbance through variable to device response becomes as

$$\frac{e^{res}}{i^{dis}} = 1 - \frac{g_{dis}}{s + g_{dis}} = \frac{s}{s + g_{dis}}. \quad (2.33)$$

As shown in (2.33), the disturbance  $i^{dis}$  can be suppressed by high-pass filter.

The AVF control system can be interpreted from the perspective of power flow by using bond graph. Fig. 2-6 shows the bond graph of AVF control system. In the physical device part, it is shown that a source absorbs power  $e^{ref} i^{dis}$  and it disturbs the power flowing into the capacitive element. From the bond graph, it turns out that the disturbance observer injects almost same amount of power  $e^{ref} \hat{i}^{dis}$ , and it cancels the power absorption. Moreover, the power  $(C_{cvt} - 1) \dot{e}^{ref} e^{ref}$  is applied as the supplement for realizing the response to be  $e^{ref}$ .

The notable feature of the system is that the device acts for controller as if it had unit value of single capacitive element, as shown in Fig. 2-7. The normalization realized by the internal power injection is beneficial for control system in a sense that the controlled plant is unified to be single  $1/s$  in Laplace domain. From this perspective, this dissertation employs the system as a unit for the bilateral control.

## 2.5 Case of Thermodynamic Systems

In thermodynamic systems, the across and through variables correspond to temperature and entropy flow. However, the entropy flow has difficulty in actual treatment and heat flow is generally taken as an alternative. The graph with the use of the temperature and heat flow is called as pseudo bond graph. In this section, difference between the uses of entropy flow and heat flow is discussed.

The entropy flow is defined as follows

$$\begin{aligned}\dot{S}^{res} &= \frac{1}{T_{dv}} \frac{d'Q_{dv}}{dt} \\ &= \frac{1}{T_{dv}} \frac{C_{dv}dT_{dv} + p_{dv}dV_{dv}}{dt},\end{aligned}\quad (2.34)$$

where  $S$ ,  $Q$ ,  $p$  and  $V$  denote entropy, quantity of heat, pressure and volume (not voltage here), respectively. Note that “ $'$ ” is added at the right hand side of first line of (2.34), since the  $Q$  is not state quantity actually. Here,  $T_{dv}$  is absolute temperature of device. When solid material is used as thermal device, the change of volume can be neglected; therefore, the multiplication of temperature and entropy flow becomes equal to heat flow ( $\dot{S}^{res}T_{dv} = C_{dv}\frac{dT_{dv}}{dt} = q^{res}$ ).

The integral of (2.34) yields

$$\begin{aligned}S^{res} &= C_{dv} \int_{T_{amb}}^{T_{dv}} \frac{dT}{T} dt = C_{dv} \ln \frac{T_{dv}}{T_{amb}} \\ &\simeq C_{dv} \frac{T_{dv} - T_{amb}}{T_{amb}} = C_{dv} \frac{T^{res}}{T_{amb}},\end{aligned}\quad (2.35)$$

where  $T_{amb}$  denotes ambient temperature which is generally constant and initial value of device temperature. Then,  $T^{res}$  represents the relative temperature from  $T_{amb}$ . For the approximation of natural logarithm, first-order Taylor expansion is utilized [100]. In the same manner, the entropy flow can be approximated as

$$\begin{aligned}\dot{S}^{res} &\simeq \frac{C_{dv}}{T_{amb}} \dot{T}^{res} \\ &= \frac{1}{T_{amb}} q^{res}.\end{aligned}\quad (2.36)$$

From (2.36), supposing that the variation of  $T^{res}$  is small enough, the entropy flow  $\dot{S}^{res}$  is almost proportional to heat flow  $q^{res}$ . Moreover,  $\frac{C_{dv}}{T_{amb}}$  can be comprehended as the equivalent C element in generalized system. The assumption is thought to be valid for the haptic instruments, since the temperature range of the application is relatively small (283 K  $\sim$  323 K or 10 °C  $\sim$  50 °C) among the general thermal

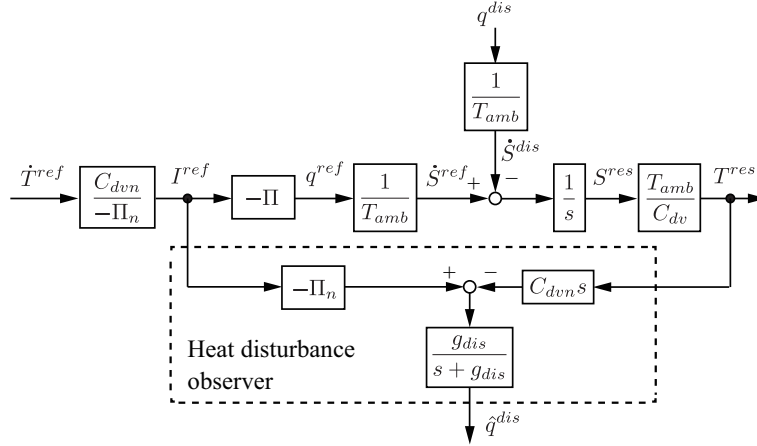


Fig. 2-8: Estimation of disturbance heat flow.

engineering. Therefore, compensating for the disturbance entropy flow and heat flow is almost equivalent. The block diagram of system in the case of thermoelectric device is shown in Fig. 2-8. In Fig. 2-8,  $\Pi$  denotes Peltier coefficient of thermoelectric material. The heat flow disturbance  $q^{dis}$  is proportional to entropy flow disturbance  $\dot{S}^{dis}$ , and compensation for the heat flow disturbance implicitly means the compensation for the  $\dot{S}^{dis}$ . When device temperature change is large, this approximation loses its validity. Nevertheless, general thermal engineering often prefers the control of thermal energy rather than that of entropy, and pseudo bond graph fits for the practical requirements. In experiments, this study also employs the pseudo bond graph.

## 2.6 Generalized Control Conductance and Control Systems

### 2.6.1 Generalized Control Conductance

This study designs the control system based on the AVF controller. For constructing the concrete system and dealing with various kinds of control tasks, considering the characteristics of the systems plays an important role. In this dissertation, generalized control conductance is defined as

$$\kappa = \frac{\partial i}{\partial e}, \quad (2.37)$$

where the variable  $\kappa$  represents the control conductance. Here,  $i$  and  $e$  mean the total through variables flowing into the device and response of the across variable, respectively.

The generalized conductance corresponds to the control stiffness [35] in the field of motion control, and it is capable of indicating the characteristics of generalized control systems. When the across variable

of device is controlled perfectly, deviation of  $e$  is always zero even when the through variables flow into the device from external environment. In this case, the conductance becomes infinite. On the other hand, under the explanations in [35], the infinite deviation of  $e$  is allowed in the ideal control of through variable except the case that the error of through variable is zero. Therefore, ideal control of through variable is equivalent to realizing the system to have zero  $\kappa$ . The conductance becomes between zero and infinite in the generalized impedance control systems, since the relation between across and through variables are given as impedance commands [35].

Generally, the control systems are required to deal with various kinds of tasks. From the perspective of the generalized control conductance, wide range of  $\kappa$  should be covered in controlling the system. From here, control systems of across and through variables with the use of AVF controller are introduced.

### 2.6.2 Control System of Across Variable

The AVF reference in across variable control is calculated as

$$\dot{e}^{ref} = K_{pe}(e^{cmd} - e^{res}), \quad (2.38)$$

where  $e^{cmd}$  and  $K_{pe}$  denote command of across variable and proportional gain, respectively. From Fig. 2-7, following is achieved when AVF control is perfect

$$\dot{e}^{res} = \dot{e}^{ref} = K_{pe}(e^{cmd} - e^{res}). \quad (2.39)$$

Based on (2.39), bond graph of control system can be described as shown in Fig. 2-9. The inversed gain  $1/K_{pe}$  corresponds to dissipation element, and normalized capacitive element is connected. The part of command generation (represented as “SA”) can be handled as the source which injects the power

$$P_{sa} = e^{cmd} \dot{e}^{ref} = K_{pe} e^{cmd} (e^{cmd} - e^{res}). \quad (2.40)$$

In the case that  $K_{pe}$  is set at infinite, the  $P_{sa}$  also becomes infinite. The injection continues until the response reaches to the command, and injecting the infinite power realizes the instantaneous tracking; however, it leads to generation of enormous inrush through variable  $1 \cdot \dot{e}^{ref}$ , and the implementation is actually impossible. The decrease of gain  $K_{pe}$  works to relieve the problem at the cost of tracking performance. This is like introducing the current-limiting resistor in electrical circuit, and the  $K_{pe}$  should be determined considering the trade-off between the tracking performance and increase of reference variable.

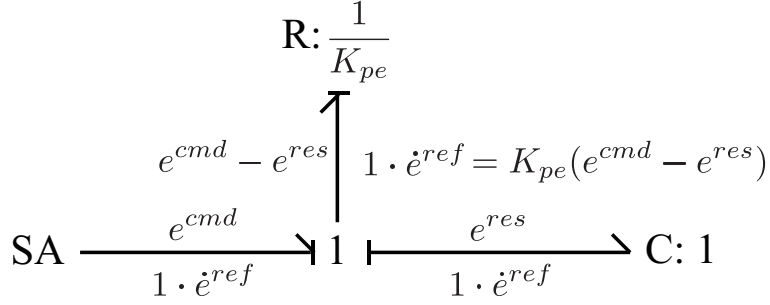


Fig. 2-9: Bond graph of across variable control.

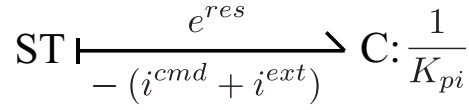


Fig. 2-10: Bond graph of through variable control.

When the AVF control is perfect, disturbance through variable  $i^{dis}$  is totally canceled and it does not appear in the control system. In this case the denominator of (2.37) becomes zero, and the system with infinite control conductance is realized.

### 2.6.3 Control System of Through Variable

In through variable control, the AVF reference is given by

$$\dot{e}^{ref} = -K_{pi}(i^{cmd} + i^{ext}), \quad (2.41)$$

where  $i^{cmd}$  and  $K_{pi}$  denote the command and proportional gain for through variable control, respectively. Assuming that AVF control is perfect, following holds

$$\dot{e}^{res} = \dot{e}^{ref} = -K_{pi}(i^{cmd} + i^{ext}). \quad (2.42)$$

The bond graph of the control system is shown in Fig. 2-10. The perfect AVF control realizes the unification of capacitive element, and it is shown that the addition of the through variable controller again varies the amount of the element. Note that the disturbance terms are suppressed even when (2.42) is employed. Then the external through variable  $i^{ext}$ , which is one of the components of  $i^{dis}$ , flows into the modified capacitive element. Here,  $i^{cmd}$  is an offset for this flow injection.

The infinite  $K_{pi}$  realizes the zero amount of the equivalent capacitance. When  $i^{cmd} + i^{ext} \neq 0$ , the response of across variable  $e^{res}$  becomes infinite in this case. Since the power injection can be calculated

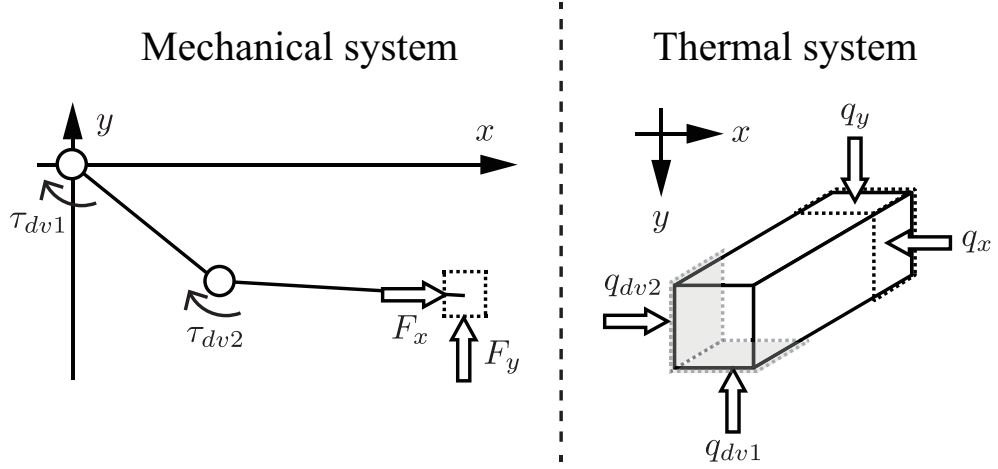


Fig. 2-11: Examples of multi-degree-of-freedom system.

as below, and the system keeps the injection of infinite power until the error of through variables reaches to zero.

$$P_{st} = -e^{res}(i^{cmd} + i^{ext}) \quad (2.43)$$

On this point, the system with infinite  $K_{pi}$  realizes the zero value of control conductance. Of course, the gain should have moderate value in actual implementation; however, the control conductance can be reduced enough by setting the  $K_{pi}$  at high value.

From the explanations above, it is able to say that the AVF control that realizes  $\dot{e}^{ref} = \dot{e}^{res}$  with the suppression of disturbance factors plays an important role for covering the wide range of control conductances. The constructed systems become the fundamental unit for treating the various kinds of control tasks, including the bilateral reproduction of power interaction.

## 2.7 Control of Multi-Degree-of-Freedom System

This dissertation only treats the one dimensional physical phenomena, and use of the single-degree-of-freedom system is focused. In this section, the case of controlling multi-degree-of-freedom system is briefly introduced. Fig. 2-11 shows the example of multi-degree-of-freedom system. Here, multiple actuators and devices are utilized in the system, and these input  $\tau_{dv1}$ ,  $\tau_{dv2}$ ,  $q_{dv1}$  and  $q_{dv2}$  to the system. By increasing the number of actuators and devices, the control of multiple axes becomes possible; for example, in Fig. 2-11, lateral and vertical motions and thermal states can be controlled. In the control

of robotic manipulator, Jacobian matrix that relates the angles of the motors and velocities of the end effector is generally utilized. As well as this, the model of relationship between the input of thermal device and thermal states of the end part of the system should be derived in the multi-degree-of-freedom thermal system.

In controlling the multi-degree-of-freedom system, the inversed model can be utilized to calculate the reference for each actuator or device, like the transformation of the reference in workspace into that in motor space using inversed Jacobian matrix. For deriving the heat transfer model of thermal system, analyses on the multi-dimensional distributed parameter system or use of the thermal network method [101] should be considered. Though the modeling becomes complex, the AVF-based control plays an important role also in the case of controlling multi-degree-of-freedom system, in a sense that the accurate reproduction of the applied references is imperative for the performance enhancement of the multi-degree-of-freedom control.

## 2.8 Experiments on Across Variable Control

From here, some experimental examples are shown. Firstly the control of across variable is experimented in this section, and then the experiments on through variable control are conducted in next section. The discussions so far were conducted in generalized way. On the other hand, mechanical and thermal experiments are demonstrated as the concrete examples in the experiments.

### 2.8.1 Overview of Experiments (Across Variable Control)

In experiments, control law shown in (2.38) is used. Then, the gains were set at 2.0, 3.0 and 4.0 for mechanical system and at 0.1, 0.2 and 0.5 for thermal system, respectively. When the AVF control is perfect, the transfer function from command to response is derived from From (2.39) as

$$\frac{e^{res}}{e^{cmd}} = \frac{1}{\frac{1}{K_{pe}}s + 1}. \quad (2.44)$$

This is a general first order transfer function, and  $1/K_{pe}$  corresponds to the time coefficient; when  $e^{cmd}$  is set to be constant, the response reaches to 63.2 % of the command at the time  $1/K_{pe}$  s. Therefore, the performance of the constructed system can be checked using the constant.

In mechanical system, the across variable and its flow in mechanical system correspond to velocity and acceleration, respectively. On the other hand, those for thermal system can be handled as temperature



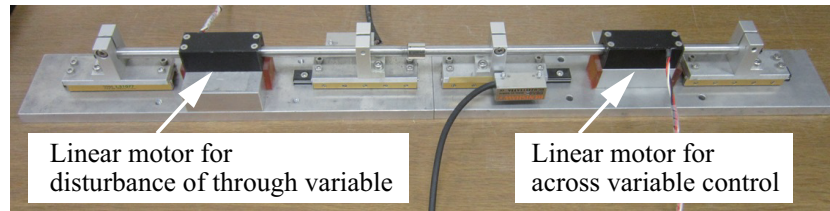


Fig. 2-12: Experimental setup of across variable control (mechanical system).

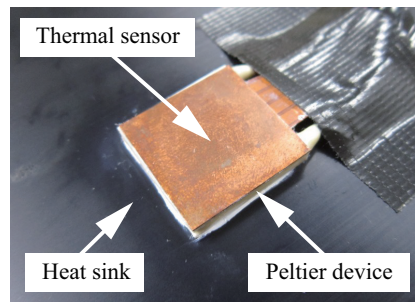


Fig. 2-13: Experimental setup of across variable control (thermal system).

and its varying rate. Therefore, it is able to say that the experiment for mechanical system is a velocity control with acceleration controller, whereas that for thermal system internally controls changing rate of temperature for temperature control. Experimental setups for mechanical and thermal systems are shown in Figs. 2-12 and 2-13, respectively. The setup shown in Fig. 2-12 consists of two linear motors; one is for across variable control and the other one is used to generate disturbance through variable. In disturbance motor, constant current (0.01 A) is applied to generate external force (through variable in mechanical system). In the experiments, linear motors provided by GMC hillstone corp. (model number: S080T, rated force: 2.7 N, rated current: 0.84 A) are utilized. As for the velocity response that corresponds to across variable, differentiation of position response obtained by encoder is conducted. In thermal system, Peltier device that can facilitate the heat flow is employed as the thermal device. On the device, thermal sensor that incorporates heat flow sensor and thermocouple is mounted. Then, the information on temperature obtained by the sensor is used for feedback control. The Peltier device and heat flow sensor used in the experiments are from Z-MAX corp. (model number: FPH 1-7104NC, max current: 3.9 A, max cooling capacity: 18.7 W) and CAPTEC Enterprise (model number: HF-20, size:  $20 \times 20 \times 0.4$  mm, nominal sensitivity:  $2.0 \mu\text{V}/\text{W}/\text{m}^2$ ), respectively. Since the disturbance heat flow is naturally generated by the temperature gradient at interior of the device, thermal device for generating the disturbance is not used for the thermal control.

Table 2.2: Parameter values for experiments (mechanical system).

Variables	Value	Unit
Nominal mass of motor, $M_n$	0.23	kg
Nominal torque coefficient, $K_{tn}$	3.33	N/A
Cut-off frequency of DOB, $g_{dis}$	1000.0	rad/s
Cut-off frequency of pseudo derivative, $g_{pd}$	1000.0	rad/s

Table 2.3: Parameter values for experiments (thermal system).

Variables	Value	Unit
Nominal capacitance of device, $C_{dvn}$	2.0	J/K
Nominal Seebeck coefficient, $\alpha_{sn}$	0.03	V/K
Cut-off frequency of DOB, $g_{dis}$	2.0	rad/s

Parameter values for each experiment are shown in Tables 2.2 and 2.3, respectively. The nominal mass  $M_n$  and capacitance  $C_n$  correspond to generalized C element. Here, the generation of through variables by the actuator and the device are described as

$$F^{ref} = K_t I^{ref} \quad (2.45)$$

$$q^{ref} = -\Pi I^{ref} = -\alpha_s (T_{amb} + T^{res}) I^{ref}, \quad (2.46)$$

where  $\alpha_s$  denotes Seebeck coefficient of thermoelectric device. The cut-off frequency for AVF control is set as large as possible within the region that does not affect the stable operation.

### 2.8.2 Results of Experiments (Across Variable Control)

The results of across variable control are shown in Figs. 2-14 and 2-15, respectively. For each experiment, command  $e^{cmd}$  was set at  $-0.004$  m/s and  $1.0$  K (relative value to ambient temperature), respectively. Since the response performance of thermal device is slower than that of electrical motor,  $K_{pe}$  and  $g_{dis}$  are set lower in thermal control. However, within the bandwidth in which the AVF control based on disturbance observer is effective, the time constant  $\frac{1}{K_{pe}}$  is well realized in both cases. In this sense, it is able to say that the control of across variable based on robust AVF control is successfully conducted.

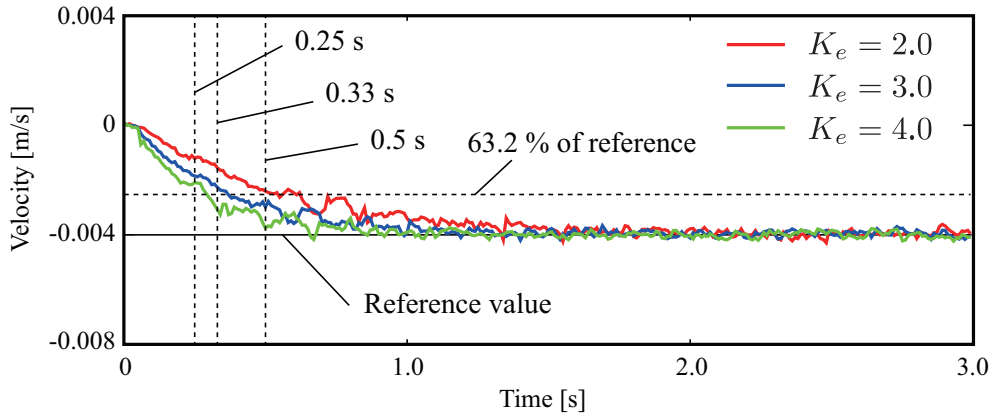


Fig. 2-14: Experimental results of across variable control (mechanical system).

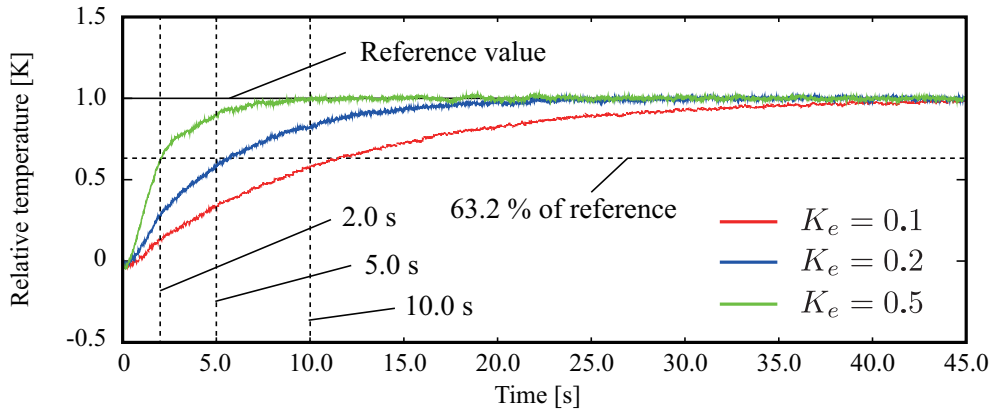


Fig. 2-15: Experimental results of across variable control (thermal system).

Figs. 2-16 and 2-17 are the cases without using disturbance observer. In mechanical case shown in Fig. 2-16,  $K_{pe}$  was set at 200.0 since the linear motor did not move due to the disturbance force and slight frictions; yet, the steady state error exists. Also in the case of thermal control in which the gain was set at  $K_{pe} = 0.5$ , the error occurs due to the disturbance heat flows. According to [63], the threshold for warming of the skin of the thenar eminence is  $0.2\text{ }^{\circ}\text{C}$  (when the changing rate of temperature is  $2.1\text{ }^{\circ}\text{C}$ ). Although the thermal sensation changes according to the conditions such as the changing rate and initial value of temperature, ensuring the resolution of temperature control to be around at least  $0.1\text{ }^{\circ}\text{C}$  is thought to be important for rendering fine thermal sensation. Comparing Figs. 2-15 and 2-17, the temperature difference in steady state is around  $0.5\text{ }^{\circ}\text{C}$ , and the proposed system is thought to be effective for enhancing the rendering quality of thermal sensation.

As for the steady state error, those can be decreased or removed by increasing the controller gain or

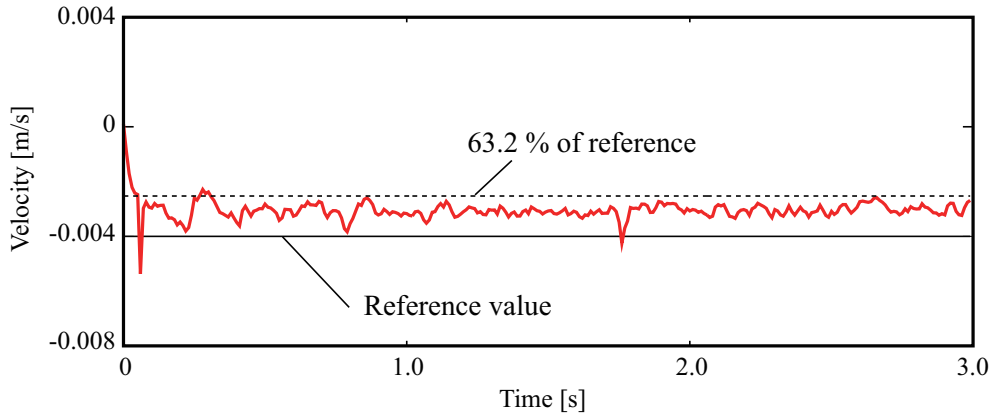


Fig. 2-16: Experimental results of across variable control (mechanical system and without disturbance observer).

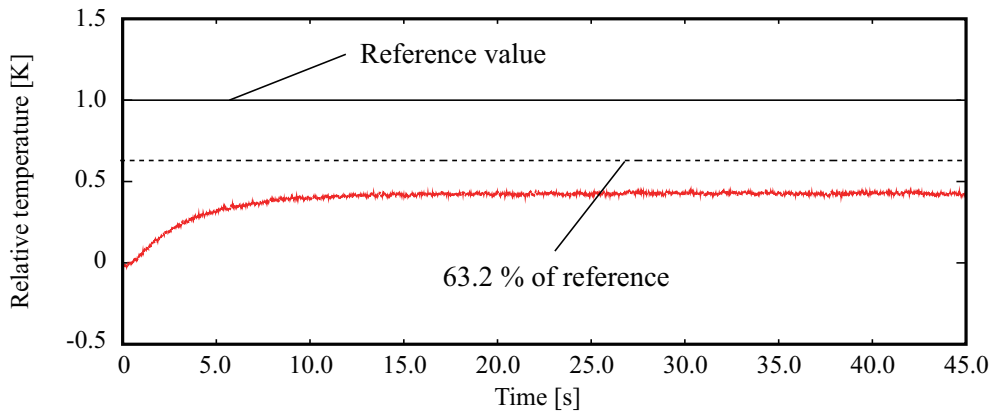


Fig. 2-17: Experimental results of across variable control (thermal system and without disturbance observer).

employing integral controller like PI and PID control, respectively. However, these types of systems basically cannot handle the suppressing the disturbance through variable and designing the transient tracking performance independently; increase of gain or use of integral controller can induce the vibrational transient response for the sake of attenuating the disturbance. The system developed in this chapter can treat the performances independently by the observer of disturbance through variable and controller gain. The comparison between the proposed system and the system with PI controller is conducted in [103]. Since the transient responses are also important for the thermal sensation, the proposed system is thought to have superiority for the thermal rendering.

When the AVF control based on disturbance observer is employed, the systems can realize the tracking

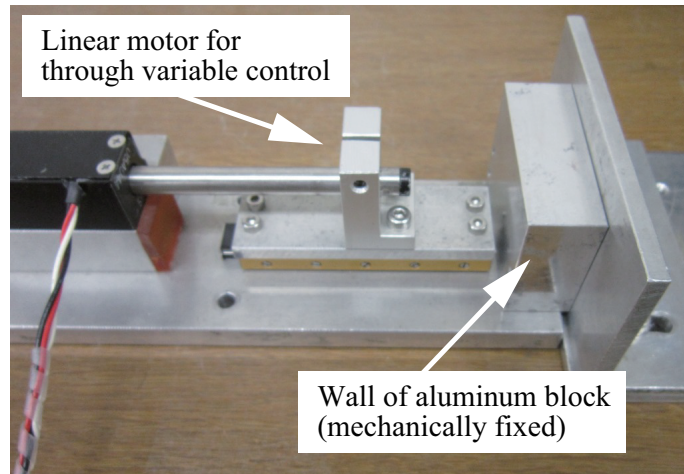


Fig. 2-18: Experimental setup of through variable control (mechanical system).



Fig. 2-19: Aluminum block used for through variable control of thermal system.

without steady state errors. Even though the  $g_{dis}$  cannot be set at infinite in actual cases, the control with  $\kappa = \infty$  is achieved within the bandwidth of observer by compensating for the disturbance through variables.

## 2.9 Experiments on Through Variable Control

### 2.9.1 Overview of Experiments (Through Variable Control)

In experiments on controlling through variables, (2.41) is utilized. In mechanical and thermal systems, the controlled variables correspond to force and heat flow, respectively. Fig. 2-18 shows the setup for force control; mechanically fixed aluminum block is prepared as the external environment. The thermal control employed same setup shown in Fig. 2-13, and cubic aluminum block shown in Fig. 2-19 is put

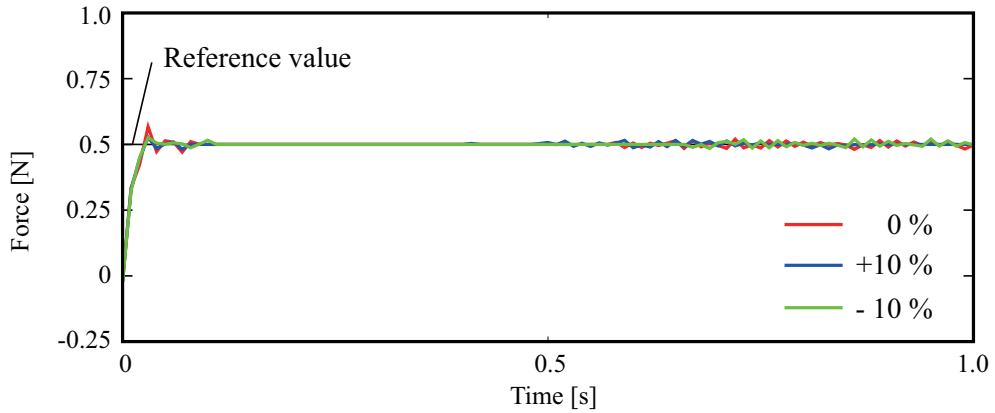


Fig. 2-20: Experimental results of through variable control (mechanical system).

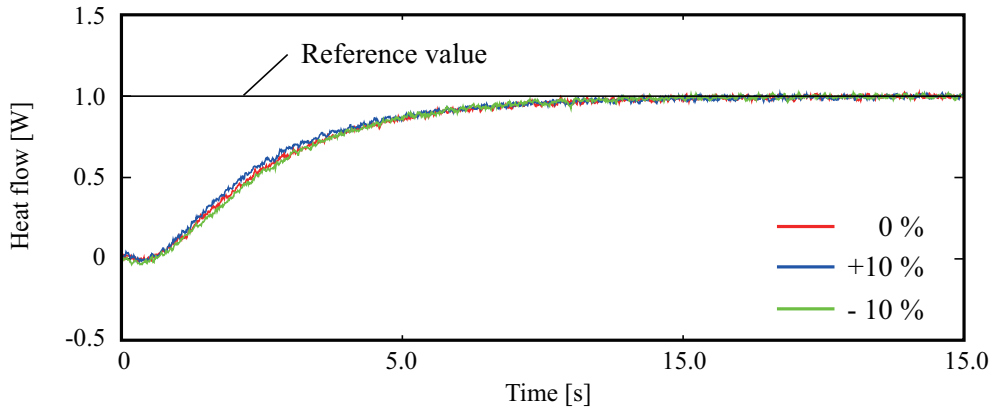


Fig. 2-21: Experimental results of through variable control (thermal system).

on the system so that the interactive heat flow is generated. As for the obtaining information on force and heat flow, reaction force observer and heat inflow observer that modifies the output of heat flow sensor are used [102]. Here, this dissertation assumes that the estimations are perfectly conducted.

The gain  $K_{pi}$  is set at 1.0 and 2.0 for mechanical and thermal experiments, respectively. Then, the nominal capacitive elements ( $M_n$  and  $C_n$ ) are changed  $\pm 10\%$  to generate the modeling errors relatively. In the experiments, the robustness of the AVF control against the errors is tested.

### 2.9.2 Results of Experiments (Through Variable Control)

The experimental results of mechanical and thermal control are shown in Figs. 2-20 and 2-21, respectively. In both cases, the control of through variable is conducted without steady state error. The notable thing here is that the responses change little even when the nominal parameters are varied. This means

that the AVF control based on disturbance observer has robustness against the errors of system modeling.

From the experiments on control of across and through variables, it is shown that the disturbance observer-based AVF control enhances the robustness and realizes normalization of capacitive element. This feature contributes for simplifying the total flow of control design. In this sense, the system becomes strong candidate as a unit for bilateral control systems.

## 2.10 Summary of Chapter 2

In this chapter, the robust control of AVF in generalized physical systems was explained. The control device mainly consists of actuation, input from environment and passive element parts. Then, the operation of the device can be described in unified way by using the across and through variables. The robust control systems were constructed using the observer of disturbance through variables, and the power regarded as the disturbance was compensated by injecting the counter power based on the estimation by the observer. Therefore, the adverse effects of disturbance that cause the undesirable response are able to be suppressed. The perfect control of AVF corresponds to unifying the control device to have single and normalized capacitive element, and this feature is quite beneficial for designing control systems. In this chapter, control conductance was defined. Then, it was used for discussions on control of across and through variables with the use of AVF controller. It was shown that the AVF controller contributes for widening the range of the index values. The constructed systems will be used for the bilateral reproduction of power interaction in next section.



## Chapter 3

# Bilateral Control Based on Across Variable Flow for Reproduction of Physical Power Interaction

---

### 3.1 Introduction

Utilizing the AVF controller introduced in previous chapter as a unit system, bilateral control system is constructed in this chapter. Bilateral control system consists of master and slave systems, and the power exchange by physical interaction is able to be reproduced at the distant place by realizing the synchronization of both master and slave systems. By controlling the difference of across variables and summation of through variables to be zero, the perfect synchronization is realized. The acceleration-based 4ch bilateral control [44], which has already been established in the field of motion control, is the strong candidate for the precise synchronization. One of the most important themes in this dissertation is the expansion of the notion for generalized physical systems. On this point, AVF-based 4ch bilateral control system is constructed. The contents in this chapter are mainly to investigate the validity of the system, and analyses on the system are conducted from various viewpoints, with comparing the other control schemes.

The contents in this chapter are as follows. In Section 3.2, the control objectives of the bilateral control are reviewed. Next, several control systems are constructed in Section 3.3. Through Sections from 3.4 to 3.6, characteristics of the systems are analyzed from the perspective of generalized intermediate impedance, bond graph and pole placements of control systems. The special case on controlling the thermodynamic systems is explained in Section 3.7. Section 3.8 shows several kinds of experiments,

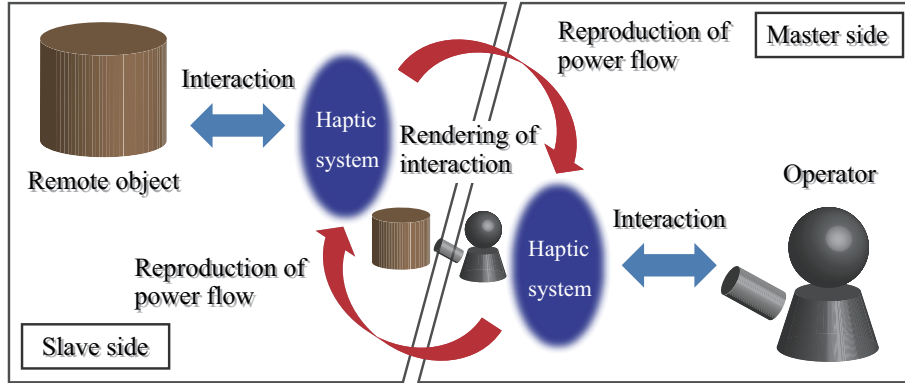


Fig. 3-1: Schematic of bilateral control for reproduction of power interaction.

including mechanical and thermal bilateral control. Finally, this chapter is concluded in Section 3.9.

### 3.2 Reproduction of Generalized Power Interaction

First, the bilateral control for reproducing the power interaction is explained in this section. Fig. 3-1 shows the schematic illustration of the bilateral control. The system consists of master and slave haptic systems, and there exist an operator at master side and remote object at slave side, respectively. The physical interactions are actually done at each system locally. The purpose of developing the bilateral control system is to render the direct contact between the operator and the object, by reproducing the external environments (operator and remote object) of each side at the other side.

The concrete objectives of the control system are shown as

$$e_m - e_s = 0 \quad (3.1)$$

$$i_m^{ext} + i_s^{ext} = 0, \quad (3.2)$$

where the subscripts  $m$  and  $s$  denote master and slave system, and superscript  $ext$  means external value. (3.1) and (3.2) mean that differential mode of across variables and common mode of external through variables should be controlled. For example, in mechanical systems, the negative force should be reproduced while maintaining the velocities of master and slave systems to be same. In the same manner, temperature and entropy flow are controlled in thermal systems. When the above control objectives are fulfilled, following holds

$$P_m = e_m i_m^{ext} = -e_s i_s^{ext} = -P_s. \quad (3.3)$$

Table 3.1: Control objectives for each physical system.

Variables	Mechanical system	Electrical system	Thermal system
Differential mode	Velocity synch.	Voltage synch.	Temperature synch.
Common mode	Action-reaction law	Kirchhoff's current law	Thermal energy conservation

This means that the perfect synchronization of across variables and rendering of external through variables realize the perfect reproduction of power exchange between master and slave systems. Therefore, the physical power injected by the operator is directly transmitted to remote object without any losses, and vice versa.

The control objectives for each system are summarized in Table 3.1. In mechanical system, control of differential mode means trajectory synchronization by velocity control. Then, action-reaction law is artificially realized between remote systems. In thermal systems, temperature and entropy flow are treated to realize thermal energy conservation artificially. Since the multiplication of across and through variables in each system yields the common unit “power,” the (3.1) and (3.2) are valid in bilateral control regardless of the kinds of physical systems.

### 3.3 Generalized Reproduction of Bilateral Power Flow

In this section, using the AVF control system as the unit, several types of bilateral control systems are constructed.

#### 3.3.1 AVF-based 4ch Control System

The block diagram of AVF-based 4ch control system is shown in Fig. 3-2. In Fig. 3-2,  $C_e$  and  $C_f$  are controller for across and through variables, respectively. The system consists of master and slave sides, and through variables ( $i_m^{ext}$  and  $i_s^{ext}$ ) are applied from external environment. In this system, the through variables play the main role for driving the whole system.

The control laws for master and slave systems are calculated as follows:

$$\dot{e}_m^{ref} = C_e(e_s - e_m) - C_i(\hat{i}_m^{ext} + \hat{i}_s^{ext}) \quad (3.4)$$

$$\dot{e}_s^{ref} = C_e(e_m - e_s) - C_i(\hat{i}_m^{ext} + \hat{i}_s^{ext}). \quad (3.5)$$

In (3.4) and (3.5), AVF references are calculated on the basis of information on current state of across and through variables. For obtaining the information on  $i_m^{ext}$  and  $i_s^{ext}$ , both sensors and observer-based

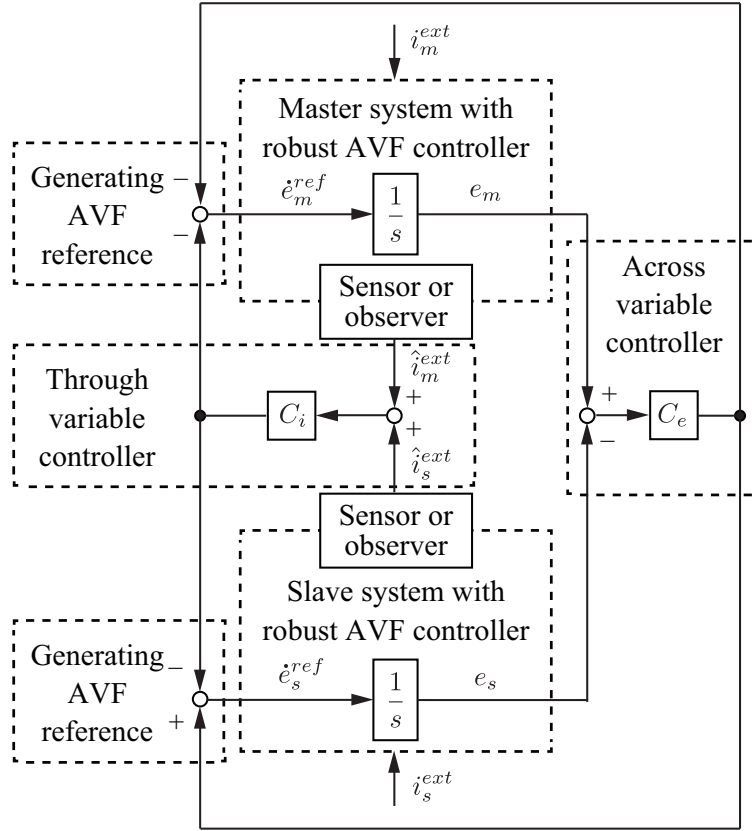


Fig. 3-2: Block diagram of the AVF-based 4ch control system.

techniques can be utilized. As for the latter one, reaction force observer can be employed and it is preferred from the viewpoint of bandwidth for estimation [36]. In thermal control, heat inflow observer is proposed in the same manner. The control laws contain two parts: across variable controller and through variable controller. These controllers work to fulfill the (3.1) and (3.2), and calculated AVF reference is realized by the AVF controller locally. The system shown in Fig. 3-2 is represented in unified manner; therefore, by setting the variables for corresponding ones of each physical system, the bilateral control is able to be conducted. This point is one of the main themes in this dissertation.

### 3.3.2 Comparative Methods

As stated in Chapter 1, there have been various types of bilateral control proposed up to now. In this chapter, three methods are compared with the AVF-based 4ch type: across variable-based type, through variable-based type and reflection-based type.

The across variable-based type, which corresponds to the velocity-based (sometimes position-based

type is employed) bilateral control. The control laws are shown as follows:

$$\dot{e}_m^{ref} = C_e(e_s - e_m) \quad (3.6)$$

$$\dot{e}_s^{ref} = C_e(e_m - e_s). \quad (3.7)$$

The control method only focuses on the synchronization of across variables, and it is realized by substituting  $C_i = 0$  in (3.4) and (3.5).

On the other hand, the through variable-based type, which is the extended form of force-based bilateral control in mechanical system, has the control laws shown below:

$$\dot{e}_m^{ref} = -C_i(\hat{i}_m^{ext} + \hat{i}_s^{ext}) \quad (3.8)$$

$$\dot{e}_s^{ref} = -C_i(\hat{i}_m^{ext} + \hat{i}_s^{ext}). \quad (3.9)$$

This type focuses on the reproduction of external through variables, whereas it neglects the synchronization of across variables of master and slave systems.

The most famous type of bilateral control in mechanical system is force-reflecting scheme [11–16]. This can be generalized using across and through variables as

$$\dot{e}_m^{ref} = -C_i(\hat{i}_m^{ext} + \hat{i}_s^{ext}) \quad (3.10)$$

$$\dot{e}_s^{ref} = C_e(e_m - e_s). \quad (3.11)$$

This control system aims to clarify the roles of control objectives; the master system works to reproduce the through variable, and slave system tracks to the master's across variable. In this sense, this type can be thought to realize the best performance among the comparative systems.

### 3.4 Analyses Based on Generalized Intermediate Impedance

From this section, the characteristics of the control schemes are analyzed from the perspective of generalized intermediate impedance, bond graph and pole placements. According to the analyses, the AVF-based 4ch scheme turns out to have the best performance among the systems.

#### 3.4.1 Hybrid Parameters of Control Systems

In Section 3.4, the systems are compared using the concept of intermediate impedance. As the preliminaries of the comparison, hybrid parameters of respective control systems are derived. The hybrid

parameters [20], whose idea is based on electrical 2-port circuit, are well known in the field of mechanical bilateral control and the generalized form is defined as

$$\begin{bmatrix} i_m^{ext} \\ e_m \end{bmatrix} = \begin{bmatrix} H_{11} & H_{12} \\ H_{21} & H_{22} \end{bmatrix} \begin{bmatrix} e_s \\ -i_s^{ext} \end{bmatrix}. \quad (3.12)$$

The parameters relate the across and through variables of master and slave systems. Therefore, the performance analyses on tracking and rendering can be conducted using the parameters.

Supposing that the information on the external through variable is same as the real value ( $\hat{i}^{ext} = i^{ext}$ ), each parameter of AVF-based 4ch bilateral control is calculated as

$$H_{11} = -\frac{s^2 + 2C_e s}{2C_e C_i + K C_e + C_i s} \quad (3.13)$$

$$H_{12} = \frac{2C_e C_i + C_i s + K s + K C_e}{2C_e C_i + K C_e + C_i s} \quad (3.14)$$

$$H_{21} = \frac{2C_e C_i + C_i s + K s + K C_e}{2C_e C_i + K C_e + C_i s} \quad (3.15)$$

$$H_{22} = -\frac{2K C_i + K^2}{2C_e C_i + K C_e + C_i s}, \quad (3.16)$$

and the parameters of reflection-based type are derived as

$$H_{11} = -\frac{s^2 + C_e s}{C_i(2C_e + K + s)} \quad (3.17)$$

$$H_{12} = \frac{C_e C_i + K s}{C_i(2C_e + K + s)} \quad (3.18)$$

$$H_{21} = \frac{C_e C_i + C_i s + K s + K C_e}{C_i(2C_e + K + s)} \quad (3.19)$$

$$H_{22} = -\frac{K C_i + K^2}{C_i(2C_e + K + s)}, \quad (3.20)$$

where  $K$  shown below represents the imperfectness of disturbance compensation:

$$K = \frac{s}{s + g_{dob}} \frac{1}{C_{dv}}. \quad (3.21)$$

The parameters of across variable-based and through variable-based types can be derived by substituting  $C_i = 0$  and  $C_e = 0$  to those of the 4ch type, respectively.

### 3.4.2 Symmetric Property and Hybrid Parameters

Supposing that the remote material at the slave system can be described by generalized impedance  $Z_{env}$  and  $e_s = -Z_{env} i_s^{ext}$  holds in Laplace domain, following is derived

$$\frac{e_m}{i_m^{ext}} = \frac{H_{21} Z_{env} + H_{22}}{H_{11} Z_{env} + H_{12}}. \quad (3.22)$$

This represents the rendered impedance at the master side. When  $e_m/i_m^{ext} = Z_{env}$ , the operator at master side can feel the physical property of remote environment perfectly. In the same manner, supposing  $e_m = -Z_{env}i_m^{ext}$  yields

$$\frac{e_s}{i_s^{ext}} = \frac{H_{12}Z_{env} + H_{22}}{H_{11}Z_{env} + H_{21}}. \quad (3.23)$$

This transfer function means the rendered impedance when the operator manipulates slave system and remote material is located at the master system. The across or through variable-based type, as well as AVF-based 4ch type, has same control laws in master and slave systems. In this sense the systems can be said to have ‘‘symmetric property,’’ thus (3.22) and (3.23) become same. Therefore, the system with the property should fulfill following

$$H_{12} = H_{21}. \quad (3.24)$$

The inversed hybrid parameters are derived as

$$\begin{bmatrix} i_s^{ext} \\ e_s \end{bmatrix} = \frac{1}{\Delta} \begin{bmatrix} H_{11} & H_{21} \\ H_{12} & H_{22} \end{bmatrix} \begin{bmatrix} e_m \\ -i_m^{ext} \end{bmatrix}, \quad (3.25)$$

where

$$\Delta = H_{12}H_{21} - H_{11}H_{22}. \quad (3.26)$$

The matrix represents the transferring performance when the operator manipulates slave system. As well as the discussions by (3.22) and (3.23), the system with symmetric property should yield same parameters with those shown in (3.12). For this, following should be fulfilled in addition to (3.24).

$$\Delta = 1 \quad (3.27)$$

Summarizing the above, followings are necessary condition for symmetric bilateral control:

- The parameters  $H_{12}$  and  $H_{21}$  are identical.
- $H_{12}H_{21} - H_{11}H_{22} = 1$  holds.

Observing the parameters of AVF-based 4ch type and reflection-based type, the former fulfills the requirement of symmetric property while the latter does not. The difference is natural since the reflection-type does not have the same control laws for master and slave systems: the across and through variables are controlled at the operator and the remote side, respectively.

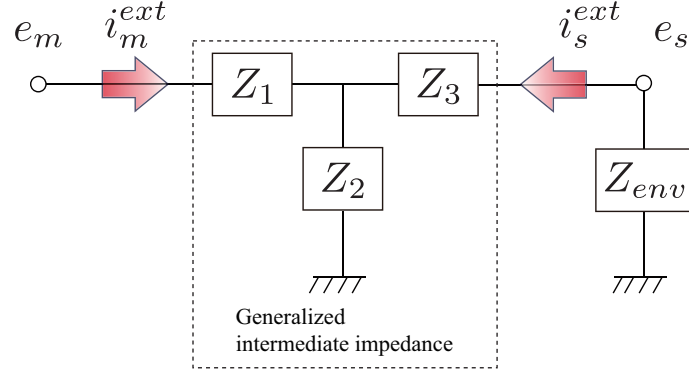


Fig. 3-3: Generalized intermediate impedance in power transmission.

### 3.4.3 Generalized Intermediate Impedance

Using the properties above, the generalized intermediate impedance of the bilateral control is discussed. The bilateral control system can be comprehended as that the total system plays a role of intermediation between operator and remote environment; transferring the power from one system to the other one. Based on this, the generalized intermediate impedance is defined as shown in Fig. 3-3. From the perspective of the impedances, the bilateral control system can be said to have good performance when the leakage and loss in power transmission are small.

The synthetic impedance for master side is derived as

$$\frac{e_m}{i_m^{ext}} = \frac{(Z_1 + Z_2)Z_{env} + (Z_1Z_2 + Z_1Z_3 + Z_2Z_3)}{Z_{env} + (Z_2 + Z_3)} \quad (3.28)$$

$$= \frac{H_{11}(Z_1 + Z_2)Z_{env} + H_{11}(Z_1Z_2 + Z_1Z_3 + Z_2Z_3)}{H_{11}Z_{env} + H_{11}(Z_2 + Z_3)}. \quad (3.29)$$

Comparing with (3.22), the relationship between impedances and hybrid parameters are derived as

$$H_{11}(Z_2 + Z_3) = H_{12} \quad (3.30)$$

$$H_{11}(Z_1 + Z_2) = H_{21} \quad (3.31)$$

$$\frac{H_{12}H_{21}}{H_{11}} - H_{11}Z_2^2 = H_{22}. \quad (3.32)$$

From the last relation, the impedance  $Z_2$  is derived as

$$Z_2 = \frac{1}{H_{11}}\sqrt{\Delta}. \quad (3.33)$$

This means that the impedance  $Z_2$  becomes the element that involves fractional calculus unless the root of  $\Delta$  is solved by the polynomial expression. For example, the reflection-based type with perfect AVF



Table 3.2: Parameter values for plotting gain diagrams.

Variables	Value
$C_e$	100.0~500.0 (changed by 100.0)
$C_i$	1.0~5.0 (changed by 1.0)
$C_{dv}$	0.3
$g_{dob}$	100.0 rad/s

control ( $K = 0$ ) produces

$$Z_2 = -\frac{C_i}{s} \sqrt{\frac{C_e}{s + C_e}}. \quad (3.34)$$

Transfer function with fractional order can often be obtained in modeling the distributed parameter systems. As the total expression of rendered impedance, the transfer function can be described by polynomial expression (like (3.12)). However, from the viewpoint of generalized intermediate impedance, there exists the possibility that each element involves complex phenomena. It is difficult to determine the phenomena actually degrade the stability performance; however, at least it is able to say that the asymmetric bilateral control system can involve complex dynamics in intermediating the power transmission.

When the bilateral control system has symmetric property,  $\sqrt{\Delta} = 1$  and polynomial expression of  $Z_2$  can be obtained. In this case, the impedances are derived as

$$Z_1 = Z_3 = \frac{H_{22}}{1 + H_{12}} \quad (3.35)$$

$$Z_2 = \frac{1}{H_{11}}. \quad (3.36)$$

Note that  $Z_1 = Z_3$  holds since the system is symmetric.

The ideal objective of bilateral control is to reproduce the power interaction between operator and remote environment without any losses and leakages. From this perspective, the impedances should ideally be  $Z_1 = Z_3 = 0$  and  $Z_2 = \infty$ , respectively. Figs. 3-4, 3-5, 3-6 and 3-7 are analytical frequency responses of each control schemes. For plotting the diagrams, parameters shown in Table 3.2 are used. The diagram of reflection-based type is omitted since the system has fractional order term and has difficulty in plotting.

From Figs. 3-4 and 3-5, DC gain is observed in  $Z_2$  of across variable-based type. This means that the system causes leakage of power transmission even when the bilateral control is in steady state. When the gain  $C_e$  is increased, the characteristics of  $Z_1$  are improved; however, the  $Z_2$  changes little. It is thought that the change of  $C_e$  cannot improve the  $Z_2$ .

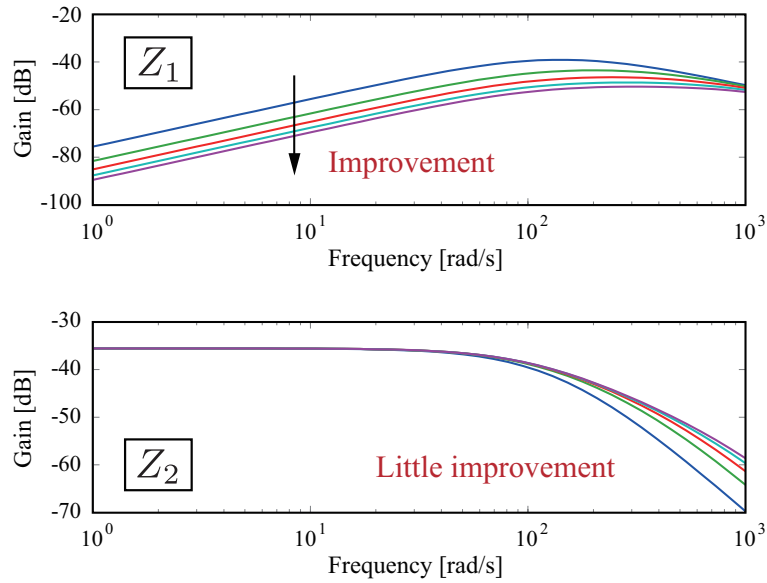


Fig. 3-4: Impedances in the case of across variable-based bilateral control.

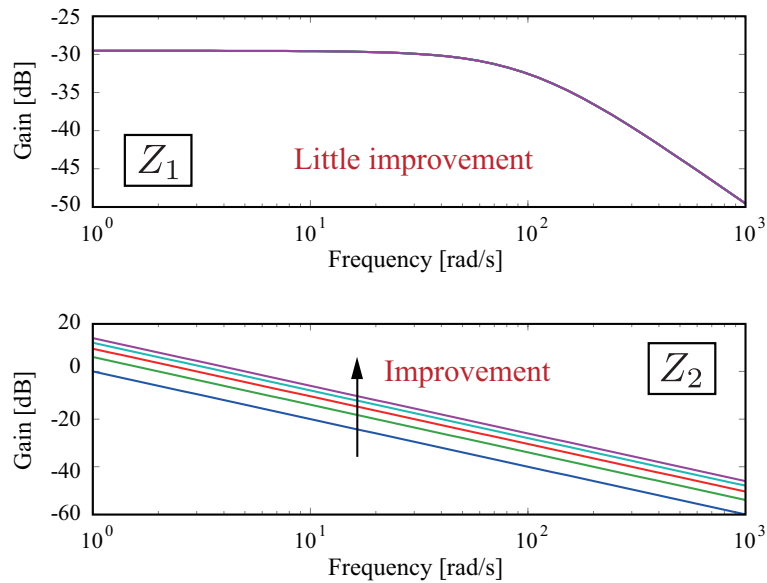


Fig. 3-5: Impedances in the case of through variable-based bilateral control.

On the other hand,  $Z_1$  has DC gain in the case of through variable-based control. In this case, power losses occur even when the system is in steady state. The change of  $C_i$  contributes for improvement of  $Z_2$ . However, the DC gain cannot be eliminated by the controller.

Figs. 3-6 and 3-7 show the gain diagrams of the AVF-based 4ch bilateral control. In this system, the

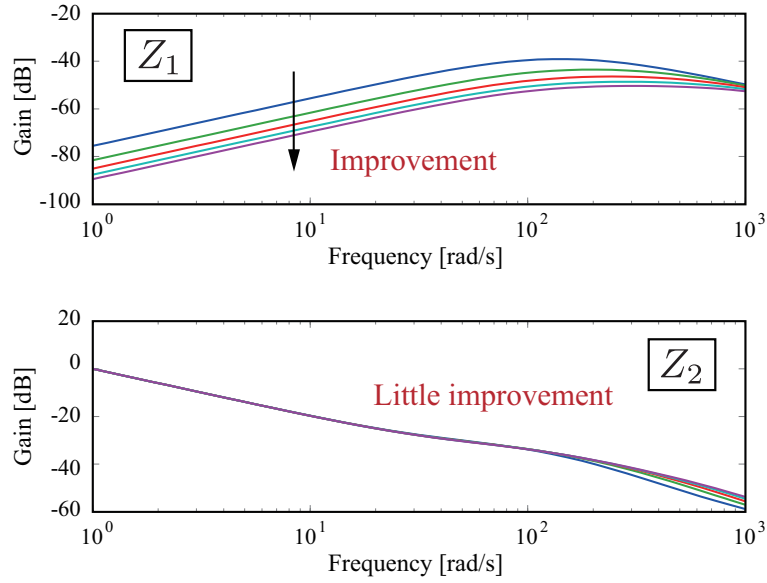


Fig. 3-6: Impedances in the case of AVF-based bilateral control ( $C_e$  is changed).

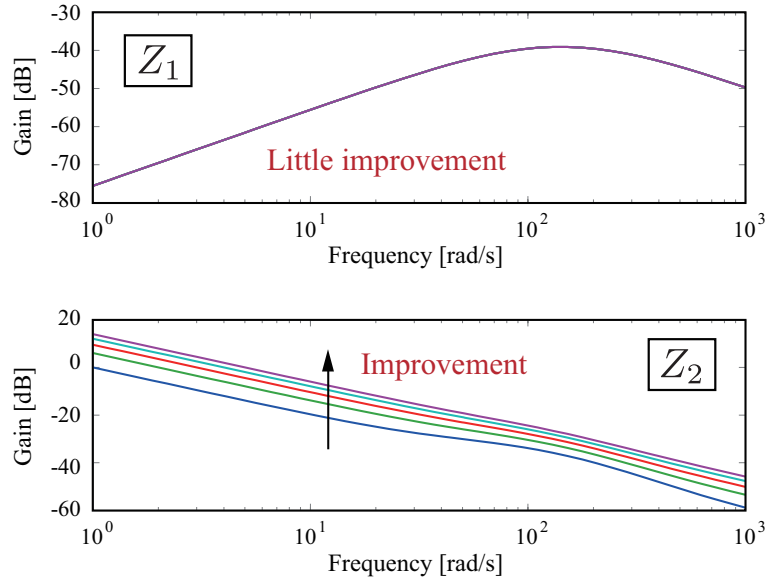


Fig. 3-7: Impedances in the case of AVF-based bilateral control ( $C_i$  is changed).

DC components of  $Z_1$  and  $Z_2$  are  $-\infty$  dB and  $\infty$  dB, respectively. Therefore, the system can transfer the power perfectly at least in the steady state. Moreover, the characteristics of  $Z_1$  and  $Z_2$  can be improved by increasing the gains  $C_e$  and  $C_i$ , respectively. Compared with across and through variable-based type, the AVF-based 4ch control can realize the better performance.

### 3.5 Analyses Based on Bond Graphs

The discussions so far indicate the necessity of both controllers of across and through variables. On this point, not only the AVF-based 4ch type but also the reflection-based type is effective for rendering the remote environment. Since the evaluation using the generalized intermediate impedances is difficult for the reflection-based type, the analyses using bond graph are conducted in this section.

#### 3.5.1 Lyapunov-based Analyses Using Bond Graph

The arrows in bond graph represent the power flow in the system. Therefore the Lyapunov-based analyses, that consider the dissipation of energy, can easily be conducted by using the graph. In [90], Lyapunov function  $V$  is established as

$$V = k_1 E_1 + k_2 E_2 \cdots k_n E_n, \quad (3.37)$$

where  $k$  and  $E$  denote constant and energy stored in element, respectively.  $n$  is a total number of storage (C and I) elements, and (3.37) represents the summation of stored energies. Lyapunov-based stability analyses focuses on the definiteness of  $\dot{V}$ ; when it is negative definite, asymptotic stability of total system is ensured. The derivative of the Lyapunov function yields

$$\begin{aligned} \dot{V} &= \frac{\partial V}{\partial E_1} \frac{dE_1}{dt} + \frac{\partial V}{\partial E_2} \frac{dE_2}{dt} + \cdots + \frac{\partial V}{\partial E_n} \frac{dE_n}{dt} \\ &= \sum_{i=1}^n k_i P_i, \end{aligned} \quad (3.38)$$

where  $P_i$  denotes power flowing into each element. Therefore, the Lyapunov stability can be analyzed by checking whether the summation of power flows becomes negative definite or not. In [90], the external inputs (power sources in bond graph) which don't correspond with control variables are omitted, and internal stability is analyzed by checking the definiteness of (3.38).

#### 3.5.2 Bond Graph of AVF-based 4ch Bilateral Control

The bond graph of AVF-based 4ch bilateral control is shown in Fig. 3-8. Here, AVF control is assumed to be perfect and relationship between  $i_s^{ext}$  and  $e_s$  is defined as follows

$$i_s^{ext} = K_{env} \frac{1}{s} e_s + D_{env} e_s. \quad (3.39)$$

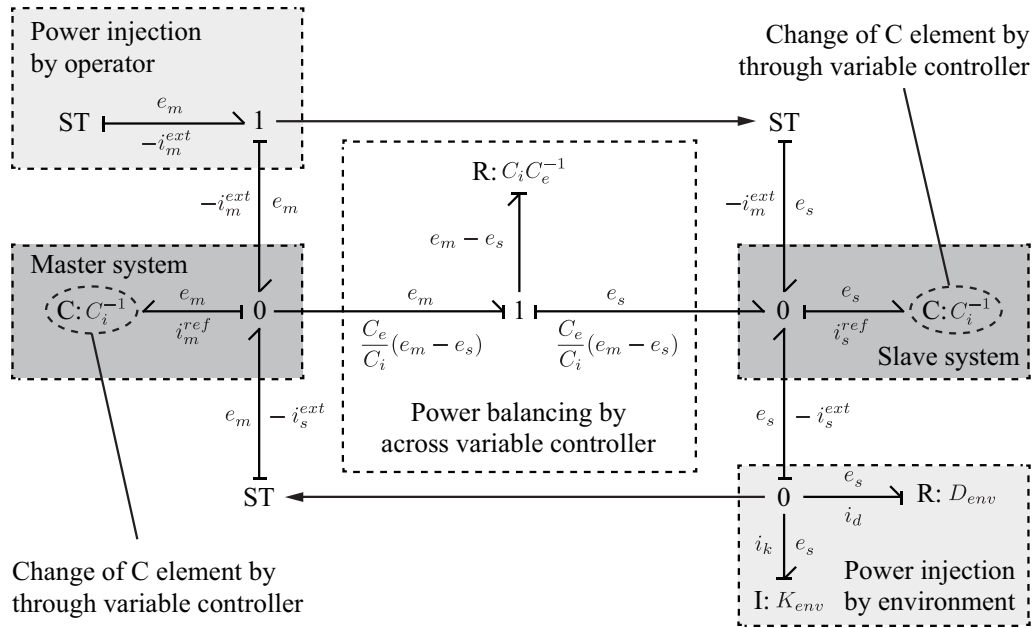


Fig. 3-8: Bond graph of AVF-based 4ch control.

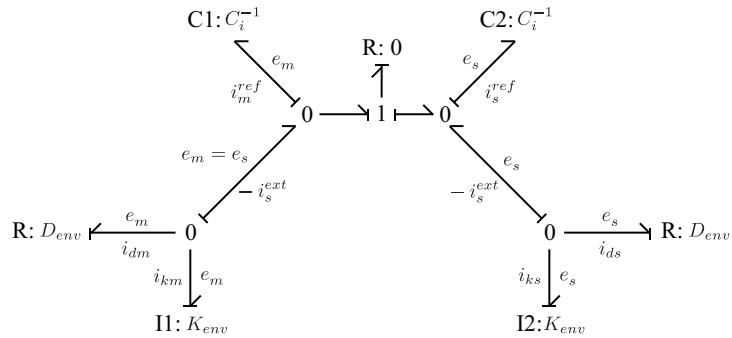


Fig. 3-9: Approximated bond graph for stability analysis of AVF-based 4ch control.

In the graph, there exist several parts: power injection from operator and external remote environment, master and slave systems. The controller of through variables plays the role of power injections. By the injections, the master and slave systems will have same amount of physical power and changes those across variable in the same way. However in actual, the imperfectness of the control leads to the error of power storing. The controller of across variable is used for balancing the power difference; the path for power transmission is prepared. By the simultaneous use of controllers of across and through variables, the power synchronization of master and slave systems are maintained.

The R element in across variable control is described as  $C_i/C_e$ . Therefore, when the gain is increased,

the element approaches to zero and the power flow can be neglected. As a result,  $e_m = e_s$  is realized and the bond graph can be approximated. With omitting the external power source for checking the internal stability [90], the bond graph can be approximated to be the one shown in Fig. 3-9. In the graph, Lyapunov function is defined as follows

$$V = E_{C1} + E_{C2} + E_{I1} + E_{I2}, \quad (3.40)$$

where the subscripts of  $E$  denote each storing element. The derivative of (3.40) becomes

$$\begin{aligned} \dot{V} &= P_{C1} + P_{C2} + P_{I1} + P_{I2} \\ &= e_m \dot{i}_m^{ref} + e_s \dot{i}_s^{ref} + e_m \dot{i}_{km} + e_s \dot{i}_{ks} \\ &= -2e_s \dot{i}_s^{ext} + e_m \dot{i}_{km} + e_s \dot{i}_{ks} \\ &= -e_m \dot{i}_{dm} - e_s \dot{i}_{ds} \\ &= -D_{env} (\dot{i}_{dm}^2 + \dot{i}_{ds}^2) \leq 0. \end{aligned} \quad (3.41)$$

Since the semi-definiteness of  $\dot{V}$  is proved, the asymptotic stability is ensured.

### 3.5.3 Bond Graph of Reflection-based Bilateral Control

The bond graph of reflection-based bilateral control is shown in Fig. 3-10. The difference between the graph of the system and that of the AVF-based 4ch control is power sources of across variables (represented as SA). When the across variable controllers are implemented at both master and slave systems, it is able to be comprehended as the path for power balancing in bond graph. On the other hand, reflection-based type has across variable controller only at the slave side; equivalently, source of across variable injects the power so that the stored energy becomes same as that of master side. Moreover, the through variable controller at the slave side is eliminated, and this causes the rejection of power flowing from remote environment at the slave system.

The approximated bond graph for stability analyses is shown in Fig. 3-11. Different from the case of AVF-based 4ch control system, the power sources stay remained since these are not external inputs. In this case, the Lyapunov function is defined as

$$V = E_{C1} + E_{C2} + E_{I1} + E_{I2}, \quad (3.42)$$

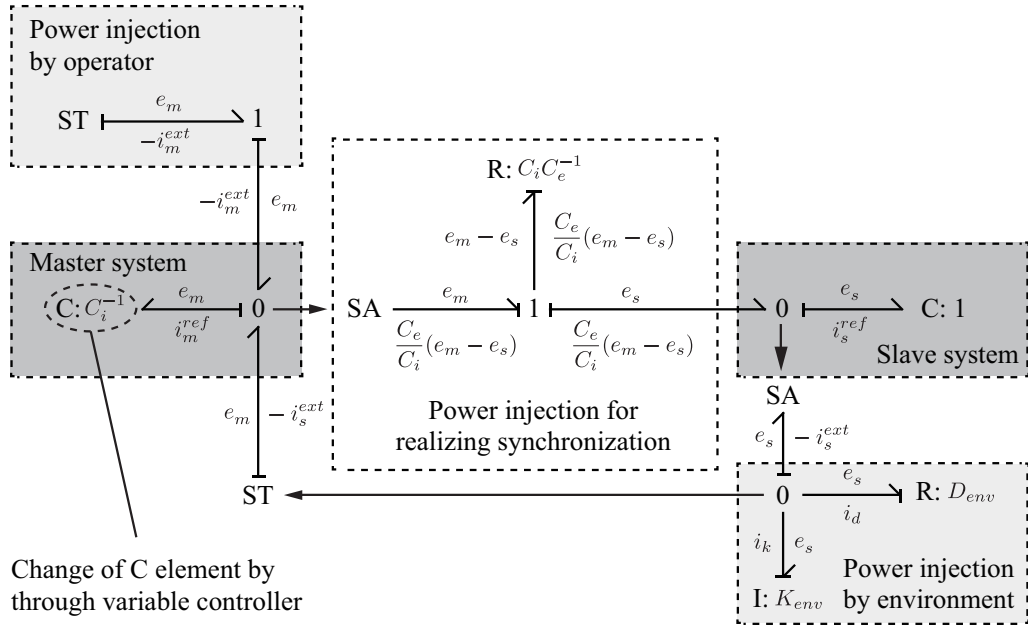


Fig. 3-10: Bond graph of reflection-based control.

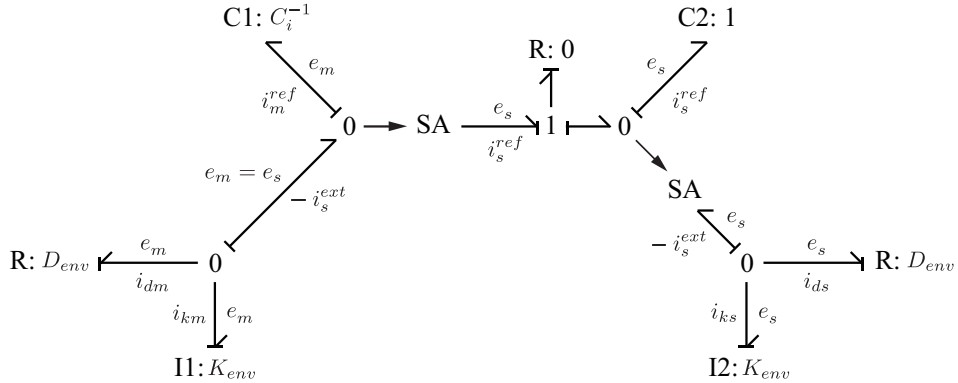


Fig. 3-11: Approximated bond graph for stability analysis of reflection-based control.

and its derivative becomes

$$\begin{aligned}
 \dot{V} &= P_{C1} + P_{C2} + P_{I1} + P_{I2} \\
 &= e_m i_m^{ref} + e_s i_s^{ref} + e_m i_{km} + e_s i_{ks} \\
 &= e_m i_s^{ext} + e_s i_s^{ref} + e_m i_{km} + e_s i_s^{ext} - e_s i_{ds} \\
 &= -e_m i_{dm} + e_s i_s^{ref} + e_s i_s^{ext} - e_s i_{ds} \\
 &= -D_{env}(i_{dm}^2 + i_{ds}^2) + e_s i_s^{ref} + e_s i_s^{ext}. \tag{3.43}
 \end{aligned}$$

Table 3.3: Parameter values for plotting pole movements.

Variables	Value
$C_e$	100.0
$C_i$	1.0
$C_{dv}$	0.3
$g_{dob}$	1000.0 rad/s
$K_{env}$	2000.0~20000.0 (changed at 2000.0)
$D_{env}$	100.0

In reflection-based bilateral control, the definiteness of the  $\dot{V}$  cannot be confirmed. Therefore, the asymptotic stability is not ensured; the system may be unstable when the terms  $e_s i_s^{ref} + e_s i_s^{ext}$  are large and  $\dot{V} > 0$  occurs.

From the viewpoint of Lyapunov stability, it is able to say that the AVF-based 4ch bilateral control has advantage over the reflection-based type.

### 3.6 Analyses Based on Pole Placements

Another approach for checking the stability is to analyze the pole placements of the system. (3.22) represents the transfer function of rendered impedance. Poles are the roots of denominator polynomial, and the transfer function is stable when all poles have negative real parts. Therefore, the stability can be checked whether the poles are located at the left half side of complex plane or not.

Fig. 3-12 shows the pole movements with different environmental impedances. For plotting the graph, parameter values shown in Table 3.3 are used. Then, environmental impedances are set to be same as (3.39). As the value of impedance  $K_{env}$  gets higher, the imaginary part of poles is increased. However, the real part of the poles keeps to be negative. From Fig. 3-12, it is able to say that the system keeps its stability against various values of impedances.

On the other hand, as shown in Fig. 3-13, the reflection-based bilateral control becomes unstable as the impedance is increased. For the lower impedance, the system can stably work to render the remote environment; the operation of the system will be limited. As well as the Lyapunov-based analyses, the AVF-based bilateral control is thought to have more stability than reflection-based scheme from the viewpoint of pole movements.



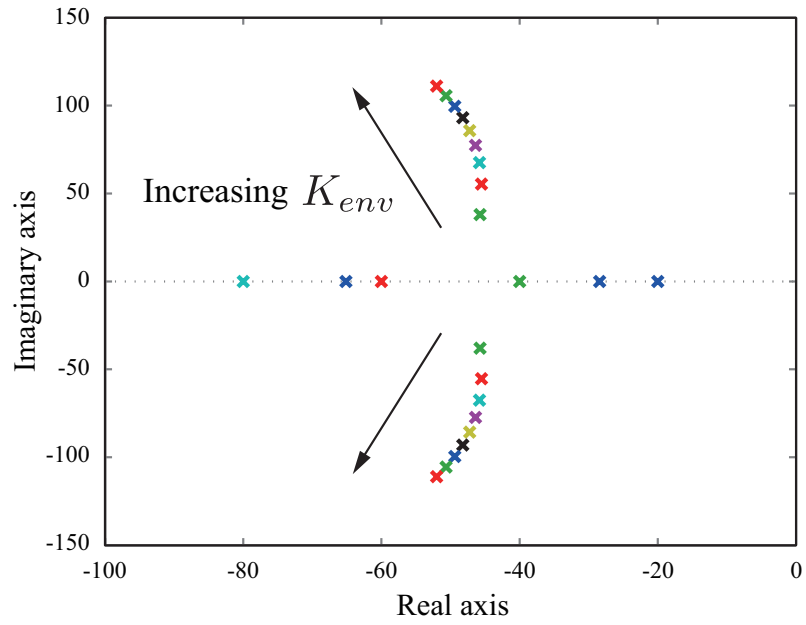


Fig. 3-12: Pole movements of AVF-based 4ch control system.

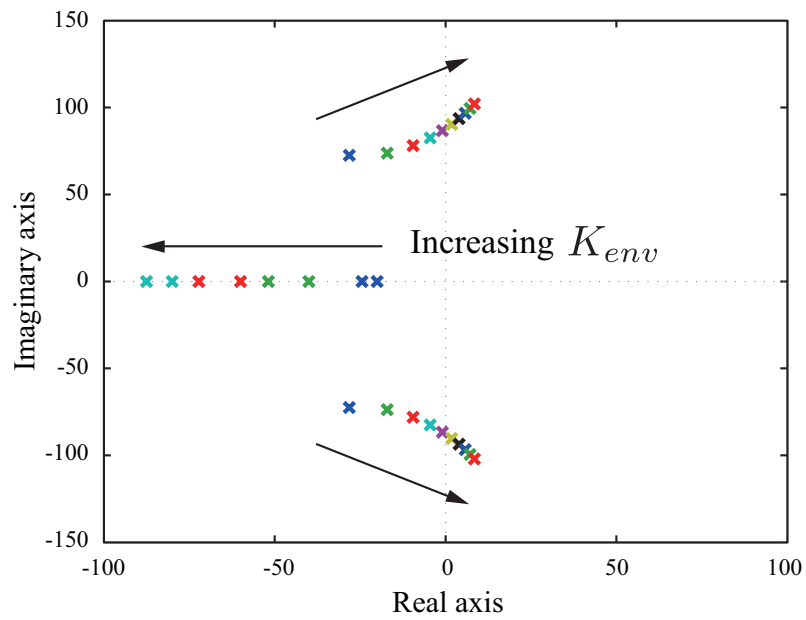


Fig. 3-13: Pole movements of reflection-based control system.

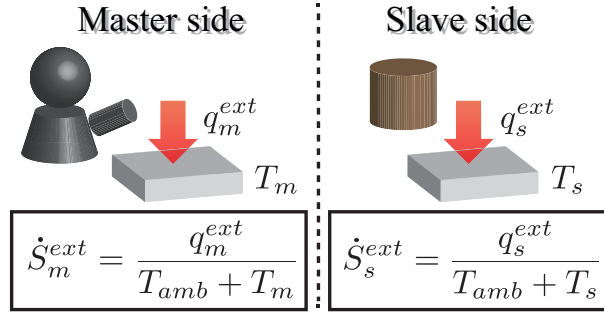


Fig. 3-14: Entropy flow in thermal bilateral control.

### 3.7 Common-Mode Control of Entropy Flows

In the case of controlling thermodynamic systems, the treatment of thermal systems that involves the generation of entropy should be discussed, as well as the robust control of across-variable flow. Fig. 3-14 shows the entropy flow in thermal bilateral control. From the analogies introduced in previous chapter, the control of external through variables corresponds to the control of entropy flows in thermal systems as

$$i_m^{ext} + i_s^{ext} = \dot{S}_m^{ext} + \dot{S}_s^{ext}. \quad (3.44)$$

In thermal bilateral control, each flow can be calculated from heat flow divided by device temperature as

$$\dot{S}_m = \frac{q_m^{ext}}{T_{amb} + T_m} \quad (3.45)$$

$$\dot{S}_s = \frac{q_s^{ext}}{T_{amb} + T_s}. \quad (3.46)$$

Then the summation of the entropy flows becomes

$$\dot{S}_m + \dot{S}_s = \frac{q_m^{ext}}{T_{amb} + T_m} + \frac{q_s^{ext}}{T_{amb} + T_s} \simeq \frac{1}{T_{amb} + T_m} (q_m^{ext} + q_s^{ext}). \quad (3.47)$$

Therefore, the common-mode control of the entropy flows becomes equal to that of heat flows when the control of differential mode is conducted well. Under the assumption, the summation of entropy flows become zero when that of heat flows are controlled to be zero. There can be a possibility that the equivalence is lost when scaling bilateral control that transmits magnified or minimized power interaction is conducted. Since the gain is set at 1.0 in the experiments (no scaling), this research utilizes heat flow as alternative of entropy flow.

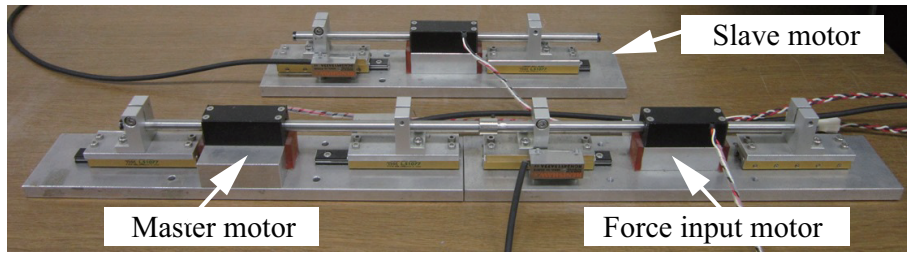


Fig. 3-15: Experimental setup of bilateral control (mechanical system).

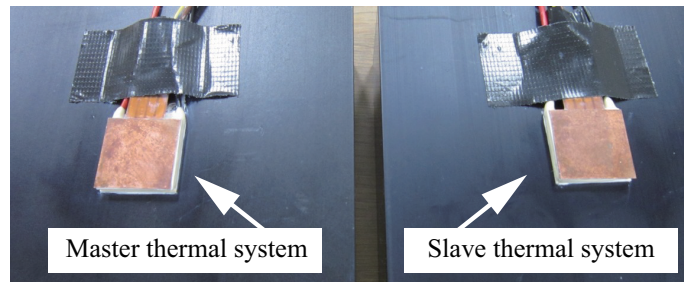


Fig. 3-16: Experimental setup of bilateral control (thermal system).

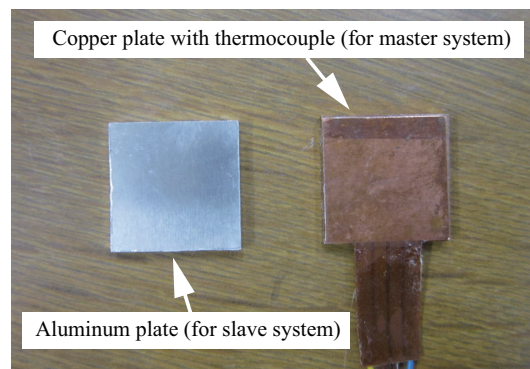


Fig. 3-17: External environments used for thermal bilateral control.

## 3.8 Experiments of Bilateral Control

In order to check the analyses on bilateral control systems, experimental results are shown in this section.

### 3.8.1 Overview of Experiments (Bilateral Control)

In the experiments, the across variable-based, through variable-based and AVF-based 4ch control systems are firstly compared. Experimental setups for mechanical and thermal control are shown in Figs.

Table 3.4: Parameter values for bilateral control (mechanical system).

Variables	Value	Unit
Gain for across-variable control, $C_e$	10.0, 50.0, 100.0	-
Gain for through-variable control, $C_i$	1.0, 2.0, 3.0	-
Nominal mass of motor, $M_n$	0.23	kg
Nominal torque coefficient, $K_{tn}$	3.33	N/A
Cut-off frequency of DOB, $g_{dis}$	1000.0	rad/s
Cut-off frequency of pseudo derivative, $g_{pd}$	1000.0	rad/s

Table 3.5: Parameter values for bilateral control (thermal system).

Variables	Value	Unit
Gain for across-variable control, $C_e$	0.1, 0.2, 0.3	-
Gain for through-variable control, $C_i$	1.0, 2.0, 3.0	-
Nominal capacitance of device, $C_{dvn}$	2.0	J/K
Nominal Seebeck coefficient, $\alpha_{sn}$	0.03	V/K
Cut-off frequency of DOB, $g_{dis}$	2.0	rad/s

3-15 and 3-16, respectively. Each setup contains master and slave systems in which AVF control based on disturbance observer is implemented. In Fig. 3-15, force input motor is attached to master motor in order to apply the external through variable. The motor is driven by constant electrical current, and the amount of the current is set at 0.1 A. Then, sponge material is utilized as the remote environment for slave system. For the thermal system, external environments shown in Fig. 3-17 are utilized. The copper plate is cooled down beforehand to generate the external through variable, and a thermocouple is attached on the plate.

Next, the generalized intermediate impedances are measured. In the experiments, bilateral control with different values of  $C_e$  and  $C_i$  are conducted, then the impedances are plotted based on the response values. Based on Fig. 3-3,  $Z_1$  and  $Z_2$  are calculated using responses processed by Fourier transformation and following equations

$$Z_1(j\omega) = \frac{(e_m - e_s)(j\omega)}{(i_m^{ext} + i_s^{ext})(j\omega)} \quad (3.48)$$

$$Z_2(j\omega) = \left. \frac{e_s(j\omega)}{i_m^{ext}(j\omega)} \right|_{i_s^{ext}=0} \quad (3.49)$$

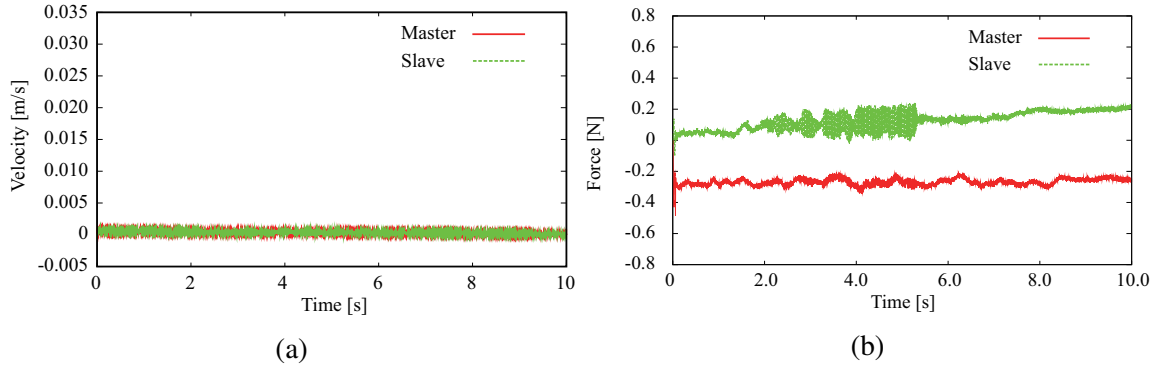


Fig. 3-18: Experimental results of across variable-based bilateral control (mechanical system). (a) Velocity responses. (b) Force responses.

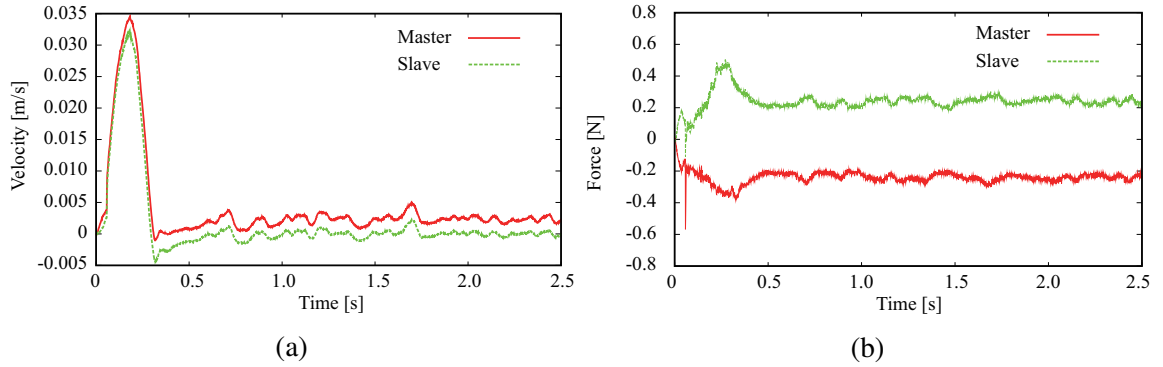


Fig. 3-19: Experimental results of through variable-based bilateral control (mechanical system). (a) Velocity responses. (b) Force responses.

Lastly, comparison with reflection-based bilateral control is conducted. The parameter values for the mechanical and thermal experiments are shown in Tables 3.4 and 3.5, respectively. In the experiments, aluminum block and cooled aluminum plate are used as external environment. Then, in the first and last experiments,  $C_e$  and  $C_i$  for mechanical and thermal control are fixed to  $(C_e, C_i) = (100.0, 3.0)$  and  $(C_e, C_i) = (0.3, 3.0)$ , respectively.

### 3.8.2 Results of Experiments (Bilateral Control)

Firstly, bilateral control of mechanical system is explained. Figs. 3-18, 3-19 and 3-20 show the results of across variable-based type, through variable-based type and AVF-based 4ch type, respectively. In the across variable-based control, master and slave motors move little even though the input motor applies force. This is thought to be caused by the compensation for external through variable (force)

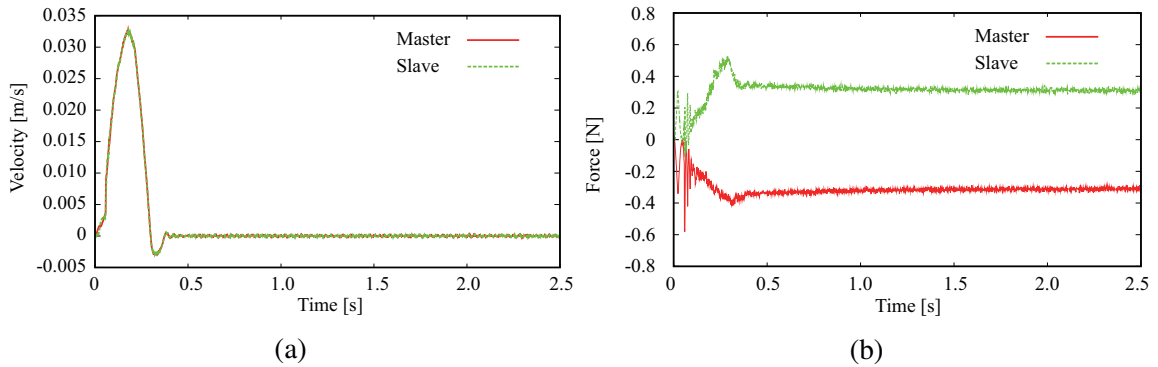


Fig. 3-20: Experimental results of AVF-based 4ch bilateral control (mechanical system). (a) Velocity responses. (b) Force responses.

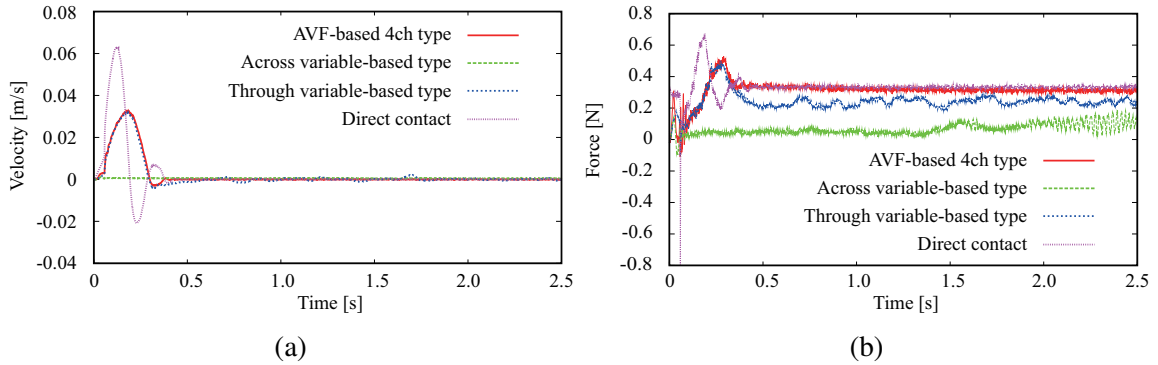


Fig. 3-21: Comparison of velocity and force responses. (a) Velocity responses. (b) Force responses.

by disturbance observer. The results indicate the necessity of including through variables in calculating AVF reference. In the through variable-based control, master and slave motors move and external through variable is generated at the slave side, as shown in Fig. 3-19. However, there exists the error of across variables (velocity). This can lead to the loss of power transmission from master system to slave system. The results shown in Fig. 3-20 indicate that the AVF-based control can realize both the synchronization of across variables and reproduction of through variables.

Fig. 3-21 shows the comparison of bilateral control systems. Here, “direct contact” represents the responses when the input motor directly contacted with environment without the bilateral control. Therefore, ideal bilateral control system should yield same results as the responses. From Fig. 3-21(a), through variable-base type and AVF-based 4ch type realize better responses than across variable-based type. On the other hand, the difference of these two control systems can be observed in the force responses shown in Fig. 3-21(b). From these results, it is able to say that the AVF-based 4ch bilateral control can realize

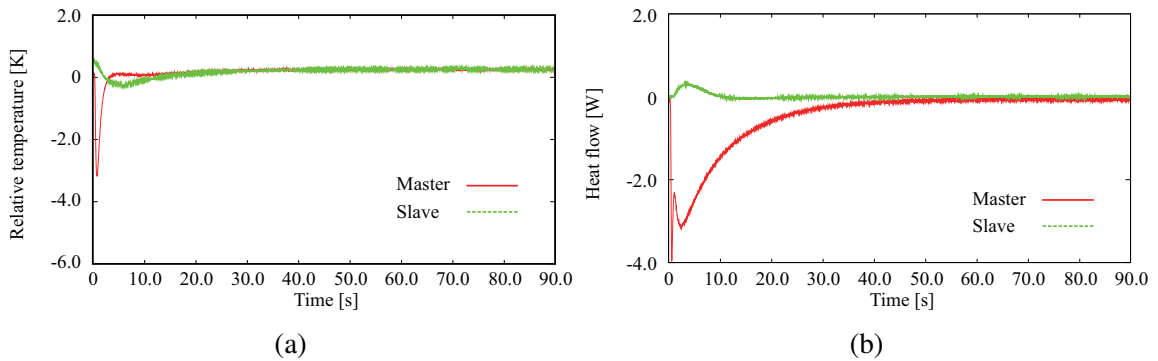


Fig. 3-22: Experimental results of across variable-based bilateral control (thermal system). (a) Temperature responses. (b) Heat flow responses.

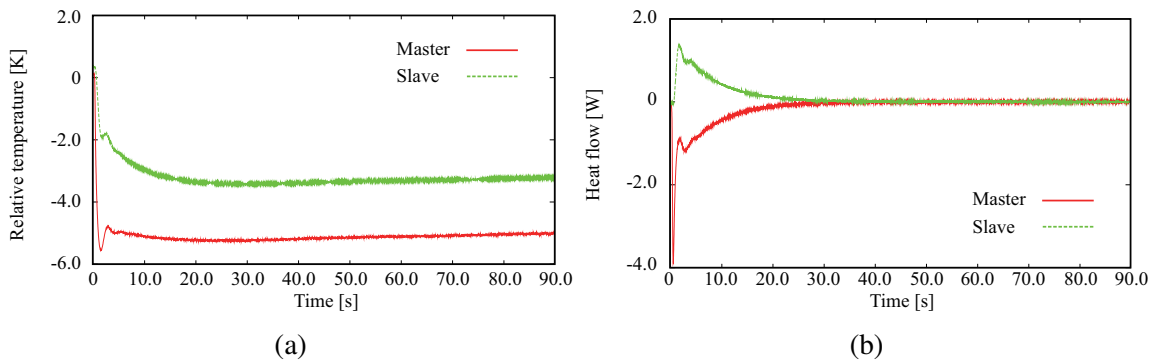


Fig. 3-23: Experimental results of through variable-based bilateral control (thermal system). (a) Temperature responses. (b) Heat flow responses.

the best performance among the systems.

Next, the results of thermal control are explained. The responses of each control system are shown in Fig. 3-22, 3-22 and 3-24, respectively. The tendencies of the results are same as those of mechanical control system, and changes in temperature are small in the case of across variable-based type, as shown in Fig. 3-22. Then, the error in across-variables exist in the through variable-based type as shown in Fig. 3-23. Though the bandwidth of the device itself is narrow and transient errors appear, the AVF-based 4ch bilateral control system whose results are shown in Fig. 3-24 can realize the control of both across and through variables.

Fig. 3-25 shows the temperature responses measured by the thermocouple attached to the external copper plate. The response of “direct contact” represents the temperature trajectory produced by the direct contact of the copper plate with aluminum plate. Among the control systems, the AVF-based 4ch

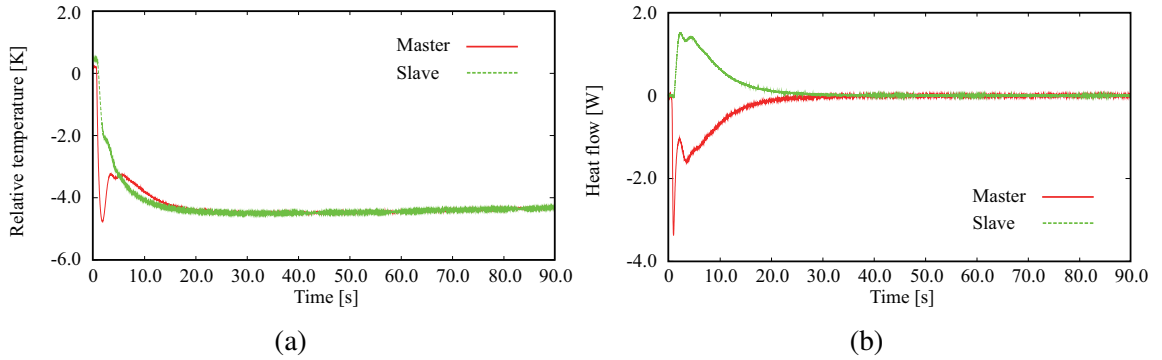


Fig. 3-24: Experimental results of AVF-based 4ch bilateral control (thermal system). (a) Temperature responses. (b) Heat flow responses.

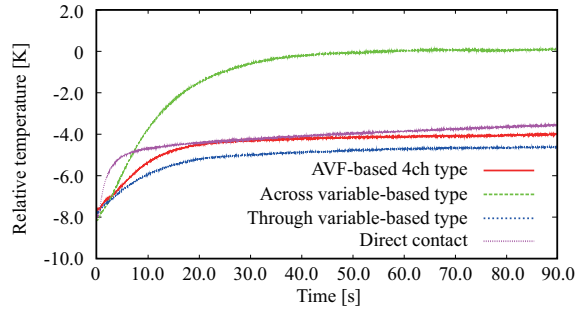


Fig. 3-25: Comparison of temperature responses.

control system yields the closest temperature response. The results so far indicate the effectiveness of AVF-based bilateral control system on reproduction of not only mechanical power interaction but also on the thermal power interaction.

### 3.8.3 Results of Experiments (Generalized Intermediate Impedances)

Next, the control systems are evaluated from the perspective of generalized intermediate impedances. For the measurement of the impedances, (3.48) and (3.49) are employed. Then, the gains of  $C_e$  and  $C_i$  in each control system are changed as shown in Tables 3.4 and 3.5.

The results of mechanical bilateral control are shown in Figs. 3-26, 3-27, 3-28 and 3-29, respectively. The results shown in Fig. 3-26 are the case of across variable-based control. The control system realizes better characteristics of  $Z_1$  among the comparative systems, whereas those of  $Z_2$  are inferior. Even when the gain of  $C_e$  is varied, the change of performance looks little. The small  $Z_2$  induces the leakage in power transmission. On the other hand, through variable-based control realizes better  $Z_2$  whereas the



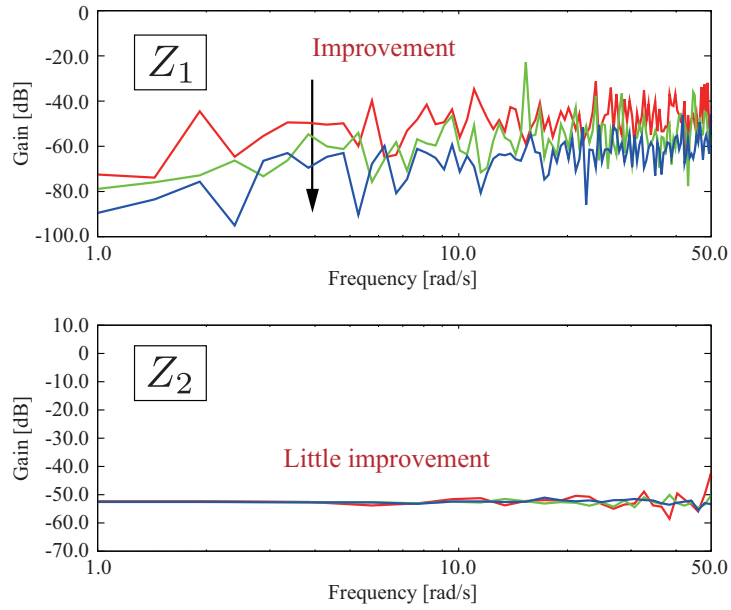


Fig. 3-26: Intermediate impedance of across variable-based bilateral control (mechanical case).

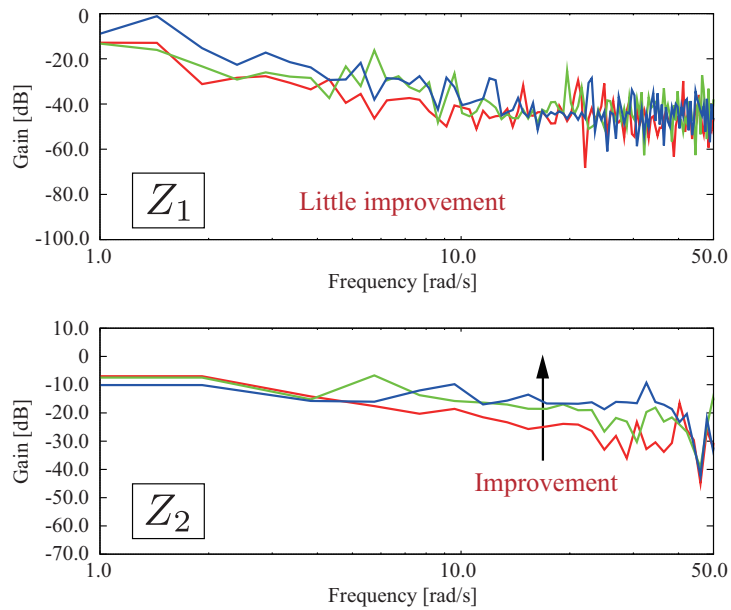


Fig. 3-27: Intermediate impedance of through variable-based bilateral control (mechanical case).

impedance  $Z_1$  is degraded. The deterioration cannot be recovered by the variation of  $C_i$ , and the results indicate the necessity of across variable controller.

Different from these control systems, the AVF-based 4ch bilateral control realizes performance en-

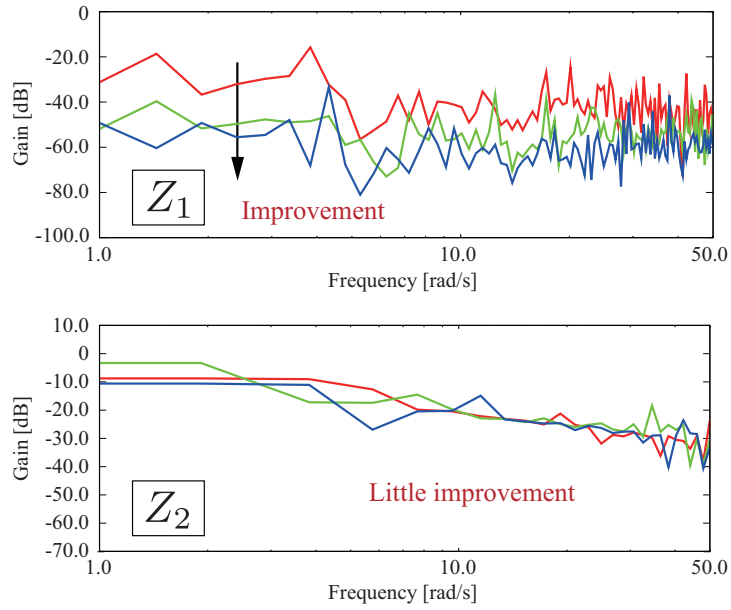


Fig. 3-28: Intermediate impedance of AVF-based bilateral control (mechanical case,  $C_e$  is changed).

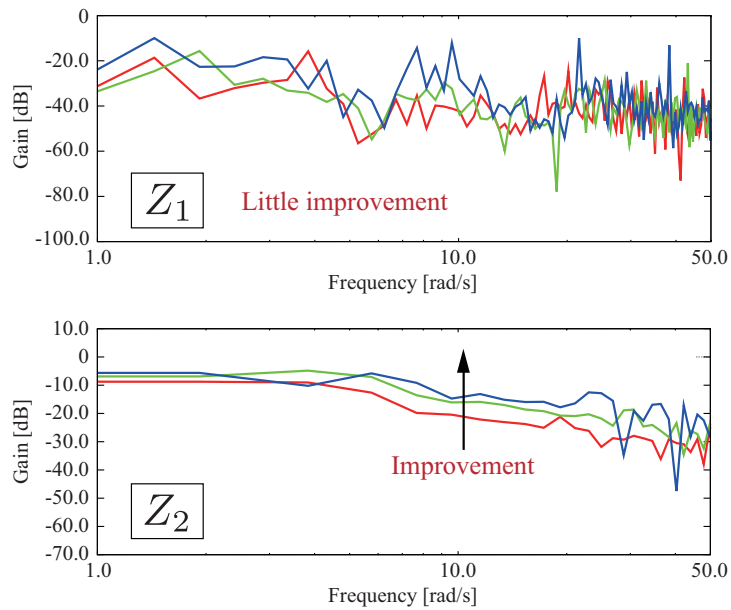


Fig. 3-29: Intermediate impedance of AVF-based bilateral control (mechanical case,  $C_i$  is changed).

hancement of  $Z_1$  and  $Z_2$ . The characteristics of the impedances are able to be enhanced respectively by changing  $C_e$  and  $C_i$ , as shown in Figs. 3-28 and 3-29.

Also in the case of thermal control, similar tendencies are observed. The results of measurement are

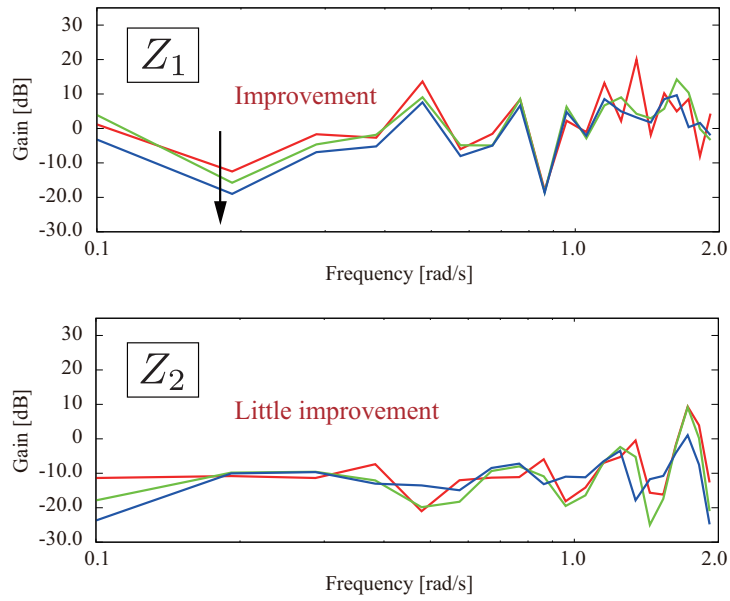


Fig. 3-30: Intermediate impedance of across variable-based bilateral control (thermal case).

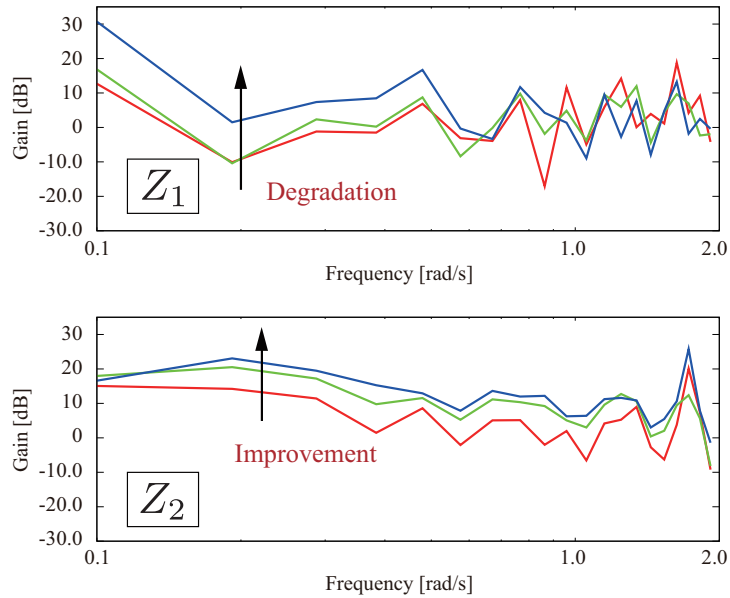


Fig. 3-31: Intermediate impedance of through variable-based bilateral control (thermal case).

shown in Figs. 3-30, 3-31, 3-32 and 3-33. As shown in Figs. 3-30 and 3-32, the across variable controller works to enhance the performance of impedance  $Z_1$ . Then, Figs. 3-31 and 3-33 indicate that the through variable controller contributes for improving the characteristics of  $Z_2$ .

In Figs. 3-31 and 3-33, the increase in  $C_i$  induces the deterioration of  $Z_1$ . This is thought to be caused

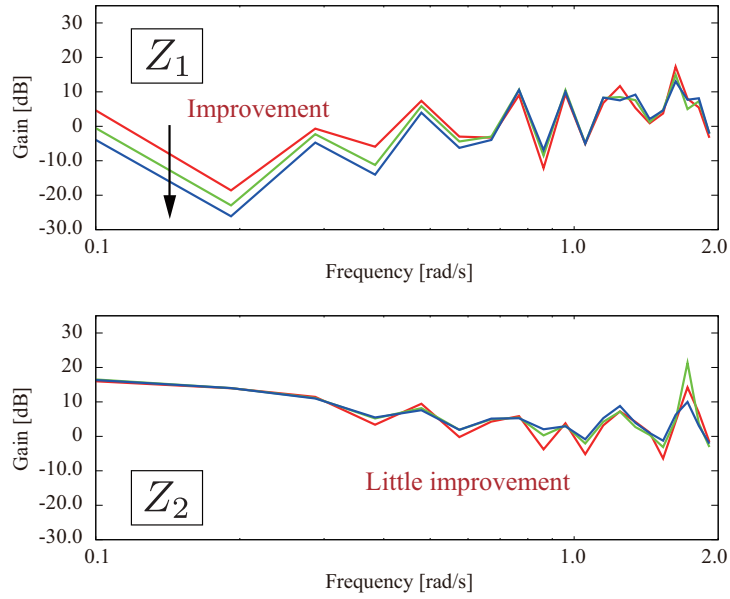


Fig. 3-32: Intermediate impedance of AVF-based bilateral control (thermal case,  $C_e$  is changed).

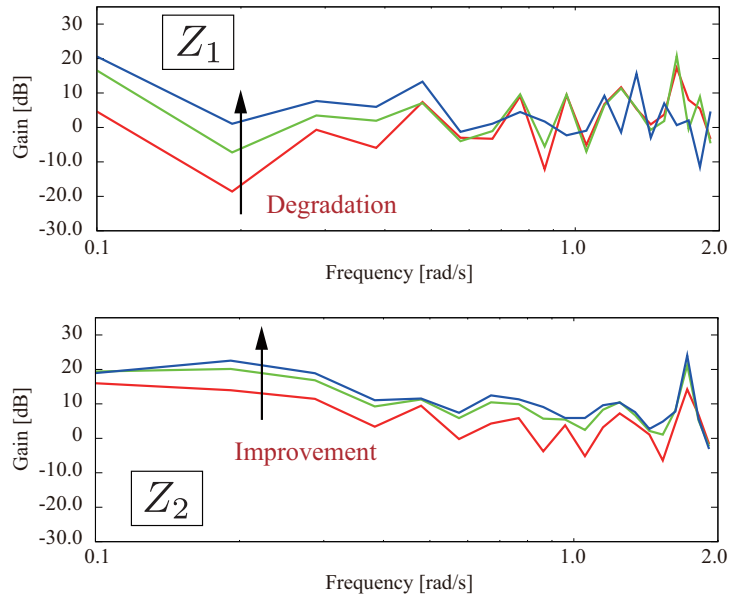


Fig. 3-33: Intermediate impedance of AVF-based bilateral control (thermal case,  $C_i$  is changed).

by the narrow bandwidth of thermal device, and some interference exist in control of across and through variables. Still, the increase of  $C_e$  does not change the performance of  $Z_2$ ; therefore, the control system has two degrees of freedom in designing the performance, and it is able to realize the reproduction of power interaction with less losses and leakages.

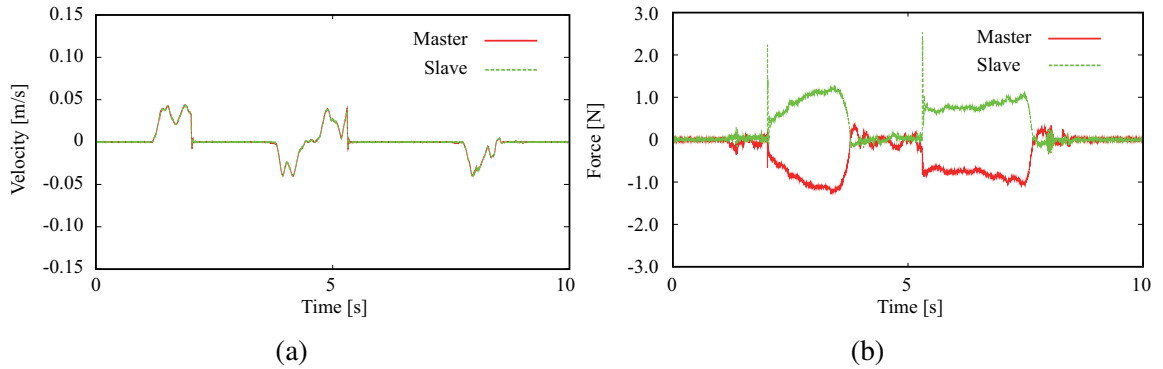


Fig. 3-34: Experimental results of AVF-based bilateral control (mechanical system, contact with aluminum block). (a) Velocity responses. (b) Force responses.

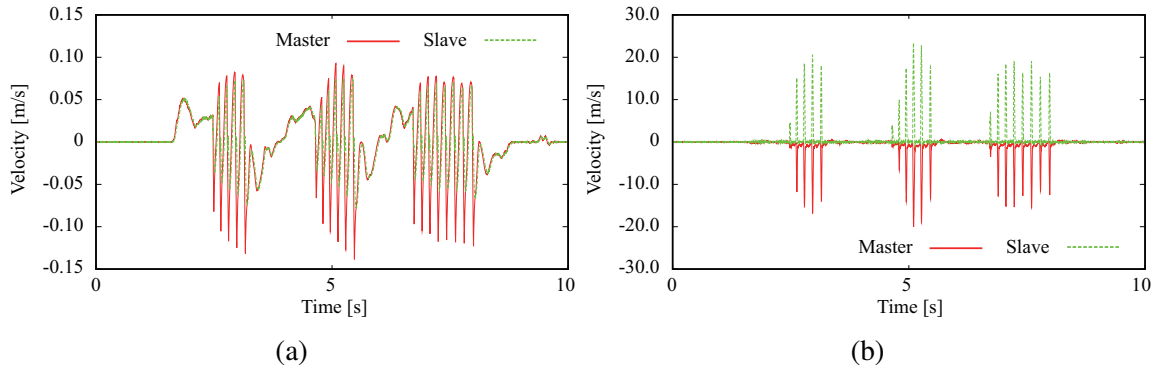


Fig. 3-35: Experimental results of reflection-based bilateral control (mechanical system, contact with aluminum block). (a) Velocity responses. (b) Force responses.

### 3.8.4 Results of Experiments (Comparison with Reflection-based Control)

Finally, the AVF-based 4ch bilateral control and reflection-based bilateral control, which include both controllers of across and through variables, are compared. For controlling mechanical system, aluminum block that has rigid impedance is prepared, while a cooled aluminum block contacts in the experiments of thermal control. Figs. 3-34 and 3-35 are the experimental results of mechanical power transmission. In the AVF-based 4ch bilateral control, the system can stably contact with the aluminum block as shown in Fig. 3-34. On the other hand, vibrations exist in the results of reflection-based control as shown in Fig. 3-35. The phenomenon is called as hunting, and the responses reflect the results of analyses on the stability described in Sections 3.5 and 3.6.

The case of thermal control is shown in Figs. 3-36 and 3-37. Comparing the responses, both control

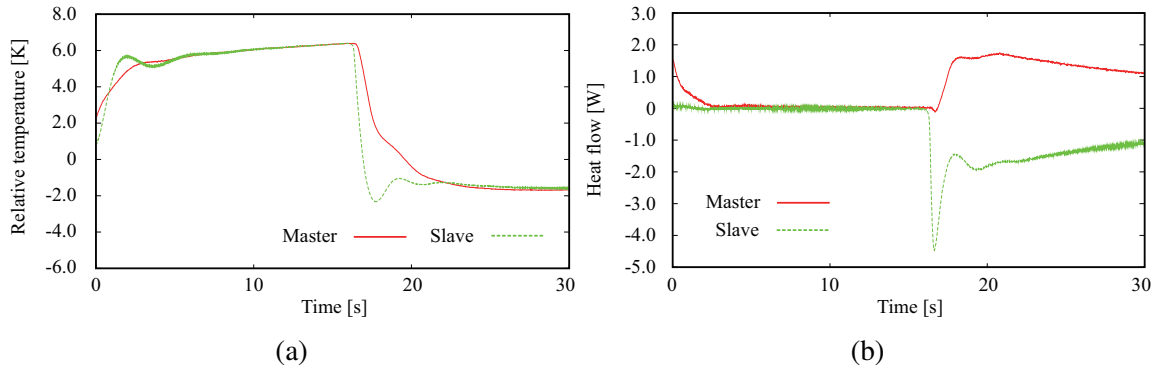


Fig. 3-36: Experimental results of AVF-based bilateral control (thermal system, contact with cooled aluminum block). (a) Temperature responses. (b) Heat flow responses.

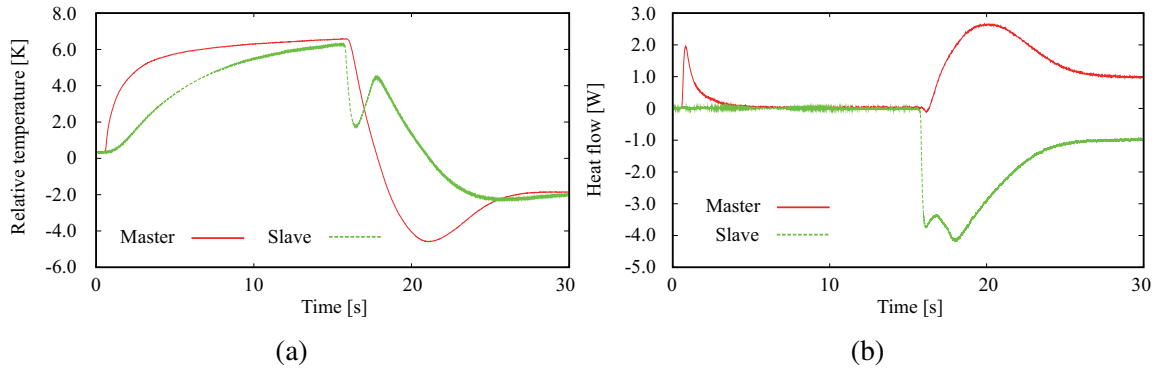


Fig. 3-37: Experimental results of reflection-based bilateral control (thermal system, contact with cooled aluminum block). (a) Temperature responses. (b) Heat flow responses.

systems realize stable contact with cooled aluminum plate, though the swing back is slightly observed in Fig. 3-37. The stable contact of reflection-based control is thought to be enabled by the narrow bandwidth of the device; the device itself works as damping for high-frequency signals, and it ended up the stabilization of control system. As the response characteristics of thermal devices are improved, the difference between the control systems is thought to be clearer.

As shown in the experimental results, the AVF-based 4ch bilateral control is effective not only for the bilateral reproduction of power transmission but also for the stable interaction with external environments. The tendencies of analyses and experimental results correspond and also this point support the validity of the AVF-based 4ch bilateral control system.

### **3.9 Summary of Chapter 3**

In this chapter, AVF-based 4ch bilateral control system was constructed. The expansion of acceleration-based 4ch bilateral control into unified framework is one of the main themes in this dissertation, and it was shown that the AVF-based 4ch control system is effective scheme for realizing the remote transmission of generalized power flow. The characteristics of the system were analyzed using generalized intermediate impedances, bond graph and pole placements. In analyses, comparison with the other control schemes was also conducted. According to the analyses, it was shown that the AVF-based 4ch type performs the best rendering of remote environment. In addition to that, the treatment that should be cared for use of thermodynamic system as the unit was explained. The analyses were checked by experiments of mechanical and thermal bilateral control. This chapter assumed that the information were communicated without any delays and local AVF control was perfect. From next chapters, the specific cases with those problems are considered.

## Chapter 4

# Performance Enhancement of Bilateral Control under Communication Delay

---

### 4.1 Introduction

The AVF-based 4ch bilateral control is a strong candidate for rendering remote environment mutually between master and slave systems. However, in practical situations, there exist some factors that disturb the operation of the system. One of the problems is time delay element in the control system. Communication of information between master and slave systems is essential for the realization of remote rendering. When the communication is conducted without delays, the control system can achieve the utmost performance. However, if it is not the case, the rendering of power interaction becomes inferior; in the worst case, the system can become unstable. Therefore, some compensation methods should be considered for expanding the applicability of the bilateral control system.

In this chapter, compensation filter for enhancing the performance of bilateral control under time delay is proposed [96]. The bilateral control with phase-lag compensation is employed as the base system, and hybrid parameters of the system are analyzed. The validity of the use of phase-lag compensator is checked by simulations. The filter is designed for through variable control, on the basis of the analyzed results. Then, the operation of the filter is changed according to the state of the system. One of the advantage of the proposed system is that it maintains the symmetric property; the master can be slave and vice versa. In this research, two kinds of experiments are conducted; one is the determination of the operation of proposed system, and the other is the comparison of methods by the measurement of hybrid parameters. In the comparative method, the communication disturbance observer-based scheme



[57] which is the famous method of delay compensation is included. By the experiments, the validity of the proposed system is confirmed.

The contents in this chapter are as follows. In Section 4.2, the AVF-based 4ch bilateral control under time delay is briefly explained. Then, as a preliminary of the proposal, bilateral control with phase-lag compensation is described in Section 4.3. Using the system with the phase-lag compensator as the basis, the compensator for through variable control is proposed in Section 4.4. Here, the adaptive algorithm for haptic communication is also explained. The used of phase-lag compensator is tested by simulations in Section 4.5. Then, the validity of the proposal is tested by the experiments in Section 4.6. The last section states conclusive remarks.

## 4.2 Bilateral Control under Time Delay

When the communication delays between master and slave systems exist, the control laws of AVF-based 4ch bilateral control become as follows:

$$\dot{e}_m^{ref} = C_e(e^{-Ts}e_s - e_m) - C_i(\hat{i}_m^{ext} + e^{-Ts}\hat{i}_s^{ext}) \quad (4.1)$$

$$\dot{e}_s^{ref} = C_e(e^{-Ts}e_m - e_s) - C_i(e^{-Ts}\hat{i}_m^{ext} + \hat{i}_s^{ext}), \quad (4.2)$$

where  $e^{-Ts}$  denotes the delay element and  $T$  represents the amount of delay. The bond graph of the control system is shown in Fig. 4-1. Here, the subscript  $d$  denotes the delayed information; for example,  $f_d(t) = f(t - T)$ . Different from Fig. 3-8, there are the sources of across variables which inject power according to the delayed information in the graph. As well as the discussions of Lyapunov-based analyses on reflection-based control system, the internal power sources can adversely effect the stability. For example, the summation of  $P_A$  and  $P_B$  in Fig. 4-1 becomes

$$\begin{aligned} P_A + P_B = & \frac{C_e}{C_f}e_s(e_{md} - e_s) + \frac{C_e}{C_f}e_m(e_{sd} - e_m) \\ & \frac{C_e}{C_f}e_{md}(e_{md} - e_s) + \frac{C_e}{C_f}e_{sd}(e_{sd} - e_m) - \frac{C_e}{C_f}(e_{md} - e_s)^2 - \frac{C_e}{C_f}(e_{sd} - e_m)^2. \end{aligned} \quad (4.3)$$

The first and second terms in (4.3) effect for losing the semi-definiteness of Lyapunov function, thus the communication delays degrade the stability of the bilateral control system. Also, the performance of power transmission is deteriorated since the controllers for balancing powers inject different power for master and slave systems. The motivation of the study in this section is to recover the performance of the system.

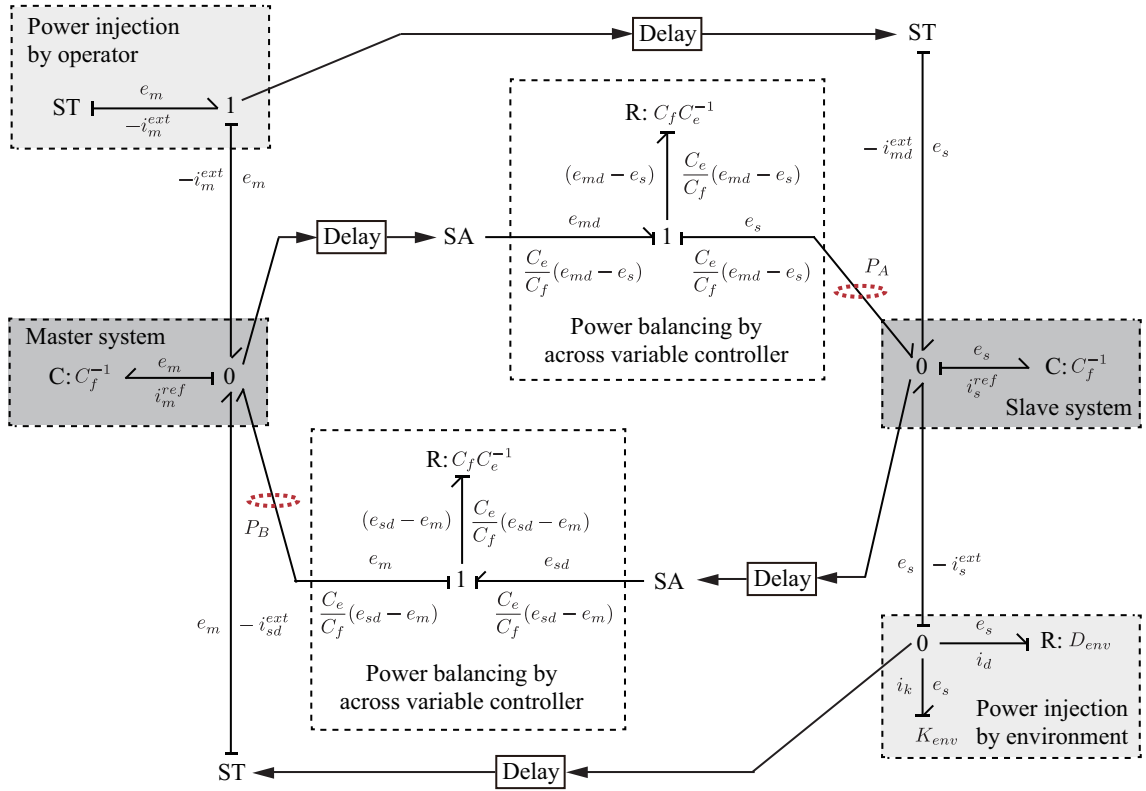


Fig. 4-1: AVF-based 4ch bilateral control under time delay.

### 4.3 Phase-lag Compensation and Stability

As a preliminary for the proposed method, compensation for gaining stability is considered here. The compensation can be conducted by implementing the certain filters and processing the signals. There are mainly two types of compensation filters: phase-lead and phase-lag types. The characteristics of the filters are as follows:

- Phase-lead type: increases the amplitude of signals, for the sake of recovering lag of signals
- Phase-lag type: induces another lag of signals, for the sake of decreasing the amplitude of signals

Among these two types, this study chooses the latter one; phase-lag compensation filter.

#### 4.3.1 Analyses on Use of Phase-lag Compensator Based on Bond Graph

The bond graph with phase-lag compensation is shown in Fig. 4-2. Here, subscript ' denotes processed value. In the graph, compensation filters are implemented as the former blocks of balancing controller.

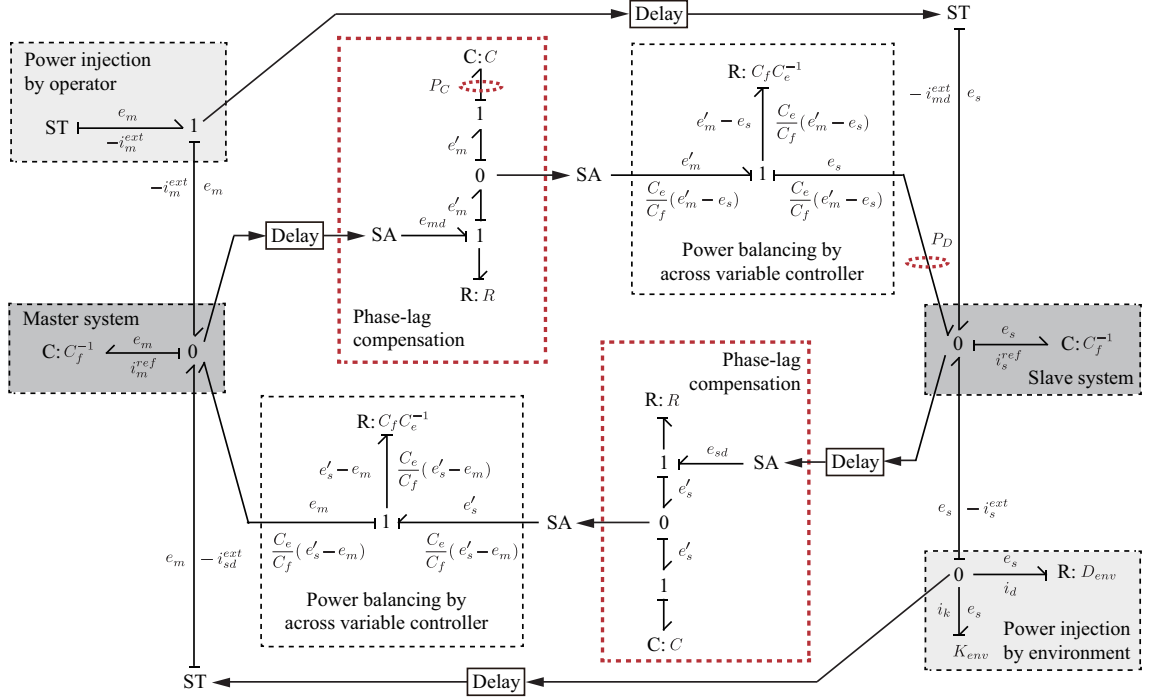


Fig. 4-2: Bilateral control with phase-lag compensator under time delay.

As the example of the filter there is a low-pass filter, and this can be constructed using R and C elements as shown in Fig. 4-2. In general, when input is given by  $u = \sin(\omega t)$ , the output of low-pass filter  $y$  becomes

$$y = G \sin(\omega t + \phi), \quad (4.4)$$

where

$$G = \frac{1}{\sqrt{1 + \omega^2 R^2 C^2}} \quad (4.5)$$

$$\phi = -\tan(\omega RC). \quad (4.6)$$

Here,  $R$  and  $C$  denote the amount of R and C elements. For this system, the power-based analyses are conducted. In the same manner with the previous section, following power is focused

$$P_C + P_D = \frac{C_e}{C_f} e'_m e_s - \frac{C_e}{C_f} e_s^2 + \frac{1}{R} e_m e'_m - \frac{1}{R} e_m^2. \quad (4.7)$$

Comparing this with the original power summation  $C_f/C_e e_m e_s - C_f/C_e e_s^2$ , the Lyapunov stability is enhanced when following holds

$$\frac{C_e}{C_f} e'_m e_s + \frac{1}{R} e_m e'_m - \frac{1}{R} e_m'^2 < \frac{C_e}{C_f} e_m e_s. \quad (4.8)$$

It is able to say that the terms in (4.7) are the factors which may lose the semi-definiteness of Lyapunov function. Therefore, if (4.8) holds, the influence of terms which are definite negative on the Lyapunov function becomes larger. Here, assuming  $e_m \simeq e_s = \sin(\omega t)$  and  $e'_m \simeq G \sin(\omega t + \phi - \omega T)$ , left side of (4.8) becomes

$$\begin{aligned} & \frac{C_e}{C_f} e'_m e_s + \frac{1}{R} e_m e'_m - \frac{1}{R} e_m'^2 \\ &= \frac{C_e}{C_f} G \left( 1 + \frac{C_f}{C_e R} \right) \sin(\omega t) \sin(\omega t + \phi - \omega T) - \frac{1}{R} G^2 \sin^2(\omega t + \phi - \omega T) \\ &= \sin(\omega t + \phi - \omega T) \left\{ \frac{C_e}{C_f} G \left( 1 + \frac{C_f}{C_e R} \right) \sin(\omega t) - \frac{1}{R} G^2 \sin(\omega t + \phi - \omega T) \right\} \\ &= \sin(\omega t + \phi - \omega T) \sin(\omega t + \delta) \cdot \\ & \quad \sqrt{\frac{C_e^2}{C_f^2} G^2 \left( \frac{C_e R + C_f}{C_e R} \right)^2 + \frac{G^4}{R^2} + 2 \frac{C_e R + C_f}{C_e R^2} G^3 \cos(\phi - \pi - \omega T)}, \end{aligned} \quad (4.9)$$

where

$$\delta = \arctan \left( \frac{\frac{G^2}{R} \sin(\phi - \pi - \omega T)}{\frac{C_e}{C_f} G \left( \frac{C_e R + C_f}{C_e R} \right) + \frac{G^2}{R} \sin(\phi - \pi - \omega T)} \right). \quad (4.10)$$

Therefore, following holds as for the absolute value

$$\begin{aligned} & \left| \frac{C_e}{C_f} e'_m e_s + \frac{1}{R} e_m e'_m - \frac{1}{R} e_m'^2 \right| \leq \\ & \quad \sqrt{\frac{C_e^2}{C_f^2} G^2 \left( \frac{C_e R + C_f}{C_e R} \right)^2 + \frac{G^4}{R^2} + 2 \frac{C_e R + C_f}{C_e R^2} G^3} = A. \end{aligned} \quad (4.11)$$

On the other hand, the absolute value of right hand side of (4.8) is limited as

$$\left| \frac{C_e}{C_f} e_m e_s \right| \leq \frac{C_e}{C_f}. \quad (4.12)$$

Considering the order of  $G$  and  $R$  in (4.11), the value of  $A$  can be adjusted to be smaller than  $C_e/C_f$ . Therefore, (4.8) is able to be realized and stability is enhanced by the phase-lag compensator.

When the phase-lead compensator is employed,  $G$  in (4.5) is more than 1.0 for all frequencies. Therefore, the absolute value of power summation can get larger and it adversely effects on the stability.

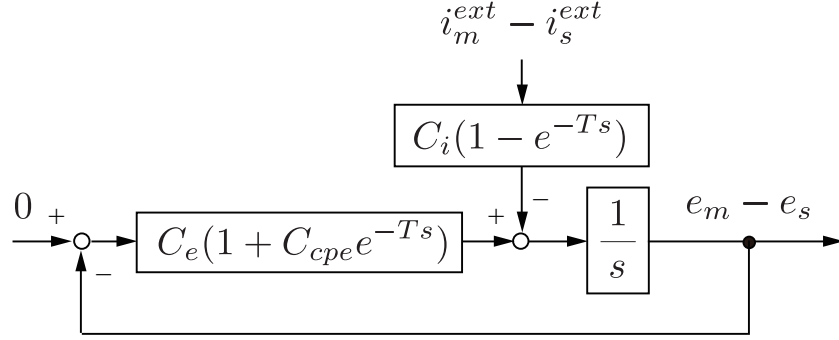


Fig. 4-3: Block diagram of differential modal space under time delay.

### 4.3.2 Analyses on Phase-lag Compensator Based on Differential Modal Space

The AVF references using the compensator are described as

$$\dot{e}_m^{ref} = C_e(C_{cpe}e^{-Ts}e_s - e_m) - C_i(\hat{i}_m^{ext} + e^{-Ts}\hat{i}_s^{ext}) \quad (4.13)$$

$$\dot{e}_s^{ref} = C_e(C_{cpe}e^{-Ts}e_m - e_s) - C_i(e^{-Ts}\hat{i}_m^{ext} + \hat{i}_s^{ext}). \quad (4.14)$$

Here,  $C_{cpe}$  denotes the compensator whose transfer function is given by

$$C_{cpe} = \frac{\alpha_{cmp}s + g_{cmp}}{s + g_{cmp}}, \quad (4.15)$$

where  $\alpha_{cmp}$  and  $g_{cmp}$  denote compensation gain and cut-off frequency, respectively. When  $\alpha_{cmp} > 1.0$ , the compensator becomes phase-lead type. On the other hand,  $\alpha_{cmp} < 1.0$  makes the compensator phase-lag type. The compensator shown in (4.15) can be comprehended as a band-limited low-pass filter.

By subtracting (4.14) from (4.13), following is derived

$$s(e_m - e_s) = -C_e(1 + C_{cpe}e^{-Ts})(e_m - e_s) - C_i(1 - e^{-Ts})(i_m^{ext} - i_s^{ext}). \quad (4.16)$$

This is the dynamics of differential modal space of bilateral control system. The block diagram of (4.16) is represented as Fig. 4-3. When there exists no communication delay, the modal disturbance  $i_m^{ext} - i_s^{ext}$  is totally erased; however, if it is not the case, the performance is degraded. From Fig. 4-3, it turns out that the  $C_e(1 + C_{cpe}e^{-Ts})/s$  becomes the loop transfer function of the modal space and stability of the control is affected by the element. Then, it is also shown that the stability can be adjusted by the compensator  $C_{cpe}$ . The part  $1 + C_{cpe}e^{-Ts}$  can be approximated by using first-order Pade approximation

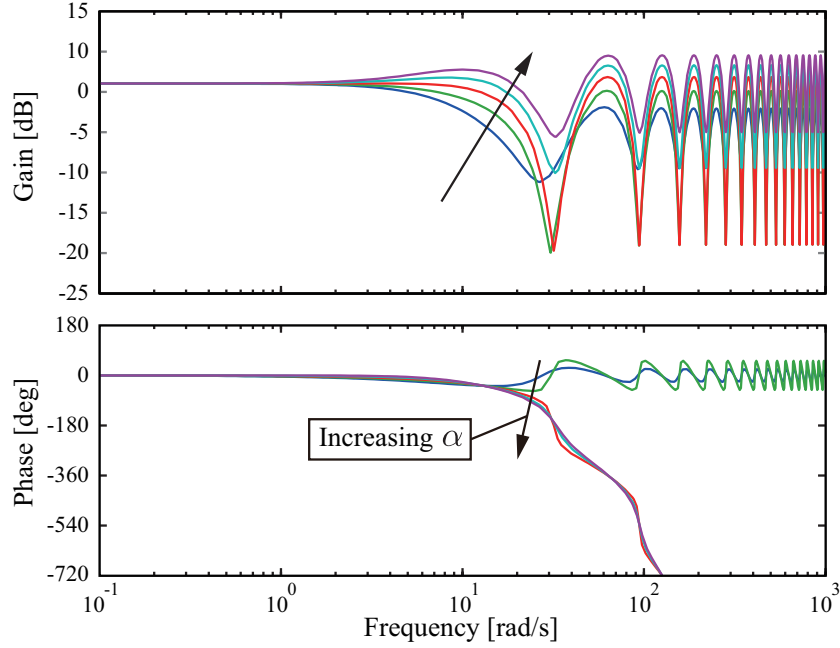


Fig. 4-4: Gain diagram of  $1 + e^{-Ts}C_{cp}$ .

as

$$\begin{aligned}
 1 + e^{-Ts}C_{cpe} &\simeq 1 + \frac{1 - \frac{T}{2}s}{1 + \frac{T}{2}s} \frac{\alpha_{cmp}s + g_{cmp}}{s + g_{cmp}} \\
 &= \frac{\frac{T}{2}(1 - \alpha_{cmp})s^2 + (1 + \alpha_{cmp})s + 2g_{cmp}}{\frac{T}{2}s^2 + (1 + \frac{T}{2}g_{cmp})s + g_{cmp}}. \tag{4.17}
 \end{aligned}$$

By the Pade approximation, the part is described as second-order transfer function. As shown in (4.17), the zeros of the transfer function can be changed by the value  $\alpha_{cmp}$ . By using quadratic formula, the zeros are derived as

$$\begin{aligned}
 s &= \frac{-(1 + \alpha_{cmp}) \pm \sqrt{(1 + \alpha_{cmp})^2 - 4g_{cmp}T(1 - \alpha_{cmp})}}{T(1 - \alpha_{cmp})} \\
 &= \frac{-a \pm b}{c}. \tag{4.18}
 \end{aligned}$$

When  $\alpha_{cmp} > 1.0$  (phase-lead compensation), the transfer function will have unstable zero since  $a > 0$ ,  $b > a$  and  $c < 0$ . Therefore, it is thought that using the phase-lead compensator may adversely effect on the control system. On the other hand, the transfer function will have stable zeros when  $0 < \alpha < 1$  (phase-lag compensator).

The bode diagram of the part  $1 + C_{cpe}e^{-Ts}$  is shown in Fig. 4-4. In plotting the diagram,  $g_{cmp}$  is set as 10.0 rad/s, and  $\alpha_{cmp}$  is changed from 0.4 with the step of 0.4. As shown in the diagram, the increase in

$\alpha_{cmp}$  causes phase lag and increase of gain. This is thought to be induced by the appearance of unstable zero. From the results, it is able to say that the use of phase-lag compensator is better for the case of bilateral control. In this dissertation, (4.13) and (4.14) with phase-lag compensator are employed as the basis for bilateral control under time delay.

#### 4.4 Design of Through Variable Compensator

Utilizing (4.13) and (4.14) as the basis of control laws, compensator for through variable controller is designed as the proposal for recovering the performance of the bilateral control. Letting  $C_{cpi}$  the compensator for through variable, novel control laws are given as follows

$$\dot{e}_m^{ref} = C_e(C_{cpe}e^{-Ts}e_s - e_m) - C_i(C_{cpi}\hat{i}_m^{ext} + e^{-Ts}\hat{i}_s^{ext}) \quad (4.19)$$

$$\dot{e}_s^{ref} = C_e(C_{cpe}e^{-Ts}e_m - e_s) - C_i(e^{-Ts}\hat{i}_m^{ext} + C_{cpi}\hat{i}_s^{ext}). \quad (4.20)$$

The aim of the control laws is to adjust the performance characteristics of bilateral control using  $C_{cpi}$ , while maintaining the stability by the compensator  $C_{cpe}$ .

The design is conducted on the basis of hybrid parameters. Assuming that the AVF control is perfect ( $\dot{e}^{ref} = \dot{e}^{res}$ ), and following the definition shown in (3.12), hybrid parameters of the system with (4.19) and (4.20) are derived as

$$H_{11} = \frac{-s^2 + 2sC_e + (1 - e^{-2Ts}C_{cpe}^2)C_e^2}{e^{-Ts}C_i\{s + (1 + C_{cpe}C_{cpi})C_e\}} \quad (4.21)$$

$$H_{12} = \frac{sC_iC_{cpi} + (C_{cpi} + e^{-2Ts}C_{cpe})C_eC_i}{e^{-Ts}C_i\{s + (1 + C_{cpe}C_{cpi})C_e\}} \quad (4.22)$$

$$H_{21} = H_{12} \quad (4.23)$$

$$H_{22} = \frac{-(C_{cpi}^2 - e^{-2Ts})C_i^2}{e^{-Ts}C_i\{s + (1 + C_{cpe}C_{cpi})C_e\}}. \quad (4.24)$$

Note that  $H_{12} = H_{21}$  since the bilateral control system keeps its symmetric property.

##### 4.4.1 Through Variable Compensator for Sub-optimal Tracking

For designing the compensator  $C_{cpi}$ , the modification of control objectives is considered. Under the communication delay, followings are set as the sub-optimal objectives

$$e^{-Ts}e_m - e_s = 0 \quad (4.25)$$

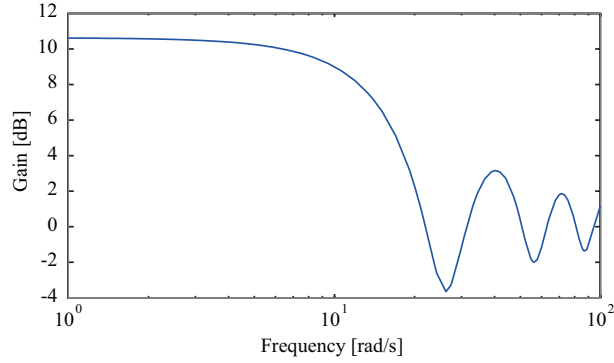


Fig. 4-5: Gain diagram of  $C_{cpi}$  (the case of  $C_e = 30.0$ ,  $T = 0.1$ ,  $C_{cpe} = (0.5s + 10.0)/(s + 10.0)$ ).

$$e^{-Ts}i_m^{ext} + i_s^{ext} = 0. \quad (4.26)$$

In the form of hybrid parameters, these are rewritten as

$$\begin{bmatrix} i_m^{ext} \\ e_m \end{bmatrix} = \begin{bmatrix} 0 & e^{Ts} \\ e^{Ts} & 0 \end{bmatrix} \begin{bmatrix} e_s \\ -i_s^{ext} \end{bmatrix}. \quad (4.27)$$

The compensator  $C_{cpi}$  should realize the hybrid parameters to be the closest to the ideal ones shown in (4.27). Among the parameters, more important parts are thought to be  $H_{12}$  and  $H_{21}$ , since these express the tracking performance of across and through variables. Therefore,  $C_{cpi}$  is designed to enhance the performance characteristics of these parameters. Comparing (4.24) with (4.27), the compensator can be derived by a back-calculation as

$$C_{cpi} = \frac{s + C_e - e^{-2Ts}C_{cpe}C_e}{s + C_e - C_{cpe}C_e}. \quad (4.28)$$

By using the compensator, the  $H_{12}$  and  $H_{21}$  will have the sub-optimal characteristics, and performance of bilateral control is recovered.

#### 4.4.2 Modification of Through Variable Compensator

One of the problems in direct use of the compensator is the degradation of  $H_{22}$ . Fig. 4-5 shows the gain diagram of (4.28), and the DC gain of the diagram has deviation from 0 dB. In this case, the DC gain of the parameter  $H_{22}$  does not become  $-\infty$  dB since the part in the parameter ( $C_{cpi}^2 - e^{-2Ts}$ ) has certain gain in DC component. Fig. 4-6 shows the gain diagram of  $H_{22}$  when the  $C_{cpi}$  is set as (4.28). As stated above, the parameter has certain steady state gain. Since  $e_m = H_{21}e_s - H_{22}i_s^{ext}$ , the parameter  $H_{22}$  is related to the interference term for synchronization control of across variables. When  $H_{22}$  has



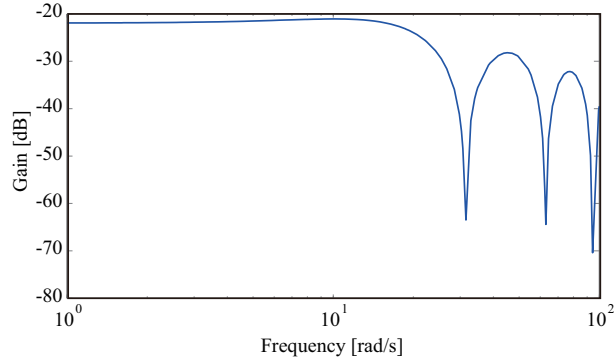


Fig. 4-6: Gain diagram of  $C_{cpi}$  (The case of  $C_e = 30.0$ ,  $C_i = 1.0$ ,  $T = 0.1$ ,  $C_{cpe} = (0.5s + 10.0)/(s + 10.0)$ ).

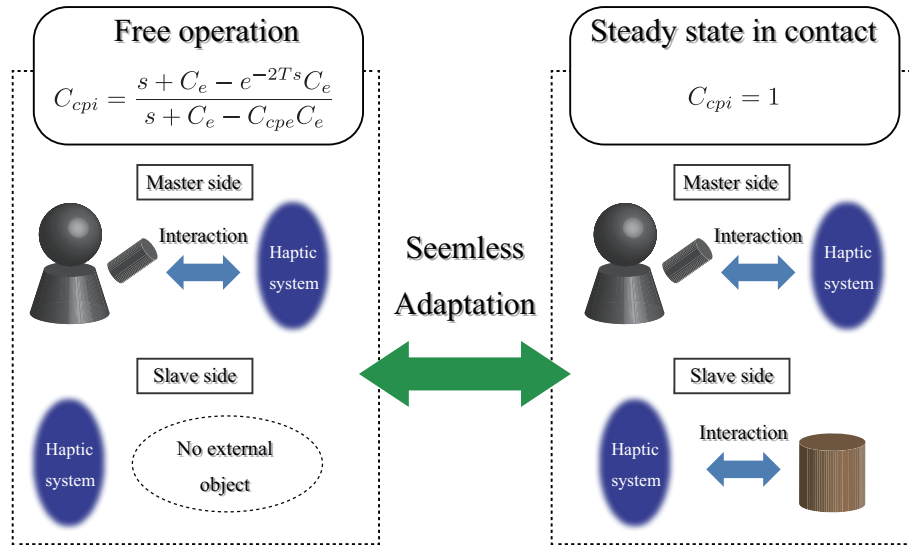


Fig. 4-7: Idea of modifying the compensator  $C_{cpi}$ .

DC gain, the interference remains even when the system is in steady state, inducing the steady state error of across variables. Recollecting the following generalized intermediate impedance, the losses occur in steady state of power transmission when  $H_{22}$  does not have  $-\infty$  dB gain in DC component

$$Z_1 = \frac{H_{22}}{1 + H_{12}}. \quad (4.29)$$

Therefore, although the compensator  $C_{cpi}$  makes the characteristics  $H_{12} = H_{21}$  sub-optimal, the performance of  $H_{22}$  is degraded.

In order to address the problem, modification of the compensator is proposed. The transfer function

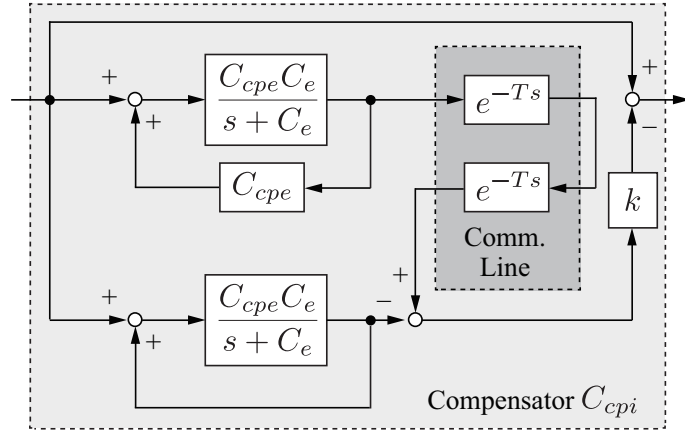


Fig. 4-8: Implementation of  $C_{cpi}$ .

of the modified compensator is

$$C_{cpi} = 1 - \frac{(e^{-2Ts} - C_{cpe})C_e}{s + (1 - C_{cpe})C_e} k, \quad (4.30)$$

where  $k$  is a gain of compensator. When the gain is  $k = 1.0$ , (4.30) becomes equivalent to (4.28). On the other hand,  $k = 0.0$  means that the compensator for through variable is off. The idea of modifying the compensator  $C_{cpi}$  is illustrated in Fig. 4-7. The operation of bilateral control can be categorized to two kinds: free operation and contact operation. In free operation, only the operator contacts with master system, whereas no external materials contact with the slave side. The contact operation is a state in which the objects are contacted with both master and slave systems. From  $e_m = H_{21}e_s - H_{22}i_s^{ext}$ , it is able to say that the system is not effected by the term  $H_{22}$  in free operation, since  $i_s^{ext} = 0$  when no objects are contacted with the slave system. Therefore, using the compensator is effective in this state. In the steady state of contact, turning off the compensator is reasonable from the viewpoint of steady state errors. From the considerations above, the compensator with variable gain is proposed in this dissertation. The detection algorithm of free and contact states is implemented in the proposal, and the gain  $k$  in (4.30) is adjusted.

Fig. 4-8 shows the implementation of the compensator. Since the  $C_{cpi}$  contains time delay element, the modeling error of the delay may cause the inappropriate operation of the filter. Therefore, the filter employs the transmission and retransmission of the signal using the real communication line [104]. By doing so, the compensator becomes free from the modeling. The lower part in the Fig. 4-8 corresponds to the second term in (4.30). The amount of the influence of the part is adjusted by the gain  $k$ .

The gain diagrams of hybrid parameters with different gain  $k$  are shown in Fig. 4-9. In plotting the

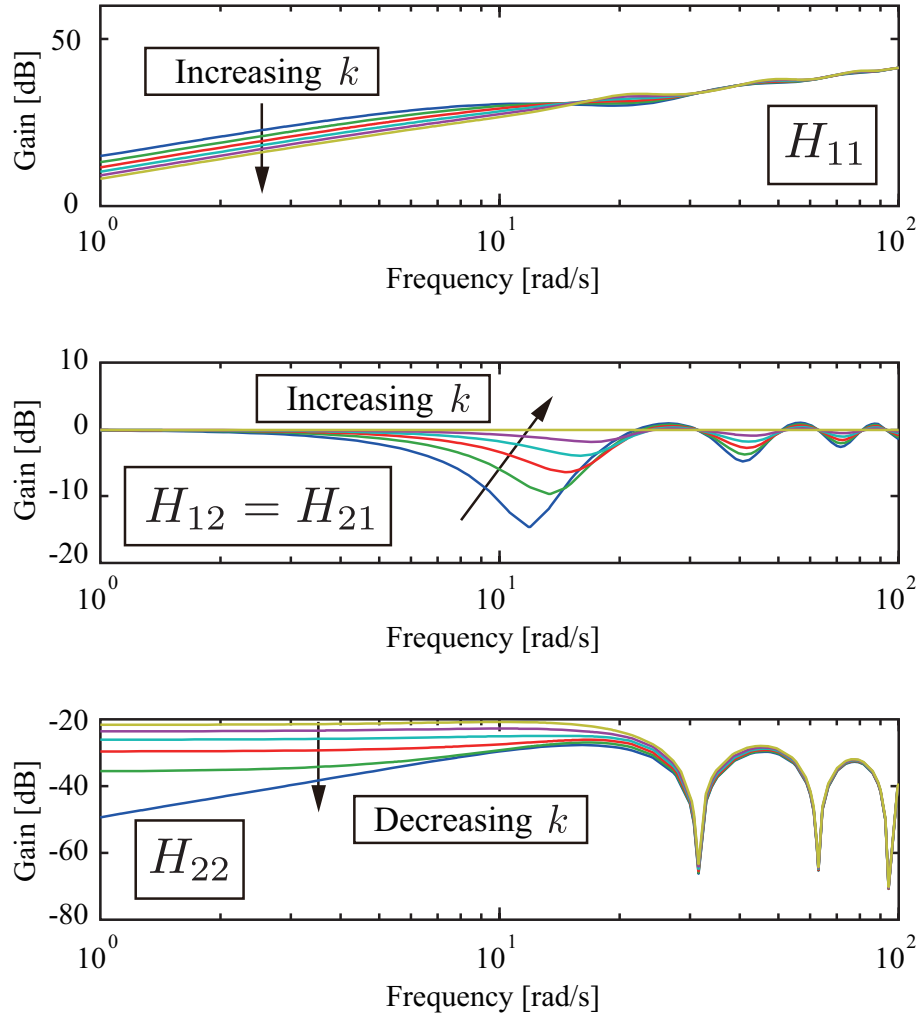


Fig. 4-9: Gain diagrams of hybrid parameters with different gain  $k$  (changed from 0.0 with increment of 0.2).

diagrams, same parameter values used for plotting Fig. 4-6 is used. From  $H_{12} = H_{21}$  in Fig. 4-9, it is shown that the anti-resonance peaks diminishes as the gain  $k$  is increased. On the other hand, it is observed that  $k = 0.0$  makes the gain of  $H_{22} -\infty$  dB. As for the  $H_{11}$ , larger  $k$  looks good since the gain of the parameter is decreased. The gain diagrams indicate the trade-off between the parameters; therefore, the control system should adaptively change the gain according to the state of the bilateral control, in order to enhance the performance of the haptic communication.

Table 4.1: Parameter values used for simulations.

Variables	Value	Unit
P gain of position control, $K_p$	500.0	-
Gain for across variable control, $K_e$	31.5	-
Gain for through variable control, $K_i$	1.0	-
Cut-off frequency of DOB, $g_{dob}$	500.0	rad/s
Cut-off frequency for deciding gain $k$ , $g_k$	10.0	rad/s
Nominal torque coefficient, $K_{tn}$	47.0	N/A
Nominal mass of motor, $M_n$	0.295	kg
Phase-lag compensator, $C_{cpe}$	$\frac{0.5s+10.0}{s+10.0}$	-
Stiffness of environment, $K_{env}$	1000.0	N/m
Viscosity of environment, $D_{env}$	100.0	Ns/m

#### 4.4.3 Determination of Gain $k$

In the proposed system, the value of  $k$  for master and slave systems are determined adaptively as

$$k_m = \frac{g_k}{s + g_k} \frac{|\hat{i}_m^{ext} + e^{-Ts}\hat{i}_s^{ext}|}{|\hat{i}_m^{ext}| + |e^{-Ts}\hat{i}_s^{ext}|} \quad (4.31)$$

$$k_s = \frac{g_k}{s + g_k} \frac{|\hat{i}_s^{ext} + e^{-Ts}\hat{i}_m^{ext}|}{|\hat{i}_s^{ext}| + |e^{-Ts}\hat{i}_m^{ext}|}, \quad (4.32)$$

where  $g_k/(s + g_k)$  is a low-pass filter used to prevent abrupt change of  $k$ . From  $|A + B| \leq |A| + |B|$ ,  $k_m$  and  $k_s$  have the value between  $0.0 \sim 1.0$ . In free operation, both gains become near to 1.0 since  $\hat{i}_s^{ext}$  is almost 0. On the other hand, in contact state, the numerators in (4.31) and (4.32) approach to 0 due to the through variable controller. Therefore, the state of compensator can be varied by checking the values of through variables.

#### 4.5 Simulations of Using Phase-lag Compensator

From here, verification of the proposed system is conducted. Firstly, the use of phase-lag compensator is tested by simulations. The parameter values for the simulations are shown in Table 4.1. As for the communication delay,  $T = 0.1$  s with random jitter (normal distribution with 0.005 s variance, the values are limited by  $0.09 \sim 0.11$  s) is simulated. In this section, different from the experiments in other

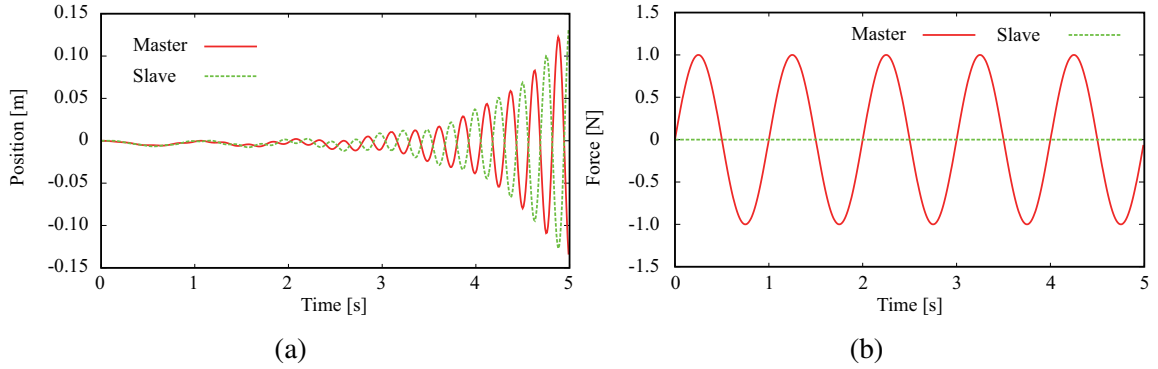


Fig. 4-10: Simulation results of bilateral control without phase-lag compensation (free operation). (a) Position responses. (b) Force responses.

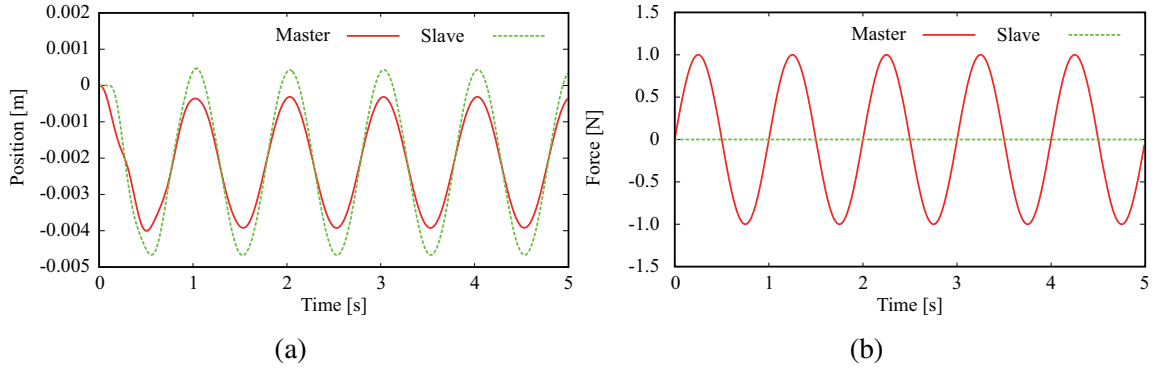


Fig. 4-11: Simulation results of bilateral control with phase-lag compensation (free operation). (a) Position responses. (b) Force responses.

chapters, following is used for across-variable control

$$C_e = \frac{1}{s}K_p + K_e. \quad (4.33)$$

This is PI controller and this considers the integral of across variables. In mechanical system, position corresponds to the variable. Practically, synchronization of position is desired in many cases of teleoperation. As for the control laws, the ones shown in (4.13) and (4.14) are used. Then, the AVF references are controlled locally by the observer for through variables. The simulation results of the system without the compensator are shown in Fig. 4-10. Here, sinusoidal through variable (force in mechanical system) is applied to the master system. As shown in Fig. 4-10(a), the system without compensation becomes unstable and responses diverge. The results indicate the adverse effect caused by communication delays between master and slave systems.

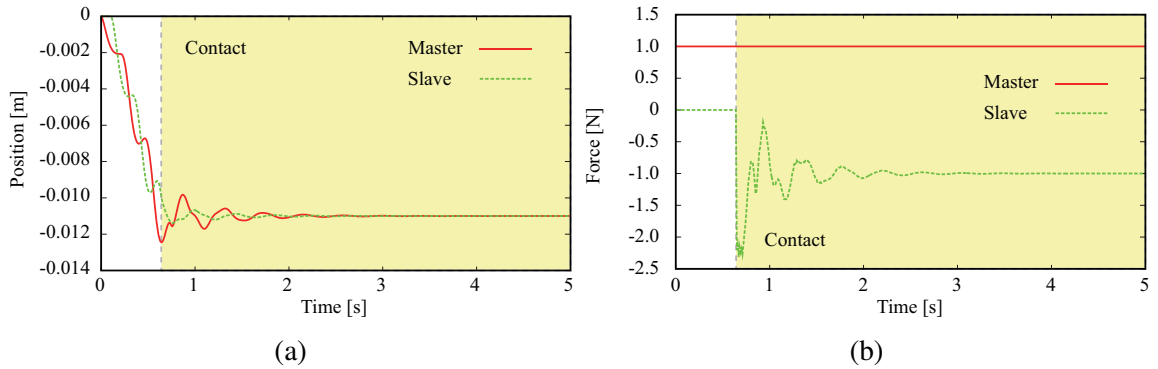


Fig. 4-12: Simulation results of bilateral control without phase-lag compensation (contact motion). (a) Position responses. (b) Force responses.

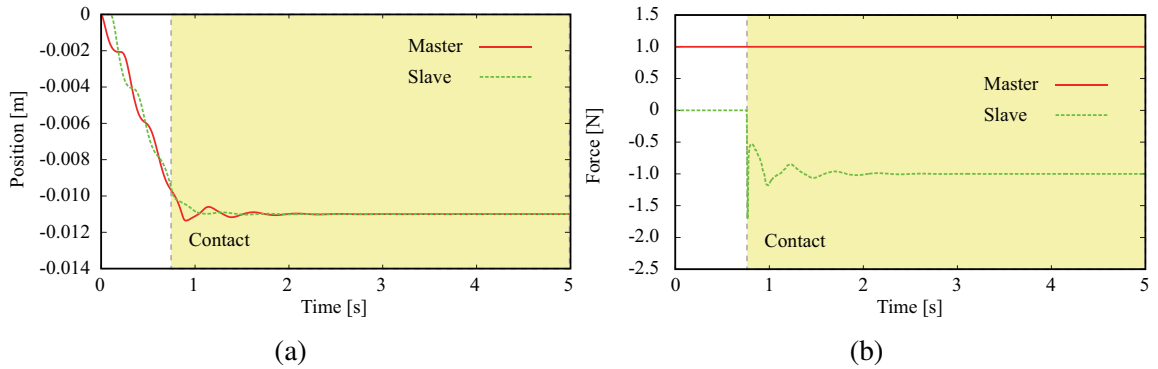


Fig. 4-13: Simulation results of bilateral control with phase-lag compensation (contact motion). (a) Position responses. (b) Force responses.

Fig. 4-11 shows the simulation results when the phase-lag compensator is utilized. In this case, although there remains the amplitude error in position responses, the stability of the system is maintained. The reducing the amplitude of communicated reference of across variable can increase the margin of stability.

Figs. 4-12 and 4-13 show the responses of contact states. As well as the case of free operation, the oscillations in force responses are decreased when the phase-lag compensator is employed. As explained by the analyses of Lyapunov stability, the phase-lag compensator contributes for the stable haptic communication.

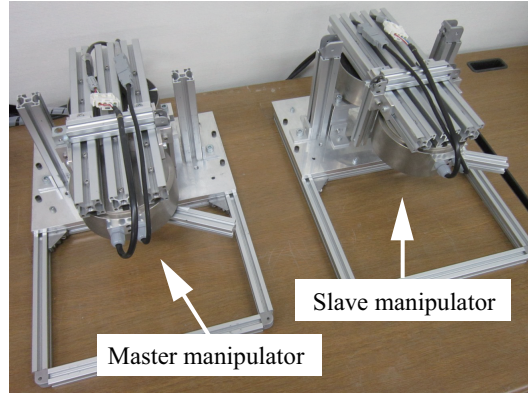


Fig. 4-14: Experimental setup for checking the compensator in through variable control.

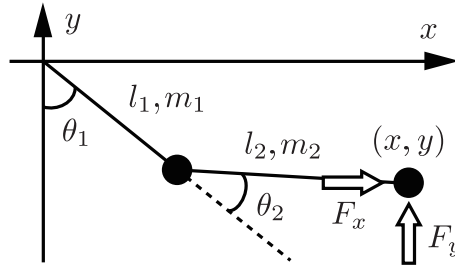


Fig. 4-15: Schematic illustration of 2-link manipulator.

## 4.6 Experiments of Using Compensator for Through Variable Control

Next, the operation of the proposed compensator is checked by experiments.

### 4.6.1 Overview of Experiments (Compensator for Through Variable Control)

Fig. 4-14 shows the setup used for the experiments. The master and slave manipulators in Fig. 4-14 are the 2-link manipulators that consist of two direct drive motors. Here, the motors used for the experiments are from Yasukawa corp. (model number: SGMCS-02BDC41, rated torque: 2.0 Nm, rated current: 1.8 Arms). In the experiments, the lateral ( $x$  direction) and vertical ( $y$  direction) mechanical motions are controlled; (4.19) and (4.20) are prepared for both directions. In the control system, the AVF references in operational space are transformed into joint space, and each joint is controlled robustly. Fig. 4-15 shows the schematic illustration of 2-link manipulator. Here,  $l$ ,  $m$ ,  $\theta$  denote length, mass and angle, respectively. Based on this, the relationship between the AVF in joint space and operational space

Table 4.2: Parameter values used for experiments of controlling 2-link manipulators.

Variables	Value	Unit
P gain of position control (for both directions), $K_p$	600.0	-
Gain for across variable control, $K_e$	49.0	-
Gain for through variable control ( $x$ direction), $K_{ix}$	0.2	-
Gain for through variable control ( $y$ direction), $K_{iy}$	0.5	-
Length of link 1, $l_1$	0.15	m
Length of link 2, $l_2$	0.15	m
Mass of link 1, $m_1$	2.0	kg
Mass of link 2, $m_2$	0.2	kg
Gain for through variable control ( $y$ direction), $K_{iy}$	0.5	-
Phase-lag compensator, $C_{cpe}$	$\frac{0.5s+10.0}{s+10.0}$	-
Cut-off frequency of DOB, $g_{dob}$	100.0	rad/s
Cut-off frequency for deciding gain $k$ , $g_k$	10.0	rad/s
Nominal torque coefficient, $K_{tn}$	1.18	N/A
Nominal inertia of motor, $J_n$	0.0028	kgm <sup>2</sup>

is described as

$$\ddot{\mathbf{x}} = \mathbf{J}_{aco}(\boldsymbol{\theta})\ddot{\boldsymbol{\theta}} + \dot{\mathbf{J}}_{aco}(\boldsymbol{\theta})\dot{\boldsymbol{\theta}}, \quad (4.34)$$

where  $\mathbf{x} = [x, y]^T$  and  $\boldsymbol{\theta} = [\theta_1, \theta_2]^T$ . The  $\mathbf{J}_{aco}$  is a Jacobian matrix, and the elements of the matrix are as follows:

$$\mathbf{J}_{aco} = \begin{bmatrix} J_{11} & J_{12} \\ J_{21} & J_{22} \end{bmatrix}, \quad (4.35)$$

where

$$J_{11} = l_1 \cos \theta_1 + l_2 \cos(\theta_1 + \theta_2) \quad (4.36)$$

$$J_{12} = l_2 \cos(\theta_1 + \theta_2) \quad (4.37)$$

$$J_{21} = l_1 \sin \theta_1 + l_2 \sin(\theta_1 + \theta_2) \quad (4.38)$$

$$J_{22} = l_2 \sin(\theta_1 + \theta_2). \quad (4.39)$$

Therefore, the AVF reference for joint space is calculated by

$$\ddot{\boldsymbol{\theta}}^{ref} = \mathbf{J}_{aco}^{-1}(\boldsymbol{\theta})(\ddot{\mathbf{x}}^{ref} - \dot{\mathbf{J}}_{aco}(\boldsymbol{\theta})\dot{\boldsymbol{\theta}}). \quad (4.40)$$



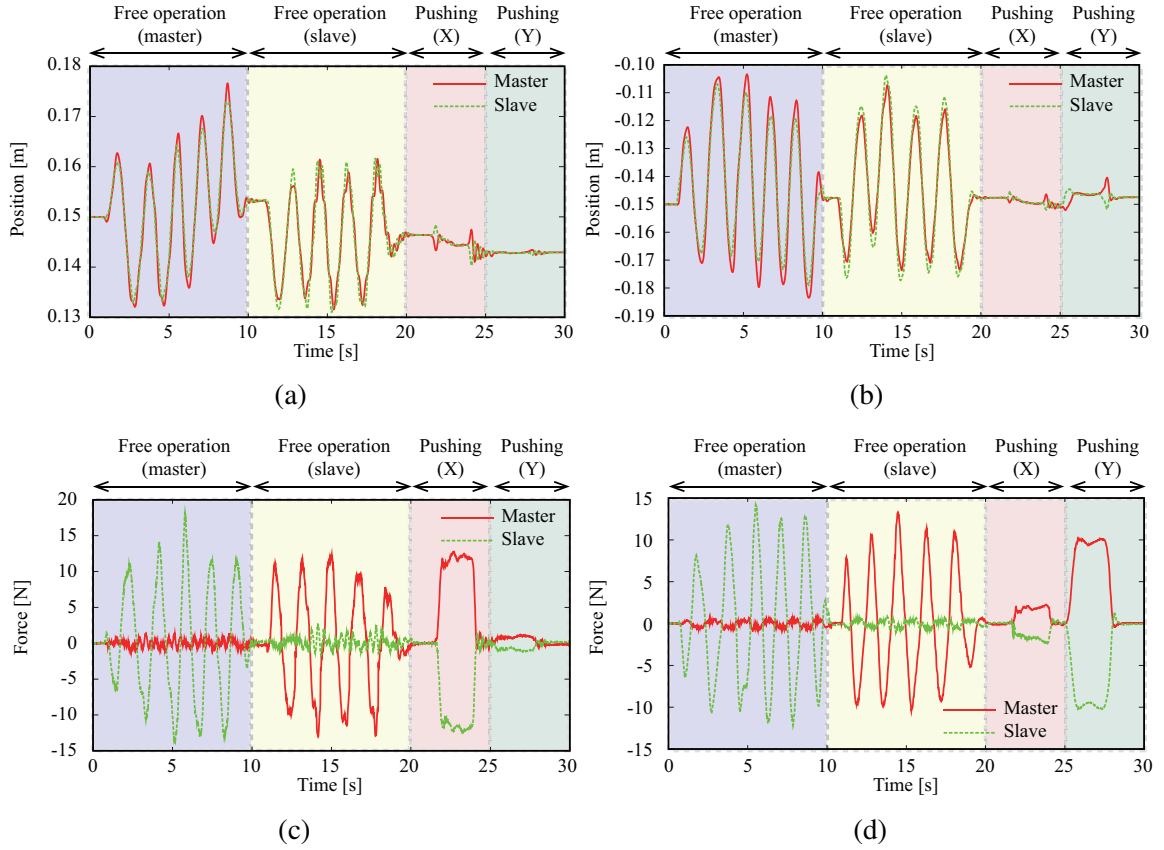


Fig. 4-16: Experimental results of bilateral control under time delay (without compensator). (a) Position responses in  $X$  direction. (b) Position responses in  $Y$  direction. (c) Force responses in  $X$  direction. (d) Force responses in  $Y$  direction.

In this section, the experiments of the system with only phase-lag compensator and the proposed method are conducted. Firstly, the operator manipulates the master system freely, then next the slave system is manipulated. After that, the operators at both sides applies kinesthetic force each other in  $x$  and  $y$  directions. The parameter values used for the experiments are shown in Table 4.2. The communication delays are simulated to be 0.1 s in one way with the 0.003 s variance (the values are limited by 0.09 ~ 0.11 s).

#### 4.6.2 Results of Experiments (Compensator for Through Variable Control)

Fig. 4-16 shows the experimental results of the haptic communication with only phase-lag compensator. As described in the simulations, the system achieves the bilateral control without the diverge of responses. However, as shown in Fig. 4-16, there exist overshoots in position responses (the integral

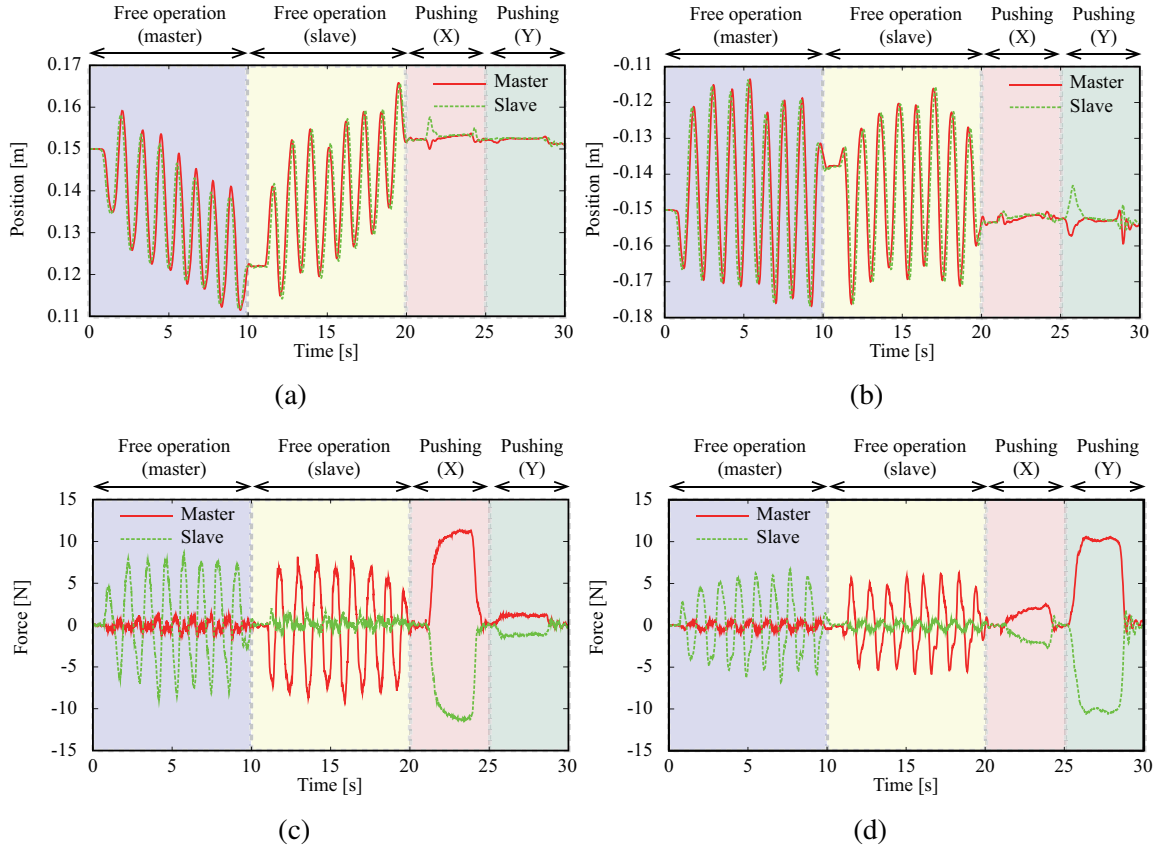


Fig. 4-17: Experimental results of bilateral control under time delay (with compensator). (a) Position responses in  $X$  direction. (b) Position responses in  $Y$  direction. (c) Force responses in  $X$  direction. (d) Force responses in  $Y$  direction.

of across variables). This is the adverse effect caused by communication delays. As for the contacting operations, the steady state errors are not observed. Since the system has symmetric control laws, the performance stays same for master-manipulation and slave-manipulation.

The experimental results of the proposed system are shown in Fig. 4-17. Different from the results of conventional system, the position overshoots are suppressed; the free operation of master system is purely reproduced. The suppression of overshoots is valid also for the free operation of slave side. In contact operation, as well as the conventional case, the steady state errors are not observed. In a sense that the responses in free operation are improved while maintaining the performance of contact operation same, the proposed system has superiority over the conventional system.

The responses of variable gains  $k$  in control of  $x$  and  $y$  directions are shown in Fig. 4-18. In free operation, the gains are near to 1.0, whereas those drop to 0.0 in contact operation. The gains changed

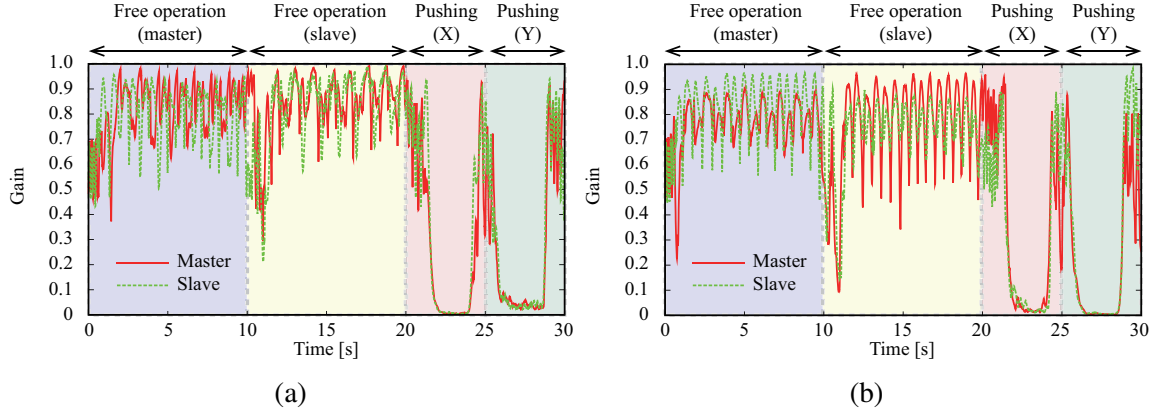


Fig. 4-18: Values of compensator gain  $k$ . (a)  $k$  for control in  $X$  direction. (b)  $k$  for control in  $Y$  direction.

to realize the Fig. 4-7, and it is shown that the proposed algorithm appropriately works according to the state of haptic communication.

## 4.7 Experiments of Comparison Using Hybrid Parameters

Lastly, the proposed method is compared quantitatively by using hybrid parameters.

### 4.7.1 Overview of Experiments (Comparison Using Hybrid Parameters)

When position is employed instead of velocity, the hybrid parameters are re-defined as

$$\begin{bmatrix} F_m^{ext} \\ X_m \end{bmatrix} = \begin{bmatrix} H_{11} & H_{12} \\ H_{21} & H_{22} \end{bmatrix} \begin{bmatrix} X_s \\ -F_s^{ext} \end{bmatrix}, \quad (4.41)$$

where  $X$  and  $F$  denote position and force, respectively. In practical situations, there can be the cases in which the operator contacts with slave side and manipulate the system. Considering this, ensuring the duplex manipulation can extend the applicability of the bilateral control system [105]. Similar to the content in Chapter 2, the inverse of (4.41) is derived as

$$\begin{aligned} \begin{bmatrix} F_s^{ext} \\ X_s \end{bmatrix} &= \frac{1}{\Delta} \begin{bmatrix} H_{11} & H_{12} \\ H_{21} & H_{22} \end{bmatrix} \begin{bmatrix} X_m \\ -F_m^{ext} \end{bmatrix} \\ &= \begin{bmatrix} H'_{11} & H'_{12} \\ H'_{21} & H'_{22} \end{bmatrix} \begin{bmatrix} X_m \\ -F_m^{ext} \end{bmatrix}, \end{aligned} \quad (4.42)$$

where

$$\Delta = H_{12}H_{21} - H_{11}H_{22}. \quad (4.43)$$

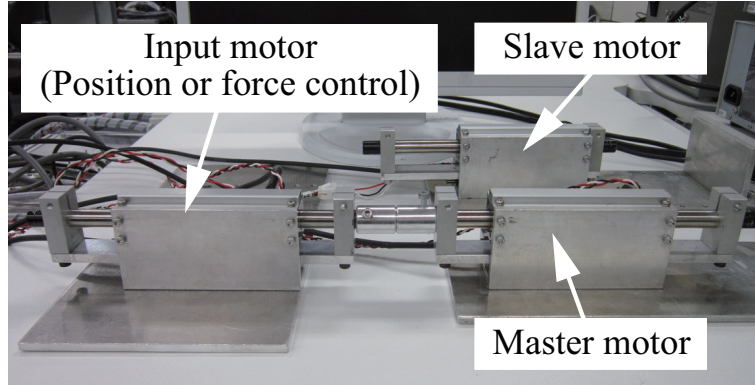


Fig. 4-19: Experimental setup used for comparing with other compensation methods.

Table 4.3: Parameter values used for comparative methods.

Parameter	Description	Value
$g_{cdob}$	Cut-off frequency of CDOB	20.0 rad/s
$C_{dm}$	Amount of FDD	$\frac{70.0s}{s+10.0}$

Moreover, it is able to define the value  $R = H/H'$  as “symmetric ratio.” The values of hybrid parameters can be measured by applying constraint conditions. For instance,  $H_{12}$ ,  $H_{21}$ ,  $H'_{12}$  and  $H'_{21}$  are derived by

$$H_{12} = \left. \frac{F_{mM}^{ext}}{-F_{sM}^{ext}} \right|_{X_{sM}=0} \quad (4.44)$$

$$H_{21} = \left. \frac{X_{mM}}{X_{sM}} \right|_{F_{sM}^{ext}=0} \quad (4.45)$$

$$H'_{12} = \left. \frac{F_{sS}^{ext}}{-F_{mS}^{ext}} \right|_{X_{mS}=0} \quad (4.46)$$

$$H'_{21} = \left. \frac{X_{sS}}{X_{mS}} \right|_{F_{mS}^{ext}=0} \quad (4.47)$$

Here, the subscripts  $M$  and  $S$  mean that operator is at master and slave side, respectively. For example,  $F_{sM}^{ext}$  denotes the amount of force detected at slave system when operator is contacting with master system. The constraint conditions can easily be implemented;  $X_s = 0$  and  $F_s^{ext} = 0$  are realized by mechanical fixing of the slave system and removing object at slave system, respectively. In this chapter, these are used for evaluating the methods.

The experimental setup is shown in Fig. 4-19. In the setup, position or force control is conducted in input motor, and the responses of bilateral control are used for calculating the hybrid parameters. The linear motors used for the experiments are from GMC hillstone corp. (model number: S120Q, rated

force: 9.7 N, rated current: 0.24 A). For the control, chirp signal (frequency: 2.0 ~ 20.0 rad/s) is applied as the control command. The responses are processed by Fourier transformation and the ratio of amplitude is calculated.

In experiments, three methods are compared: proposed method, system with only phase-lag compensator and CDOB with FDD system. The control laws of the system with phase-lag compensator are given by (4.13) and (4.14). The CDOB (Communication Disturbance Observer) with FDD (Frequency Domain Damping) is the method shown in [57], whose control laws as the generalized form are

$$\dot{e}_m^{ref} = C_e(e^{-Ts}e_s - e_m + e_d) - C_{dm}e_m - C_i(e^{-Ts}\hat{i}_s^{ext} + \hat{i}_m^{ext}) \quad (4.48)$$

$$\dot{e}_s^{ref} = C_e(e^{-Ts}e_m - e_s) - C_{dm}e_s - C_i(e^{-Ts}\hat{i}_m^{ext} + \hat{i}_s^{ext}), \quad (4.49)$$

where  $C_{dm}$  is used for velocity damping.  $e_d$  is a compensation value of CDOB, which is calculated as

$$e_d = \frac{1}{C_{dvn}s + g_{cdob}}(i_{sm}^{ref} - C_{dvn}e^{-Ts}\dot{e}_s) \quad (4.50)$$

$$\dot{i}_{sm}^{ref} = C_{dvn}C_e(e_m - e_{sm}) = C_{dvn}\dot{e}_{sm}, \quad (4.51)$$

where the subscripts *cdob* and *sm* denote communication disturbance observer and slave model, respectively. As for  $C_e$ , the one shown in (4.33) is used. CDOB regards the communication delay as the kind of disturbance, and compensates for it based on the structure of disturbance observer. Then, FDD is utilized for improving the stability in contact operation. The parameter values for CDOB-based FDD scheme are shown in Table 4.3. As for the other parameters, those shown in Table 4.1 were used.

## 4.7.2 Results of Experiments (Comparison Using Hybrid Parameters)

Fig. 4-20 shows the measurement results of the parameters  $H_{12}$ ,  $H_{21}$ ,  $H'_{12}$  and  $H'_{21}$ . As explained in the simulations in this chapter, the phase-lag compensator enhances the stability of the system. However, as shown in the part labeled “normal,” the resonance peaks remain in the hybrid parameters. The existence of peaks means that the overshoots can occur in tracking of position or force in bilateral control. The CDOB with FDD succeeds in suppressing the peak in  $H_{21}$ . Therefore, it is expected that the system achieves better position tracking than the system with phase-lag compensator. On the other hand, the resonance peak in force control still exists as represented by  $H_{12}$ . The peaks can be adjusted by changing the amount of FDD. However, the increase of damping leads to the degradation of operability; the manipulation becomes heavier. The proposed system reduces the peaks of both parameters  $H_{12}$  and

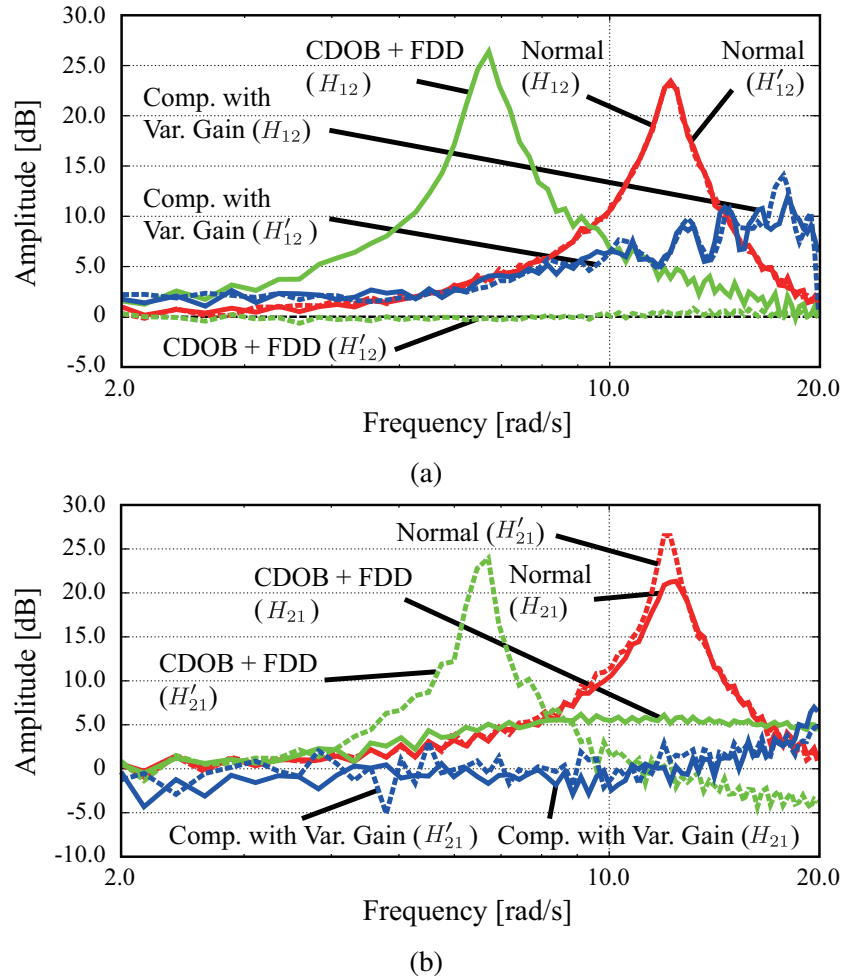


Fig. 4-20: Experimental results of measuring hybrid parameters. (a) Results of measuring  $H_{12}$  and  $H'_{12}$ . (b) Results of measuring  $H_{21}$  and  $H'_{21}$ .

$H_{21}$ . Since the gain in  $C_{cpi}$  is varied in the control, the plots are slightly deviated from sub-optimal state (0 dB). However, the reduction of the peaks indicate the validity of using the compensator  $C_{cpi}$ .

One of the advantages of the proposed system is that it maintains the symmetric property. Since the almost same control laws are employed in the proposed system, there exists little difference between the parameter  $H$  and the inversed one  $H'$ . Fig. 4-21 shows the symmetric ratios of the comparative methods. The system with phase-lag compensator also utilizes same control laws, thus the ratios become 0 dB. On the other hand, the master and slave systems in CDOB with FDD type have different controllers, and the ratios are deviated from 0 dB in this case. Whether the system should have the flat ratio characteristics depends on the application of the system; however, at least it is able to say that the proposed system can

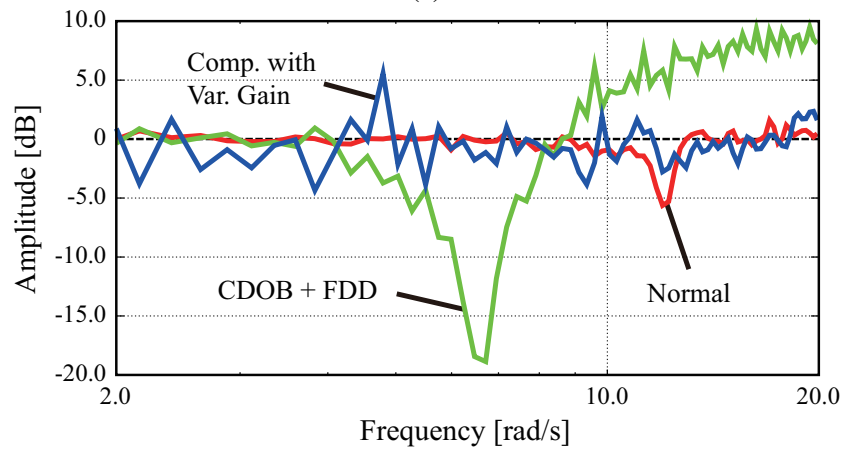
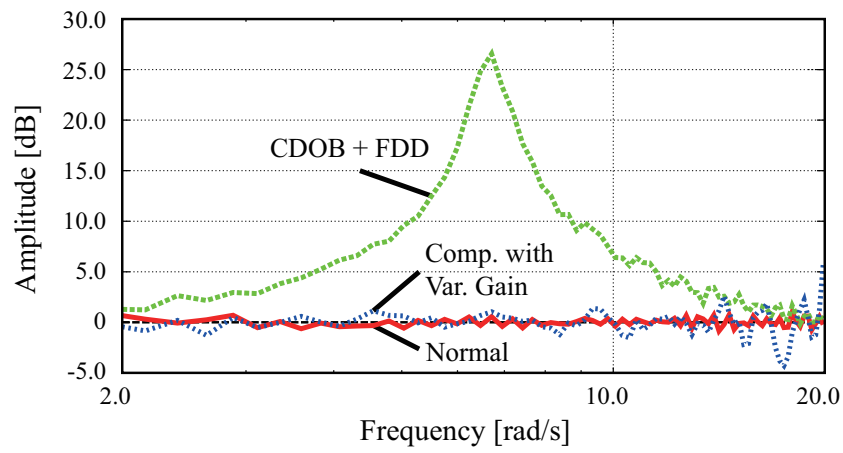


Fig. 4-21: Experimental results of measuring symmetric ratios. (a) Symmetric ratio  $R_{12}$ . (b) Symmetric ratio  $R_{21}$ .

recover the performance of the haptic communication under communication delay while maintaining the symmetric property of the bilateral control system.

## 4.8 Summary of Chapter 4

In this chapter, the compensator in through variable controller for bilateral control under communication delay was proposed. The time-delay existing between master and slave systems easily degrade the performance of haptic communication; the overshoots can appear and the system becomes unstable in the worst case. For increasing the stability margin, phase-lag compensator was firstly employed in this study. The use of the compensator was analyzed using bond graph, and the tests were conducted by the simulations. Using the system with the phase-lag compensator as the base system, the proposed compensator for through variable control was constructed. The compensator was derived from the hybrid parameters of bilateral control, and the compensation filter that can achieve the sub-optimal performances of  $H_{12}$  and  $H_{21}$  were shown. In order to address the steady state errors in contact operation caused by the direct use of the filter, the adaptive algorithm was constructed. The designed system was checked its validity by experiments. The experiments on the haptic communication using 2-link manipulators showed that the proposed compensator can enhance the performance of free operation. Then, in the comparison of control schemes by measurement of hybrid parameters, it was verified that the proposed system can recover the performance characteristics of hybrid parameters.

In practical application of haptic technologies, the communication delay that can adversely affect the performance is thought to be non-negligible factor. As described in the section of experiments, the system is effective for recovering the performance of haptic communication.



## Chapter 5

# Bilateral Control Between Systems with Different Control Performances

---

### 5.1 Introduction

In this chapter, bilateral control with different control performances is treated [97]. The AVF-based 4ch bilateral control, which is the generalized form of enhanced bilateral control beyond the kinds of physical systems, is expected to enable the bilateral reproduction between even different kinds of physical powers e.g. the mutual transformation of mechanical and thermal system. This feature can extend the applicability of haptic technologies. However, as is well known, the bandwidths of electrical motor and thermal device are totally different. Also in the case of typical bilateral control of kinesthetic sensations, there can be the cases in which the master and slave systems employ the different types of actuators, causing the gap of potential device performances. As well as the communication delay handled in Chapter 4, the response performance of the haptic device is also one of the problems that the practical application of haptic technologies face. When the bandwidths of master and slave devices are different, the AVF-control of one system appears to be imperfect for the other system. In this case, the control system can become unstable, thus making the remote communication of haptic sensation difficult.

For addressing this problem, this research conducts analyses on the modal space of bilateral control system. The imperfectness of AVF control induces the interference of across and through variable controls; the error in controlling one variable adversely work as the disturbance in the control of the other variable. In order to suppress the interference terms, this study constructs the disturbance observer in the common modal space [106]: the control space of through variables. Since the difference of bandwidths

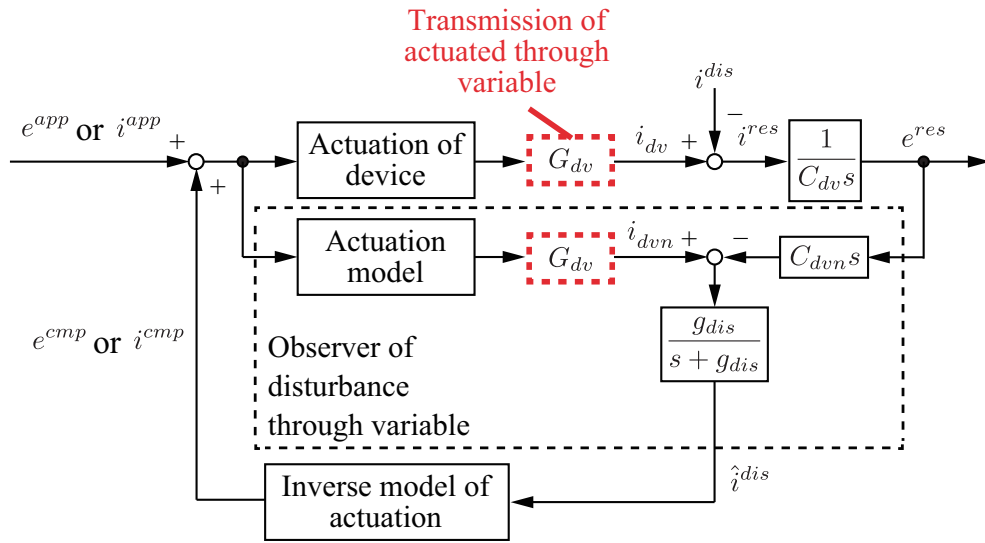


Fig. 5-1: AVF control of haptic device that has imperfect transmission characteristics.

exists, the compensation input is processed so as not to make the compensation term itself the interference factor again. By the proposed method, the unstable oscillation in bilateral control is decreased, and the performance of the haptic communication is recovered. The validity of the proposal is tested by experiments of mechanical and thermal haptic communications.

The contents in this chapter are as follows. In Section 5.2, the problems of using the devices with different control performances for bilateral control is explained. When the difference is not negligible, the AVF control of one system appears to be imperfect for the other system. Next, the modal spaces of the bilateral control system are analyzed in Section 5.3. The modal spaces are derived by adding or subtracting the AVF references of master and slave systems. According to the analyses, it turns out that the interference between across and through variable controls appears. The compensation for the interference terms are considered in Section 5.4. As the proposal, the disturbance observer is constructed in common modal space, and the compensation input is processed so as not to make the compensation itself becomes the interference again. In Section 5.5, the effectiveness of using the compensator is discussed. In Section 5.6, the experiments of bilateral control in which the performance of the master system is degraded are conducted. In the last section, conclusions are stated.

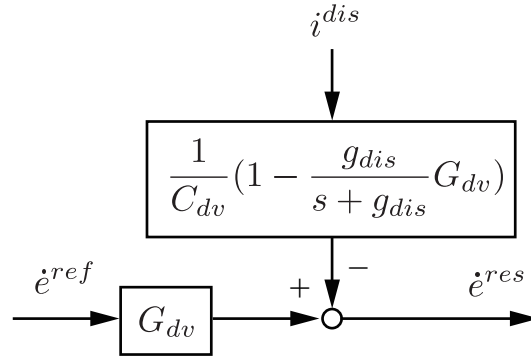


Fig. 5-2: Equivalent block diagram of the AVF control.

## 5.2 Bilateral Control Between Different Control Performances

Firstly, the Fig. 5-1 shows the AVF control of device with imperfect transmission characteristics. Here,  $G_{dv}$  denotes the transfer function of the characteristics. When  $G_{dv} = 1.0$ , it means that the generated through variable is directly transmitted to the passive C element of the device  $C_{dv}$ . However, there can be cases that the certain time is needed to transmit the through variable or the damping elements suppress the amount of facilitated variable.  $G_{dv}$  represents such kind of factors, and it can degrade the total performance of haptic communication. In this dissertation, it is assumed that the  $G_{dv}$  can be described by first order low-pass filter as

$$G_{dv} = \frac{g_{dv}}{s + g_{dv}}. \quad (5.1)$$

In estimating the disturbance through variable  $i^{dis}$ , observer for through variable is employed also in this case. The problem exists in compensating for the disturbance; the inverse model of actuation as well as the inversed transfer function  $G_{dv}$  should be utilized for compensating for the disturbance factor perfectly. However, it is difficult to derive the  $G_{dv}^{-1}$ , since the unstable poles appear when  $G_{dv}$  is described by time-delay element. In the case that  $G_{dv}$  is a low-pass filter, its inversed form may cause the large gain in high frequency band. In order to avoid this, only the inverse model of actuation is applied for calculating the compensation term. In this case, the response of across variable flow becomes

$$\dot{e}^{res} = G_{dv} \dot{e}^{ref} - \frac{1}{C_{dv}} \left(1 - \frac{g_{dis}}{s + g_{dis}} G_{dv}\right) i^{dis}. \quad (5.2)$$

The transfer function is illustrated as the block diagram as shown in Fig. 5-2. When  $G_{dv} = 1.0$ , the  $i^{dis}$  can be suppressed well by increasing the cut-off frequency of the observer  $g_{dis}$ . However if it is

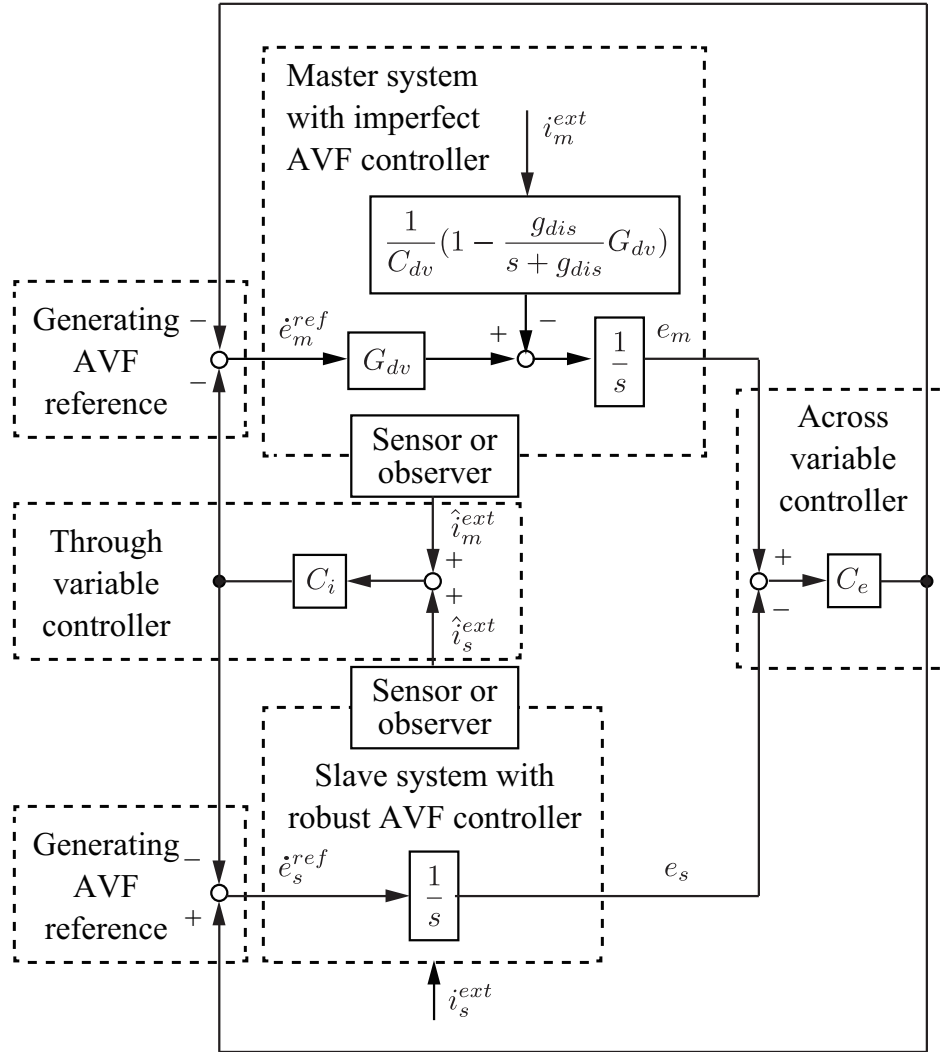


Fig. 5-3: AVF-based 4ch bilateral control with different control performances.

not the case, the suppression performance is limited by  $G_{dv}$ . In the case that the  $G_{dv}$  is low-pass filter, the imperfect disturbance suppression in high frequency band. Moreover, the  $G_{dv}$  also limits the control of across variable flow  $\dot{e}^{ref}$ . The imperfect transmission characteristics cause the degradation of AVF control.

Fig. 5-3 shows the block diagram of AVF-based 4ch bilateral control in which the master system employs the device with narrow bandwidth. In the control system, the AVF reference is calculated as

$$\dot{e}_m^{ref} = C_e(e_s - e_m) - C_i(\hat{i}_m^{ext} + \hat{i}_s^{ext}) \quad (5.3)$$

$$\dot{e}_s^{ref} = C_e(e_m - e_s) - C_i(\hat{i}_m^{ext} + \hat{i}_s^{ext}). \quad (5.4)$$

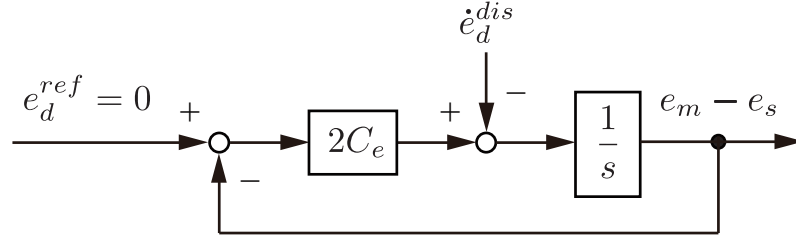


Fig. 5-4: Differential modal space of the bilateral control.

These are same as (3.4) and (3.5) in Chapter 3. However, since the AVF control at the slave system, the AVF responses become

$$\dot{e}_m = G_{dv}C_e(e_s - e_m) - G_{dv}C_i(\hat{i}_m^{ext} + \hat{i}_s^{ext}) - \frac{1}{C_{dv}} \left( 1 - \frac{g_{dis}}{s + g_{dis}} G_{dv} \right) i_m^{ext} \quad (5.5)$$

$$\dot{e}_s = C_e(e_m - e_s) - C_i(\hat{i}_m^{ext} + \hat{i}_s^{ext}). \quad (5.6)$$

Here, it is assumed that  $i^{dis} = i^{ext}$ . Therefore, the actual control is different between master and slave systems, and the performance of haptic communication is degraded. The details on this are explained in the following section.

### 5.3 Analyses on Modal Space of Bilateral Control Between Different Bandwidths

In order to analyze the operation of the bilateral control, analyses on modal spaces are conducted. There are two kinds of modal spaces in bilateral control: differential and common modal spaces. The former one corresponds to the control of across variable, while the latter does to the control of through variable. The subtraction of (5.5) from (5.6) yields

$$s(e_m - e_s) = -2C_e(e_m - e_s) - \dot{e}_d^{dis}, \quad (5.7)$$

where  $\dot{e}_d^{dis}$  denotes the disturbance term in differential modal space, whose contents are shown below

$$\dot{e}_d^{dis} = (1 - G_{dv})C_e(e_m - e_s) - (1 - G_{dv})C_i(i_m^{ext} + i_s^{ext}) + \frac{1}{C_{dv}} \left( 1 - \frac{g_{dv}}{s + g_{dv}} G_{dv} \right) i_m^{ext}. \quad (5.8)$$

The block diagram of the modal space is shown in Fig. 5-4. Actually, the  $\dot{e}_d^{dis}$  contains the term of across variable control, and the loop transfer function in the modal space is degraded. Therefore,  $C_e$  has to be designed carefully so that the control in the space is conducted stably. When  $G_{dv} = 1$  and  $g_{dis} \rightarrow \infty$

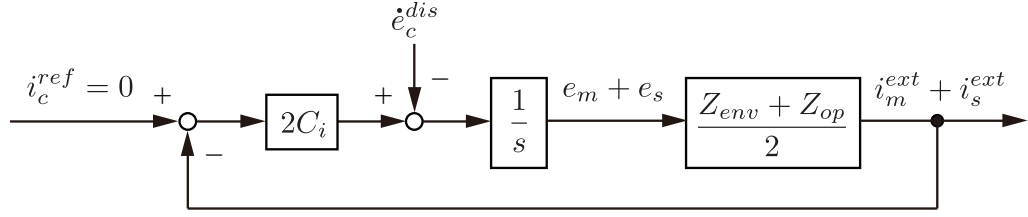


Fig. 5-5: Common modal space of the bilateral control.

the disturbance term  $\dot{e}_d^{dis}$  approach to zero. However, if it is not the case, the error of through variable control comes into the differential modal space as the disturbance term. This is an interference between the across and through variable controls.

The summation of AVF responses yields the common modal space of bilateral control system

$$s(e_m + e_s) = -2C_i(i_m^{ext} + i_s^{ext}) - \dot{e}_c^{dis}, \quad (5.9)$$

where

$$\dot{e}_c^{dis} = -(1 - G_{dv})C_e(e_m - e_s) + (1 - G_{dv})C_i(i_m^{ext} + i_s^{ext}) + \frac{1}{C_{dv}} \left( 1 - \frac{g_{dv}}{s + g_{dv}} G_{dv} \right) i_m^{ext}. \quad (5.10)$$

The block diagram of the modal space is shown in Fig. 5-5. For constructing the feedback loop in the modal space, the relation between the summation of across variables and that of through variables are approximated by  $(Z_{env} + Z_{op})/2$ , where  $Z_{op}$  denotes the impedance of operator contacted with master system [57]. As well as the differential modal space, the disturbance term that contains the error of across variable exists. When the interference terms are compensated, it is expected that the performance of the bilateral control is recovered.

## 5.4 Construction of Compensator for Interference Terms

For addressing the problem, compensator for the interference in common modal space is proposed in this research [97]. In the proposed system, the interference term  $\dot{e}_c^{dis}$  is estimated by constructing the disturbance observer in the modal space.

Transformation of (5.9) yields

$$\dot{e}_c^{dis} = -2C_i(i_m^{ext} + i_s^{ext}) - s(e_m + e_s). \quad (5.11)$$

By comparing the reference of through variable control with the summation of AVF responses, it becomes possible to estimate the  $\dot{e}_c^{dis}$ . This is the kind of disturbance observer, and it is constructed as shown in

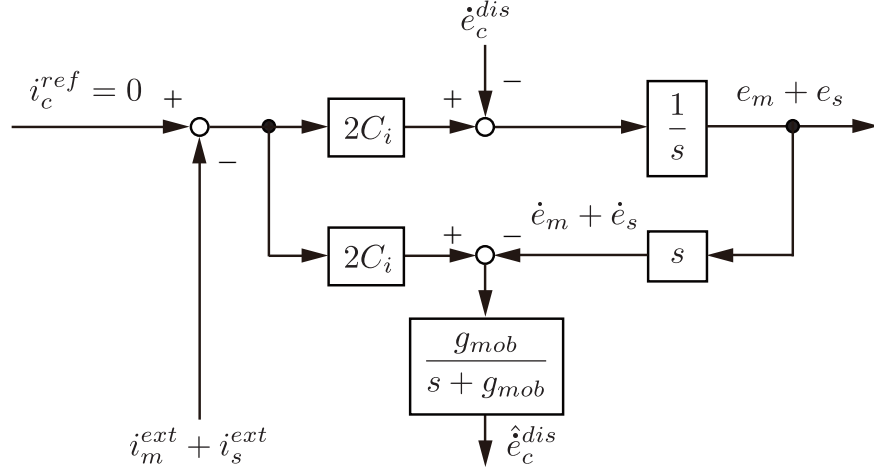


Fig. 5-6: Disturbance observer constructed in common modal space.

Fig. 5-6. Here, the subscript *mob* denotes the modal disturbance observer [106]. The low-pass filter is used to decrease the noise amplification caused by differentiating the responses of across variables. By the observer, the information on the amount of the interference disturbance becomes available.

The disturbance observer enables the suppressing the disturbance factor by the positive feedback of the estimated information. However, in the case of systems with different performances, the direct positive feedback can cause another problem. The AVF references including the direct compensation become

$$\dot{e}_m^{ref} = C_e(e_s - e_m) - C_i(\hat{i}_m^{ext} + \hat{i}_s^{ext}) + \frac{1}{2}\hat{e}_c^{dis} \quad (5.12)$$

$$\dot{e}_s^{ref} = C_e(e_m - e_s) - C_i(\hat{i}_m^{ext} + \hat{i}_s^{ext}) + \frac{1}{2}\hat{e}_c^{dis}. \quad (5.13)$$

However, the AVF responses actually become

$$\dot{e}_m = G_{dv}C_e(e_s - e_m) - G_{dv}C_i(\hat{i}_m^{ext} + \hat{i}_s^{ext}) - \frac{1}{C_{dv}} \left( 1 - \frac{g_{dis}}{s + g_{dis}} G_{dv} \right) i_m^{ext} + G_{dv} \frac{1}{2} \hat{e}_c^{dis}. \quad (5.14)$$

$$\dot{e}_s = C_e(e_m - e_s) - C_i(\hat{i}_m^{ext} + \hat{i}_s^{ext}) + \frac{1}{2}\hat{e}_c^{dis}. \quad (5.15)$$

Therefore, subtraction of (5.14) and (5.15) yields

$$s(e_m - e_s) = -2C_e(e_m - e_s) - \dot{e}_d^{dis} - (1 - G_{dv})\hat{e}_c^{dis}. \quad (5.16)$$

From (5.16), it turns out that the direct compensation induces the another interference term for differential modal space. This may deteriorate the control performance of across variables.

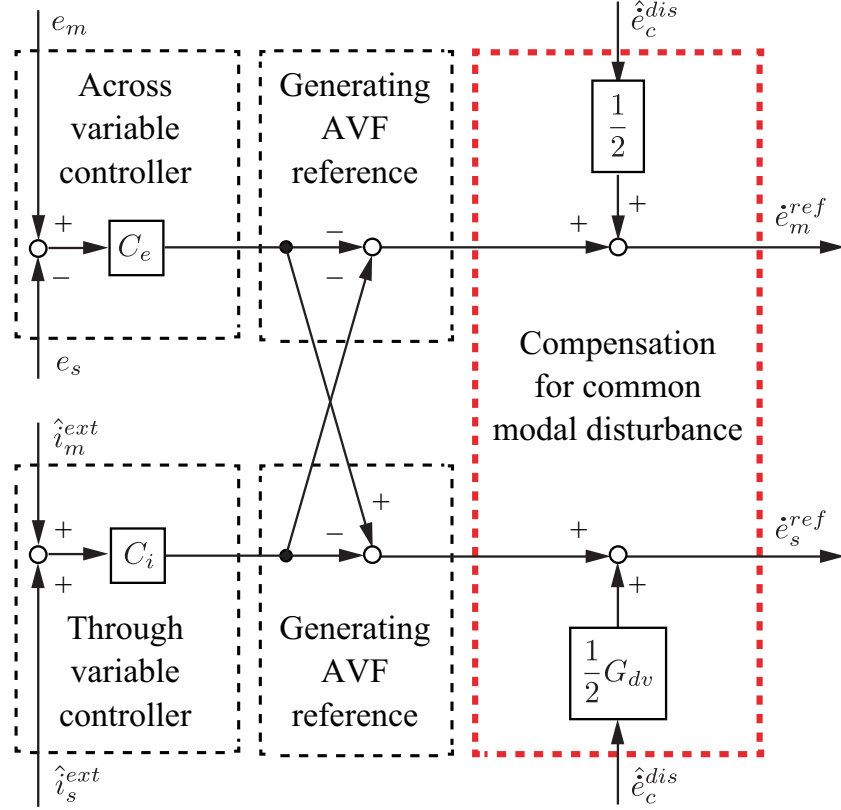


Fig. 5-7: Compensation for the disturbance in common modal space.

In order to avoid the problem, this research proposes the process of compensation shown in Fig. 5-7. The modified AVF references are shown as

$$\dot{e}_m^{ref} = C_e(e_s - e_m) - C_i(\hat{i}_m^{ext} + \hat{i}_s^{ext}) + \frac{1}{2}\hat{e}_c^{dis} \quad (5.17)$$

$$\dot{e}_s^{ref} = C_e(e_m - e_s) - C_i(\hat{i}_m^{ext} + \hat{i}_s^{ext}) + \frac{1}{2}G_{dv}\hat{e}_c^{dis}. \quad (5.18)$$

Here, the model of transmission characteristics  $G_{dv}$  is multiplied to the estimated disturbance term. In this case, the subtraction of AVF responses does not yield the additional interference term. Therefore, it is able to enhance the performance of the common modal space without effecting on the differential one.

The summation of AVF responses become

$$s(e_m + e_s) = -2C_i(\hat{i}_m^{ext} + \hat{i}_s^{ext}) - \left(1 - \frac{g_{mob}}{s + g_{mob}}G_{dv}\right)\hat{e}_c^{dis}. \quad (5.19)$$

The block diagram of the common modal space with the proposed compensation is shown in Fig. 5-8. Although the compensation again limited by the bandwidth of device characteristics, the interference



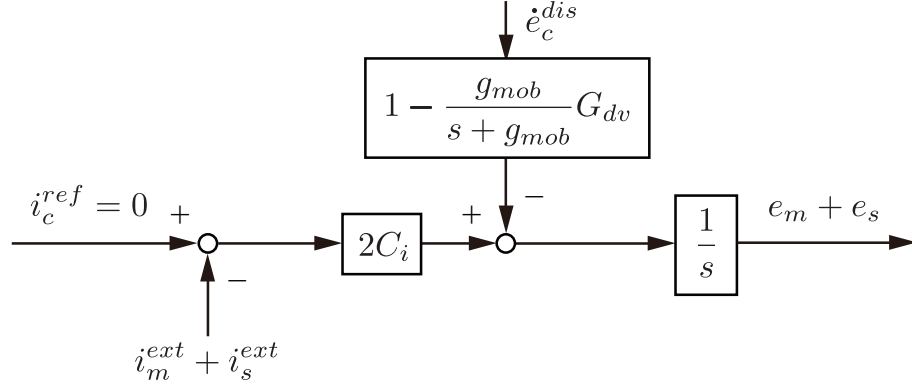


Fig. 5-8: Equivalent block diagram of common modal space.

in the band can be suppressed. Therefore, the performance of the bilateral control is expected to be enhanced.

## 5.5 Discussions on the Effectiveness of Using the Compensator

In this section, the use of the proposed compensator is discussed. From the assumption  $\hat{e}_c^{dis} = \dot{e}_c^{dis}$  and (5.17), (5.18) and (5.10), following is derived

$$\begin{aligned} \dot{e}_m^{ref} &= C_e \left( \frac{3}{2} - \frac{1}{2} G_{dv} \right) (e_s - e_m) - C_i \left( \frac{3}{2} - \frac{1}{2} G_{dv} \right) (\hat{i}_m^{ext} + \hat{i}_m^{ext}) \\ &\quad + \frac{1}{2C_{dv}} \left( 1 - \frac{g_{dis}}{s + g_{dis}} G_{dv} \right) i_s^{ext} \end{aligned} \quad (5.20)$$

$$\begin{aligned} \dot{e}_s^{ref} &= C_e \left( 1 - \frac{1}{2} G_{dv} + \frac{1}{2} G_{dv}^2 \right) (e_m - e_s) - C_i \left( 1 - \frac{1}{2} G_{dv} + \frac{1}{2} G_{dv}^2 \right) (\hat{i}_m^{ext} + \hat{i}_s^{ext}) \\ &\quad + \frac{G_{dv}}{2C_{dv}} \left( 1 - \frac{g_{dis}}{s + g_{dis}} G_{dv} \right) i_m^{ext}. \end{aligned} \quad (5.21)$$

From these, it is able to comprehend that the proposed compensation method equivalently adjusts the controller of across and through variables in order to avoid the generation of interference terms. Supposing that the  $G_{dv}$  is a low-pass filter, the gains of controllers in slave system are slightly increased, whereas those in master system is decreased. Therefore, similar effects can be obtained by the direct tuning of controller gains. The superiorities of using the compensator over the direct tuning are as follows:

- The amount of interference term can easily be estimated from the output of through variable controller and single derivation of across variables.

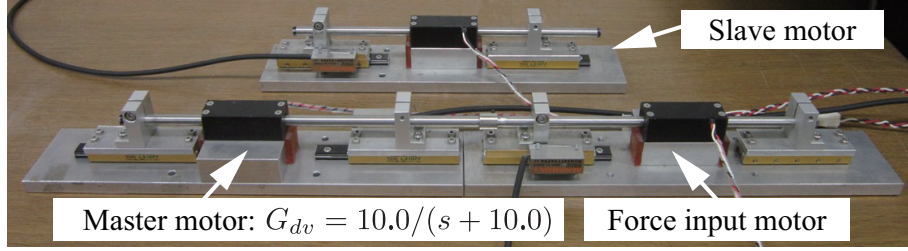


Fig. 5-9: Experimental setup of bilateral control (different bandwidths, mechanical system).

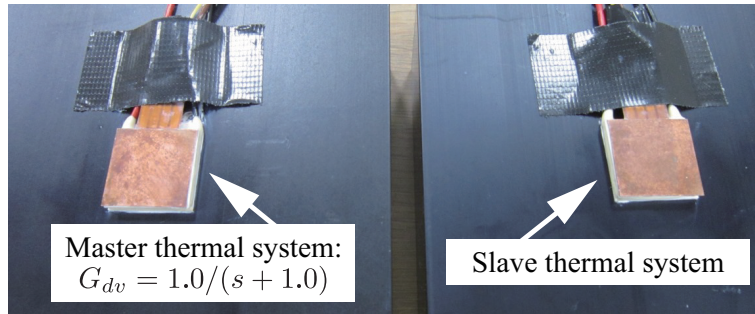


Fig. 5-10: Experimental setup of bilateral control (different bandwidths, thermal system).

- The direct tuning needs the model of  $G_{dv}$  and  $G_{dv}^2$ , whereas the proposed compensator only needs  $G_{dv}$ . This simplifies the implementation of algorithms.
- The proposed compensation considers the imperfectness of compensation for  $i_m^{dis}$ . The slave system that has wider bandwidth helps to compensate for it.

## 5.6 Experiments of Bilateral Control with Different Bandwidths

For verifying the compensation for disturbance factors in modal spaces, experiments are conducted.

### 5.6.1 Overview of Experiments (Bilateral Control with Different Bandwidths)

In this dissertation, mechanical and thermal systems are experimented, respectively. The experimental setups for respective physical systems are shown in Figs. 5-9 and 5-10. The setups are same with those shown in Figs. 3-15 and 3-16 except one thing; low-pass filter is implemented at the master system to mimic the bandwidth limitation. Here, the filters are set at  $10.0/(s + 10.0)$  and  $1.0/(s + 1.0)$ , respectively. In the mechanical bilateral control system, the constant electrical current with the value of 0.3 A is applied by the force input motor. Then, rigid aluminum block was set at the master system. Here,

CHAPTER 5 BILATERAL CONTROL BETWEEN SYSTEMS WITH DIFFERENT CONTROL PERFORMANCES

---

Table 5.1: Parameter values for bilateral control with different control performances (mechanical system).

Variables	Value	Unit
Gain for across-variable control, $C_e$	50.0	-
Gain for through-variable control, $C_i$	1.0	-
Nominal mass of motor, $M_n$	0.23	kg
Nominal torque coefficient, $K_{tn}$	3.33	N/A
Cut-off frequency of DOB, $g_{dis}$	500.0	rad/s
Cut-off frequency of pseudo derivative, $g_{pd}$	500.0	rad/s
Cut-off frequency of DOB in modal space, $g_{mob}$	500.0	rad/s

Table 5.2: Parameter values for bilateral control with different control performances (thermal system).

Variables	Value	Unit
Gain for across-variable control, $C_e$	1.0	-
Gain for through-variable control, $C_i$	1.0	-
Nominal capacitance of device, $C_{dvn}$	2.0	J/K
Nominal Seebeck coefficient, $\alpha_{sn}$	0.03	V/K
Cut-off frequency of DOB, $g_{dis}$	2.0	rad/s
Cut-off frequency of DOB in modal space, $g_{mob}$	0.5	rad/s

the input motor pushes slave motor since the degradation in haptic communication was observed more in this configuration. The bilateral control begins with the state in which the slave system is contacted with the environmental block. In the thermal system, aluminum block with ambient temperature is set at the slave system, and cooled aluminum plate is put on the master system. With these configurations, the systems with and without the proposed compensation method are compared. In the control of thermal systems, existence of large resistive element that actually effects on the AVF control should be considered. Concretely speaking, in controlling the thermal system, the estimation algorithm should take the damping characteristics of AVF control in high-frequency band into account. The modified estimation of disturbance in common modal space for thermal system is shown as

$$\hat{e}_c^{dis} = \frac{3.0}{s + 3.0} \left\{ -2C_i(i_m^{ext} + i_s^{ext}) + G_{dv}\hat{e}_c^{dis} \right\} - s(e_m + e_s). \quad (5.22)$$

Here, the first order filter corresponds to the modification. The parameter values used for the experiments are shown in Tables 5.1 and 5.2.

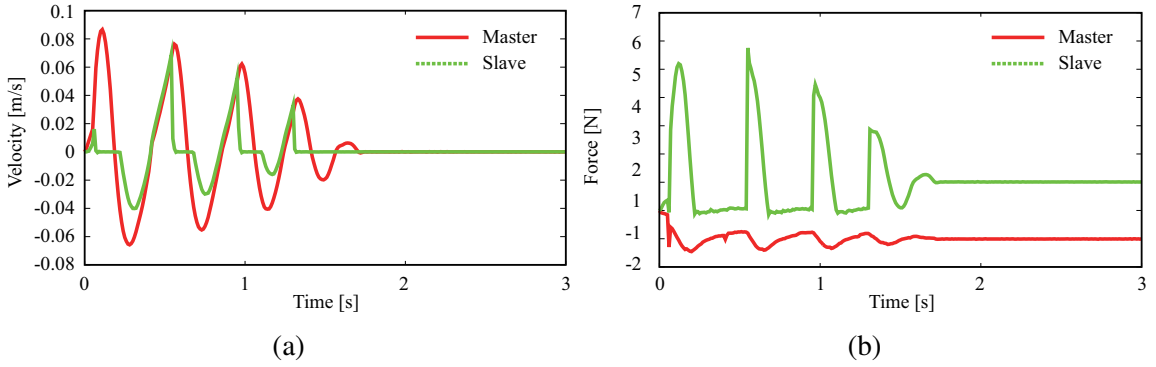


Fig. 5-11: Experimental results of system with different control performances (mechanical control, without compensation). (a) Velocity responses. (b) Force responses.

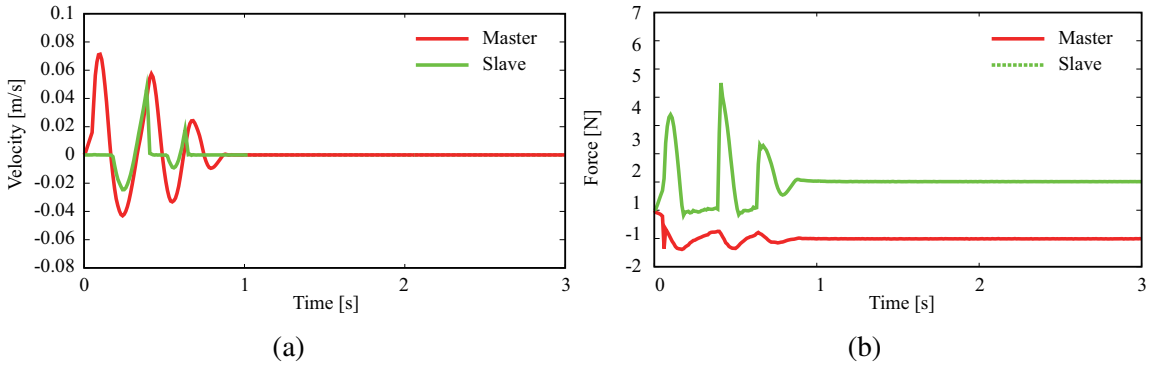


Fig. 5-12: Experimental results of system with different control performances (mechanical control, proposed system). (a) Velocity responses. (b) Force responses.

### 5.6.2 Results of Experiments (Bilateral Control with Different Bandwidths)

Firstly, the experimental results of the system without the compensation are explained. Fig. 5-11 shows the velocity (across variable) and force (through variable) responses of the experiment. Due to the difference of the control bandwidths, the AVF control is realized well only one side of the bilateral control. Thus, the physical powers of master and slave systems don't synchronize well, causing the hunting phenomena in contact with the rigid material. When the master and slave sides employed different haptic devices, there exist the possibilities that such phenomena occur in haptic communication.

Then, Fig. 5-12 shows the results of the proposed system. The proposed compensation method considers the disturbance in common modal space, and it decreases the interference between the across and through variable controls. Compared with the case of without compensation, the hunting phenomena are suppressed and more stable haptic communication is realized. As described in Section 5.5, it is

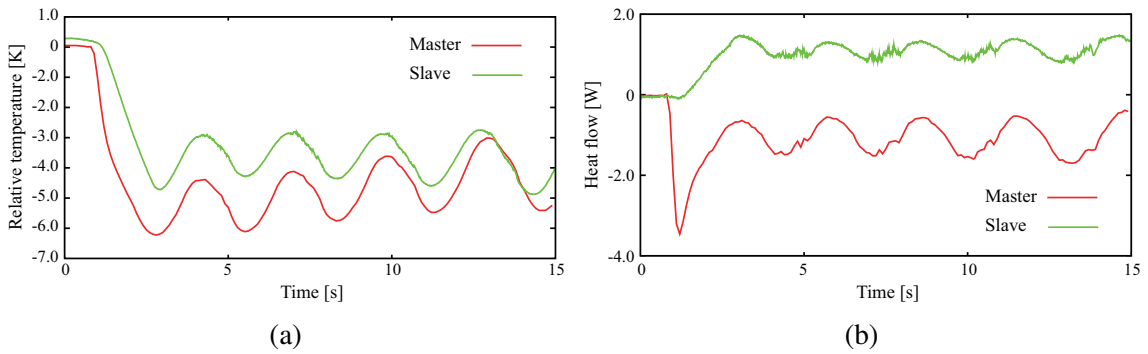


Fig. 5-13: Experimental results of system with different control performances (thermal control, without compensation). (a) Temperature responses. (b) Heat flow responses.

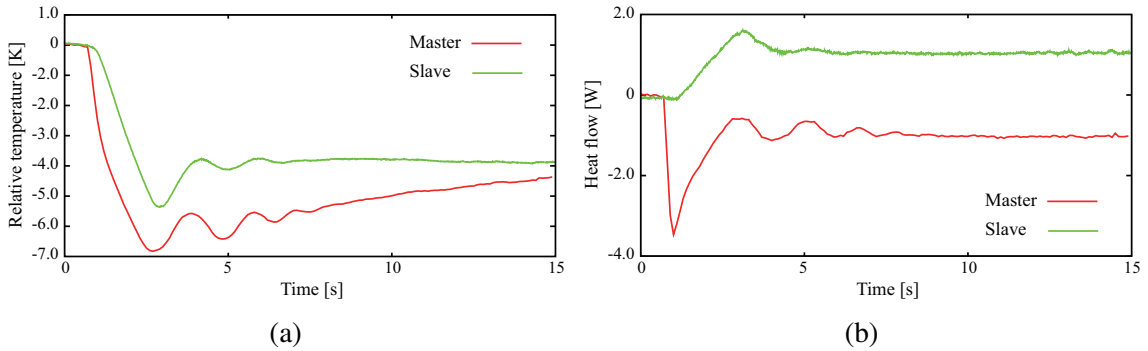


Fig. 5-14: Experimental results of system with different control performances (thermal control, proposed system). (a) Temperature responses. (b) Heat flow responses.

thought that the compensator succeeded in adjusting the across and through variable controllers of master and slave systems so that the interference in common modal space does not occur. The decrease of the vibrations indicates the validity of the proposed compensation observer.

Figs. 5-13 and 5-14 show the results of thermal haptic communication. As for the thermal control, the tendencies are similar with the case of mechanical control; the responses become oscillatory when no compensation is conducted. On the other hand, the proposed compensation method succeeds in reducing the vibration. Therefore, it is thought that the developed observer can also decrease the disturbance in common mode of thermal system. By the experimental results, it is confirmed that the proposal is effective for recovering the performance of haptic communication with different bandwidths.

## **5.7 Summary of Chapter 5**

In this chapter, compensation method for bilateral control between the systems with different control bandwidths was proposed. The difference of the bandwidth can be observed in the practical application of haptic technologies. When the haptic device has inferior control performance, the AVF control becomes incomplete. Then, according to the analyses on modal spaces, it was shown that the imperfectness becomes the interference between the control of across and through variables. Thus, the total performance of the haptic communication is degraded. In order to address the problem, the disturbance observer was constructed in the common modal space as the proposal. Since the direct use of the estimated value can additionally generate the interference term, the estimated disturbance was processed by the model of transmission characteristics. By the compensation, the influence of the interference on the through variable control was suppressed. The validity of the proposal was tested by the experiments of kinesthetic and thermal haptic communications.

## Chapter 6

# Bandwidth Improvement of Thermal Haptic Display for Mixed Rendering of Mechanical and Thermal Sensations

---

### 6.1 Introduction

As described in Chapter 5, the control bandwidth of the haptic system significantly influences on the performance of haptic communication. The bandwidth has to be increased as large as possible for providing the fine haptic power rendering. In the introduction, it is explained that the mixed rendering of mechanical and thermal sensations is the important theme in this dissertation. In this case, the bandwidth of the thermal system becomes more important, since there exists the difference of bandwidths between master and slave systems and it induces the interference terms in control. In the thermal system, heat flow sensor can be the one of the factors that degrades the response characteristics of the device. Obtaining the information on heat flow, which corresponds to the through variable in generalized physical systems, is essential and heat flow sensor is generally employed for the objective. However, the sensor usually consists of two temperature sensors inserted with the thermal resistive element, and the thermal capacitance of the sensor becomes larger than that of single temperature sensor. The system with larger thermal capacitance requires more heat flow to realize the same temperature variation, and the increase of the capacitance should be suppressed for enhancing the response characteristics of thermal systems.

Based on the background, the observer-based estimation method of heat inflow is proposed in this chapter [98]. The spread of thermal energy is able to be comprehended by distributed parameter systems, and the model of the system is derived. Then, the heat inflow observer is constructed as the alternative

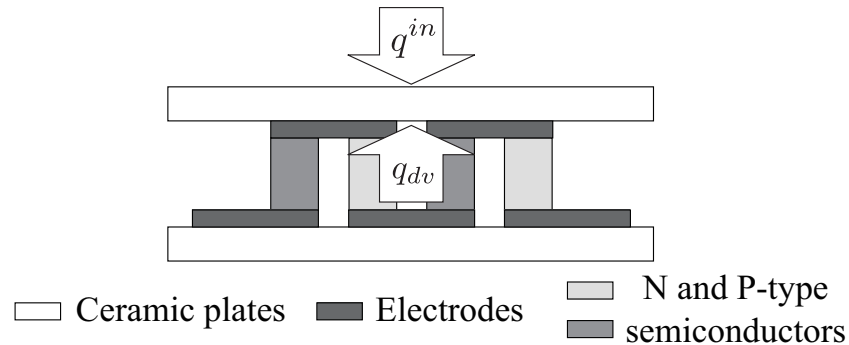


Fig. 6-1: Structure of Peltier device.

tool for obtainment of information on heat inflow. Since the observer only requires temperature sensor whose thermal capacitance is much smaller than that of heat flow sensor, the enhancement of response performance by the decrease of thermal capacitance is expected. This feature is thought to be beneficial not only for thermal bilateral control but also for the mixed rendering of mechanical and thermal sensations, which is one of the important objectives in this dissertation.

The contents of this chapter are as follows. First, the modeling of Peltier device is conducted in Section 6.2. Here, the distributed parameter systems of the consisting parts in the device are derived. Next, the heat inflow observer is constructed in Section 6.3. For the implementation of the observer, the approximation with the consideration on the poles and zeros of transfer functions is explained. The heat flow sensor is used for evaluation; however, since the sensor itself has thermal capacitance and outputs the different signals in transient state, the modification of the sensor output is described in Section 6.4. The identification of thermal contact resistance needed in the proposed observer is explained in Section 6.5. The estimation by proposed observer is experimentally tested in Section 6.6. Then, the effectiveness of using the observer for the haptic communication is checked by the thermal bilateral control and mixed rendering of mechanical and thermal sensations in Sections 6.7 and 6.8. The conclusive remarks are described in the last section.

## 6.2 Modeling of Thermoelectric Device

### 6.2.1 Structure and Coordinates of Thermoelectric Device

First, the configuration of thermal device is explained for deriving the heat inflow observer. Fig. 6-1 shows the structure of the device. Here,  $q^{in}$  denotes the heat inflow, which corresponds to the through



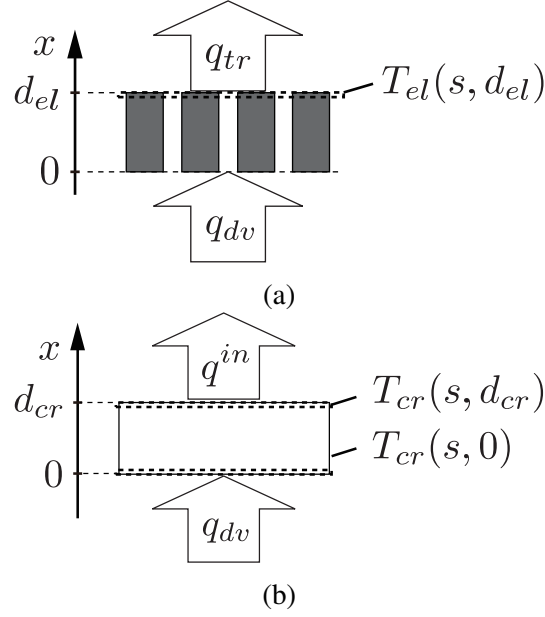


Fig. 6-2: Coordinates of each part of the device. (a) Coordinate of electrode part. (b) Coordinate of ceramic plate part.

variable  $i^{ext}$  in pseudo bond graphs. Then,  $q_{dv}$  represents the heat flow facilitated based on Peltier effect by the thermal actuator. The device consists of ceramic plates, electrodes and semiconductors. N and P-type semiconductors are prepared, and heat flow  $q_{dv}$  (corresponds to  $i_{dv}$  in generalized physical systems) is facilitated in this part. The ceramic plates are used for mechanical support of the device and insulation of electrical circuits. As for the  $q_{dv}$ , Ioffe's model [65] described below is well-known in the field of thermoelectric device:

$$q_{dv} = -\alpha_s(T_{amb} + T_c)I + \frac{1}{2}R_e I^2 + \frac{1}{R_{dv}}(T_h - T_c). \quad (6.1)$$

Here,  $T$ ,  $\alpha_s$ ,  $R$ , and  $R_e$  are the temperature, Seebeck coefficient, thermal resistance, and electrical resistance, respectively. Then, subscripts  $c$ ,  $h$ , and  $amb$  denote the cold-side temperature, hot-side temperature, and ambient temperature, respectively. The first term in (6.1) is the Peltier effect, and the facilitation of the heat flow is altered by Joule heat and heat conduction at the interior of the device.

In the device, the heat flow  $q_{dv}$  is transmitted to ceramic plate that is an interface with external environment through electrodes. Based on this point, this research defines the coordinate of the electrodes and ceramic plates. From here, followings are assumed for the simplicity of the discussion:

- Thermal energy is transferred only in the vertical direction  $x$ .

- Thermal characteristics (such as thermal diffusivity) does not change according to temperature.
- Temperature is uniform in same plane, including the electrode part which is actually distributed.

These assumptions are same as those made in Chapter 2. The coordinate of each part is shown in Fig. 6-2. In Fig. 6-2,  $d$  denotes thickness of the part. Then, the subscripts  $el$  and  $cr$  represent the electrode and ceramic plate, respectively. Between the electrode and the plate, transferring heat flow  $q_{tr}$  is defined as follows in order to link the parts

$$q_{tr}(t) = \frac{1}{R_{con}}(T_{el}(t, d_{el}) - T_{cr}(t, 0)), \quad (6.2)$$

where  $R_{con}$  denotes the thermal contact resistance between electrode and ceramic plate. The defined coordinates are used to derive the thermal equations of each part.

## 6.2.2 Transfer Functions of Electrode and Ceramic Plate Part

The thermal equation of the electrode based on the defined coordinate is described as follows:

$$\frac{\partial T_{el}(t, x_{el})}{\partial t} = a_{el} \frac{\partial^2 T_{el}(t, x_{el})}{\partial x^2} \quad (6.3)$$

$$T_{el}(0, x_{el}) = 0 \quad (6.4)$$

$$\frac{\partial T_{el}(t, 0)}{\partial x} = -\frac{1}{\lambda_{el} A_{el}} q_{dv}(t) \quad (6.5)$$

$$\frac{\partial T_{el}(t, d_{el})}{\partial x} = -\frac{1}{\lambda_{el} A_{el}} (-q_{tr}(t)), \quad (6.6)$$

where

$$a = \frac{\lambda}{\rho c}. \quad (6.7)$$

Here,  $\lambda$ ,  $A$ ,  $a$ ,  $\rho$  and  $c$  denote thermal conductivity, area, thermal diffusivity, density and specific heat, respectively. By the Laplace transformation in time domain, the transfer function between heat flows ( $q_{dv}$  and  $q_{tr}$ ) and electrode temperature can be derived as

$$T_{el}(s, x) = \frac{\cosh\left(\sqrt{\frac{s}{a_{el}}}(d_{el} - x)\right)}{\lambda_{el} A_{el} \sqrt{\frac{s}{a_{el}}} \sinh\left(\sqrt{\frac{s}{a_{el}}} d_{el}\right)} q_{dv} + \frac{\cosh\left(\sqrt{\frac{s}{a_{el}}} x\right)}{\lambda_{el} A_{el} \sqrt{\frac{s}{a_{el}}} \sinh\left(\sqrt{\frac{s}{a_{el}}} d_{el}\right)} q_{tr}. \quad (6.8)$$

The surface temperature  $T_{el}(s, d_{el})$  is derived by substituting  $x = d_{sm}$  as

$$T_{el}(s, d_{el}) = \frac{1}{\lambda_{el} A_{el} \sqrt{\frac{s}{a_{el}}} \sinh\left(\sqrt{\frac{s}{a_{el}}} d_{el}\right)} q_{dv} + \frac{\cosh\left(\sqrt{\frac{s}{a_{el}}} d_{el}\right)}{\lambda_{el} A_{el} \sqrt{\frac{s}{a_{el}}} \sinh\left(\sqrt{\frac{s}{a_{el}}} d_{el}\right)} q_{tr}. \quad (6.9)$$

Note that the derived transfer functions include hyperbolic functions. This means that the transfer functions have infinite number of poles and zeros; this can be often observed in modeling the distributed parameter system.

Similarly, the thermal equations of ceramic plate part become

$$\frac{\partial T_{cr}(t, x)}{\partial t} = a_{cr} \frac{\partial^2 T_{cr}(t, x)}{\partial x^2} \quad (6.10)$$

$$T_{cr}(0, x) = 0 \quad (6.11)$$

$$\frac{\partial T_{cr}(t, 0)}{\partial x} = -\frac{1}{\lambda_{cr} A_{cr}} q_{tr}(t) \quad (6.12)$$

$$\frac{\partial T_{cr}(t, d_{cr})}{\partial x} = -\frac{1}{\lambda_{cr} A_{cr}} (-q^{in}(t)). \quad (6.13)$$

Then, the surface and bottom temperature of the plate are derived as

$$T_{cr}(s, 0) = \frac{\cosh\left(\sqrt{\frac{s}{a_{cr}}} d_{cr}\right)}{\lambda_{cr} A_{cr} \sqrt{\frac{s}{a_{cr}}} \sinh\left(\sqrt{\frac{s}{a_{cr}}} d_{cr}\right)} q_{tr} - \frac{1}{\lambda_{cr} A_{cr} \sqrt{\frac{s}{a_{cr}}} \sinh\left(\sqrt{\frac{s}{a_{cr}}} d_{cr}\right)} (-q^{in}) \quad (6.14)$$

$$T_{cr}(s, d_{cr}) = \frac{1}{\lambda_{cr} A_{cr} \sqrt{\frac{s}{a_{cr}}} \sinh\left(\sqrt{\frac{s}{a_{cr}}} d_{cr}\right)} q_{tr} - \frac{\cosh\left(\sqrt{\frac{s}{a_{cr}}} d_{cr}\right)}{\lambda_{cr} A_{cr} \sqrt{\frac{s}{a_{cr}}} \sinh\left(\sqrt{\frac{s}{a_{cr}}} d_{cr}\right)} (-q^{in}). \quad (6.15)$$

### 6.2.3 Block Diagram of Peltier Device

Combination of the transfer functions and (6.2) enables the derivation of block diagram of the thermal actuator. Fig. 6-3 shows the constructed block diagram. Here, the  $T_{cr}(s, d_{cr})$  and nominal amount of  $q_{dv}$  are assumed to be measurable and known. The objective of the research is to estimate the  $q^{in}$  using the model and the available information.

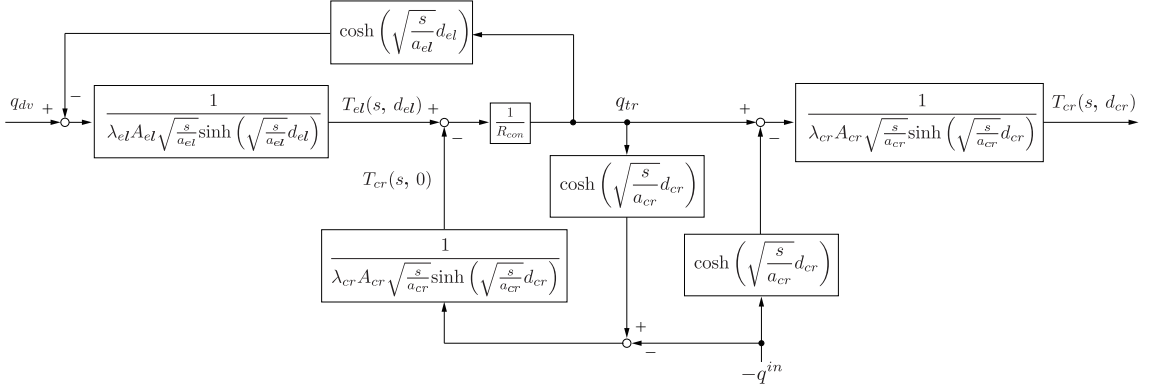


Fig. 6-3: Block diagram of heat transfer in Peltier device.

### 6.3 Heat Inflow Observer

Using the derived model of the Peltier device, the heat inflow observer is constructed.

#### 6.3.1 Construction of Heat Inflow Observer

From Fig. 6-3, the surface temperature of the ceramic plate  $T_{cr}(s, d_{cr})$  is derived as

$$T_{cr}(s, d_{cr}) = \frac{X_{el} X_{cr}}{R_{con} + X_{cr} Y_{cr} + X_{el} Y_{el}} q_{dv} + \frac{X_{cr} Y_{cr} (R_{con} + X_{cr} Y_{cr} + X_{el} Y_{el}) + X_{cr}}{R_{con} + X_{cr} Y_{cr} + X_{el} Y_{el}} q^{in}, \quad (6.16)$$

where

$$X_{cr} = \frac{1}{\lambda_{cr} A_{cr} \sqrt{\frac{s}{a_{cr}}} \sinh\left(\sqrt{\frac{s}{a_{cr}}} d_{cr}\right)} \quad (6.17)$$

$$X_{el} = \frac{1}{\lambda_{sm} A_{el} \sqrt{\frac{s}{a_{el}}} \sinh\left(\sqrt{\frac{s}{a_{el}}} d_{el}\right)} \quad (6.18)$$

$$Y_{cr} = \cosh\left(\sqrt{\frac{s}{a_{cr}}} d_{cr}\right) \quad (6.19)$$

$$Y_{el} = \cosh\left(\sqrt{\frac{s}{a_{el}}} d_{el}\right). \quad (6.20)$$

Then, the heat inflow  $q^{in}$  can be derived by inverse calculation as

$$-\hat{q}^{in} = G(-q_{dv} + HT_{cr}(s, d_{cr})), \quad (6.21)$$

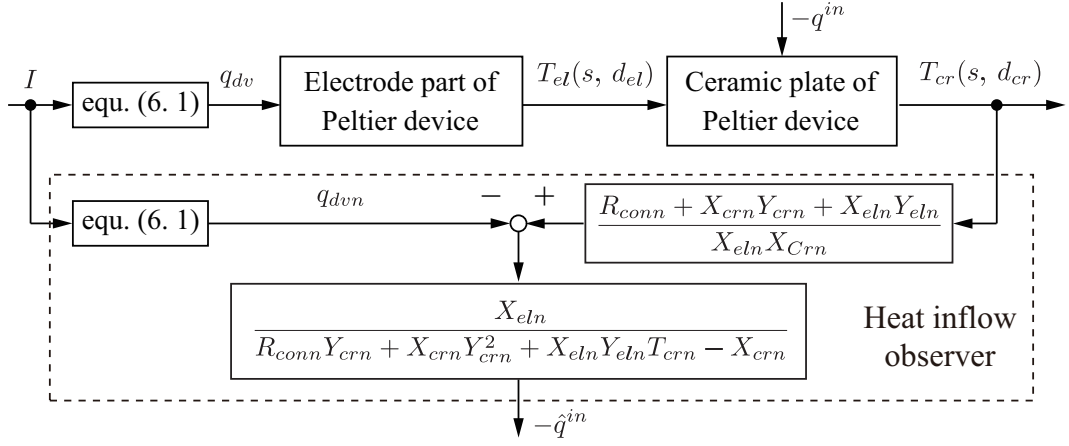


Fig. 6-4: Block diagram of the heat inflow observer.

where

$$G = \frac{X_{eln}}{R_{conn}Y_{crn} + X_{crn}Y_{crn}^2 + Y_{crn}X_{eln}Y_{eln} - X_{crn}} \quad (6.22)$$

$$H = \frac{R_{conn} + X_{crn}Y_{crn} + X_{eln}Y_{eln}}{X_{crn}X_{eln}}. \quad (6.23)$$

(6.21) is the heat inflow observer, and it enables the obtainment of information on the heat inflow without using the heat flow sensor. The block diagram of the observer is shown in Fig. 6-4. In the observer, the heat inflow  $q^{in}$  is estimated by using the nominal model and temperature information on  $T_{cr}(s, d_{cr})$ . Since the estimator only utilizes temperature sensor whose thermal capacitance is much smaller than heat flow sensor, the decrease of total thermal capacitance of the system is expected.

### 6.3.2 Approximation of Heat Inflow Observer

Since the model of the thermal system is described by hyperbolic functions and the transfer functions have infinite number of poles and zeros, the implementation of the observer is actually impossible. In order to address this, the model is approximated and rational polynomials are derived. As stated in Chapter 2, the hyperbolic functions included in the transfer functions are able to be expanded as

$$\sinh\left(\sqrt{\frac{s}{a}}d\right) = \sqrt{\frac{s}{a}}d \left(1 + \frac{d^2}{a\pi^2}s\right) \left(1 + \frac{d^2}{4a\pi^2}s\right) \cdots \quad (6.24)$$

$$\cosh\left(\sqrt{\frac{s}{a}}d\right) = 1.0 \left(1 + \frac{4d^2}{a\pi^2}s\right) \left(1 + \frac{4d^2}{9a\pi^2}s\right) \cdots \quad (6.25)$$

(6.24) and (6.25) mean that the model of the thermal system can be described by the infinite product of the first order filter. A good point in the expansion is that the approximation order can be adjusted

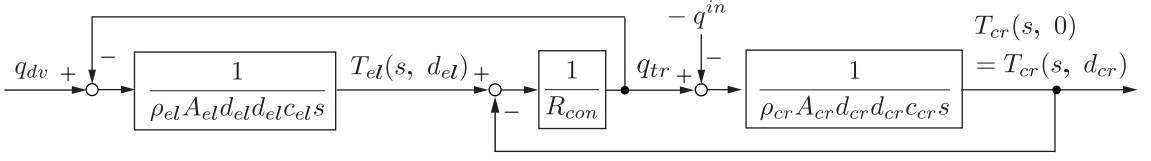


Fig. 6-5: Approximated block diagram of Peltier device.

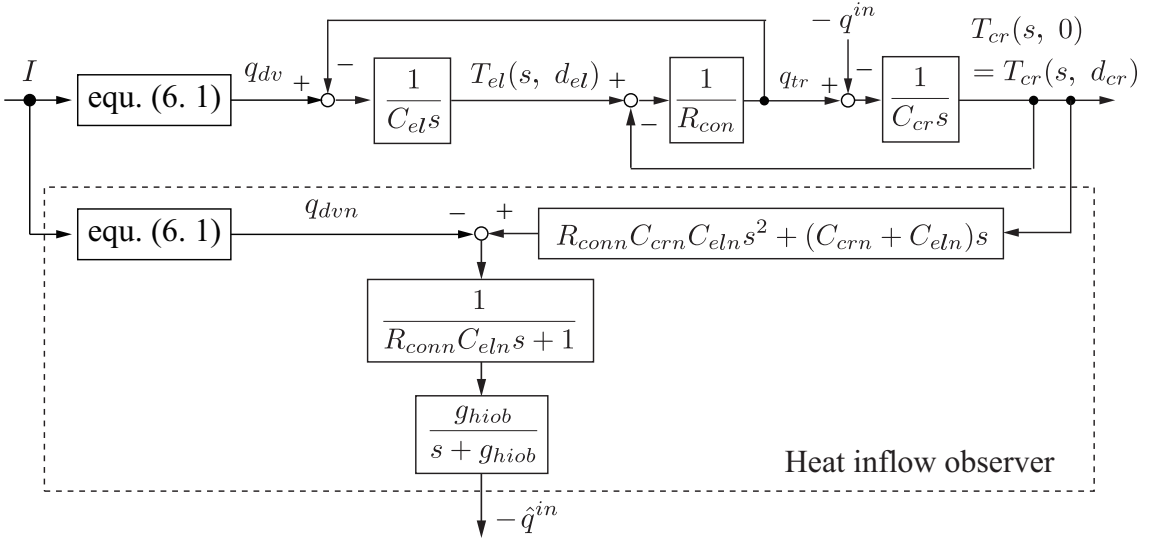


Fig. 6-6: Heat inflow observer based on approximated model.

by checking the locations of roots. Therefore, the bandwidth of validity of the model is clear. In this study, the closest roots  $(-d^2/(a\pi^2))$  and  $-4d^2/(a\pi^2)$  are considered to be far from the bandwidth of the thermal system. The simplest approximation is described below

$$\sinh\left(\sqrt{\frac{s}{a}}d\right) \cong \sqrt{\frac{s}{a}}d \quad (6.26)$$

$$\cosh\left(\sqrt{\frac{s}{a}}d\right) \cong 1.0. \quad (6.27)$$

By the approximation, the block diagram of the Peltier device can be rewritten as Fig. 6-5. The block diagram corresponds to the one modeled by thermal network method [101] in which the temperature nodes are allocated to electrode and ceramic plate part. However, different from the thermal network method, the method explained above can explicitly consider the bandwidth in modeling.

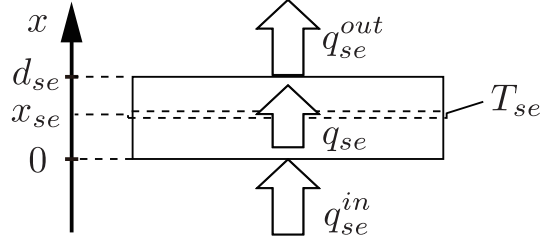


Fig. 6-7: Coordinate of thermal sensor.

In the simplified diagram, surface temperature of the plate is derived as

$$T_{cr}(s, d_{cr}) = \frac{1}{R_{con}C_{cr}C_{el}s^2 + (C_{cr} + C_{el})s} q_{dv} - \frac{R_{con}C_{el}s + 1}{R_{con}C_{cr}C_{el}s^2 + (C_{cr} + C_{el})s} q^{in}, \quad (6.28)$$

where  $C_{cr} = \rho_{cr}A_{cr}d_{cr}c_{cr}$  and  $C_{el} = \rho_{el}A_{el}d_{el}c_{el}$ . These are the thermal capacitance of the element. From the inversed system of (6.28), heat inflow observer is able to be approximated as shown in Fig. 6-6. In the observer, first-order low-pass filter is implemented to make the filters in the observer proper and realizable. The constructed observer estimates the heat inflow by

$$-\hat{q}^{in} = \frac{g_{hiob}}{s + g_{hiob}} I(-q_{dvn} + J T_{cr}(s, d_{cr})), \quad (6.29)$$

where

$$I = \frac{1}{R_{conn}C_{eln}s + 1} \quad (6.30)$$

$$J = R_{conn}C_{crn}C_{eln}s^2 + (C_{crn} + C_{eln})s. \quad (6.31)$$

In this research, the heat inflow observer based on the approximated model is experimented.

## 6.4 Modification of the Output of Heat Flow Sensor

In the experiments, comparison of the observer output with that of heat flow sensor is conducted for evaluation. However, the thermal haptics involves faster temperature variations in rendering among the thermal control engineering. Since the heat flow sensor itself has the thermal capacitance, some of the heat inflow coming into the sensor can be absorbed for changing the sensor temperature. Therefore, in order to enable the evaluation in thermal haptics, the output modification of the heat flow sensor is conducted.

Fig. 6-7 shows a coordinate configuration of thermal sensor. In Fig. 6-7,  $x_{se}$  denotes the location that thermal sensor detects its temperature  $T_{se}$  and heat flow  $q_{se}$ .  $q_{se}^{out}$  and  $q_{se}^{in}$  are heat inflow and outflow, which should be estimated for the evaluation. Note that these heat flows and  $q_{se}$  are different in transient state, which means that temperature is varying.

For the modification of the sensor output, similar techniques with the heat inflow observer are employed. The thermal equations with initial and boundary conditions of the sensor are derived as

$$\frac{\partial T_{se}(t, x)}{\partial t} = a_{se} \frac{\partial^2 T_{se}(t, x)}{\partial x^2} \quad (6.32)$$

$$T_{se}(0, x) = 0 \quad (6.33)$$

$$\frac{\partial T_{se}(t, 0)}{\partial x} = -\frac{1}{\lambda A_{se}} q_{se}^{in}(t) \quad (6.34)$$

$$\frac{\partial T_{se}(t, d_{se})}{\partial x} = -\frac{1}{\lambda A_{se}} q_{se}^{out}(t). \quad (6.35)$$

By the Laplace transformation in time domain, the transfer functions become as follows:

$$\begin{aligned} T_{se}(s, x_{se}) &= -\frac{1}{\lambda A_{se} \sqrt{\frac{s}{a_{se}}}} \frac{\cosh(\sqrt{\frac{s}{a_{se}}} x_{se})}{\sinh(\sqrt{\frac{s}{a_{se}}} d_{se})} q_{se}^{out}(s) \\ &+ \frac{1}{\lambda A_{se} \sqrt{\frac{s}{a_{se}}}} \frac{\cosh(\sqrt{\frac{s}{a_{se}}}(d_{se} - x_{se}))}{\sinh(\sqrt{\frac{s}{a_{se}}} d_{se})} q_{se}^{in}(s) \end{aligned} \quad (6.36)$$

$$\begin{aligned} q_{se}(s, x_{se}) &= \frac{\sinh(\sqrt{\frac{s}{a_{se}}} x_{se})}{\sinh(\sqrt{\frac{s}{a_{se}}} d_{se})} q_{se}^{out}(s) \\ &+ \frac{\sinh(\sqrt{\frac{s}{a_{se}}}(d_{se} - x_{se}))}{\sinh(\sqrt{\frac{s}{a_{se}}} d_{se})} q_{se}^{in}(s). \end{aligned} \quad (6.37)$$

By letting  $T_{se}(s, x_{se}) = Aq_{se}^{out} + Bq_{se}^{in}$  and  $q_{se}(s, x_{se}) = Cq_{se}^{out} + Dq_{se}^{in}$ , heat inflow  $q_{se}^{in}$  and outflow  $q_{se}^{out}$  are able to be derived as

$$q_{se}^{out} = \frac{D}{AD - BC} T_{se}(s, x_{se}) - \frac{B}{AD - BC} q_{se}(s, x_{se}) \quad (6.38)$$

$$q_{se}^{in} = -\frac{C}{AD - BC} T_{se}(s, x_{se}) + \frac{A}{AD - BC} q_{se}(s, x_{se}). \quad (6.39)$$

This is the modification algorithm for thermal sensor part. In implementation, the approximation by (6.26) and (6.27) is conducted. By the modification, amount of heat flowing into thermal sensor can be estimated more accurately, compared with only using the sensor output  $q_{se}$ .



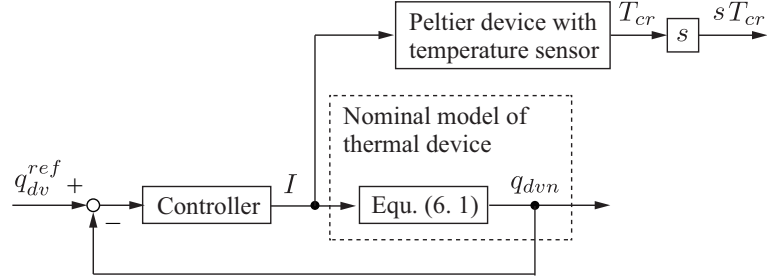


Fig. 6-8: Block diagram for identifying thermal contact resistance.

## 6.5 Identification of Thermal Contact Resistance

The proposed observer requires the nominal values of model; area, thickness, thermal conductivity, specific heat and thermal contact resistance. As for the former four elements, the nominal values can be set by the measurement of size and general physical thermal properties. However, the thermal contact resistance highly depends on the surface state between the contacting materials, and the actual value varies from devices even when the same materials are utilized. Therefore, some identification methods have to be invented.

Fig. 6-8 shows the proposed identification method. In the system, the electrical current is regulated on the basis of nominal actuation model, so that the generated heat flow  $q_{dv}$  corresponds to that of reference value  $q_{dv}^{ref}$ . The transfer function from the heat flow to the variation rate of plate temperature is derived as

$$\frac{sT_{cr}}{q_{dv}} = \frac{1}{R_{con}C_{el}C_{cr}s + C_{el} + C_{cr}}. \quad (6.40)$$

This is the general first-order filter, and the phase difference between the sinusoidal input of  $q_{dv}$  and output  $sT_{cr}$  is derived as

$$\phi = -\tan^{-1} \left( \frac{R_{con}C_{el}C_{cr}\omega}{C_{el} + C_{cr}} \right), \quad (6.41)$$

where  $\phi$  and  $\omega$  are the phase difference and frequency of sinusoidal signals. Therefore, by measuring the phase lag and substituting the nominal values of thermal capacitances, the contact resistance  $R_{con}$  can be identified.

## 6.6 Experiments of Observer-based Heat Inflow Estimation

In this section, experiments are conducted to test the performance of constructed observer.

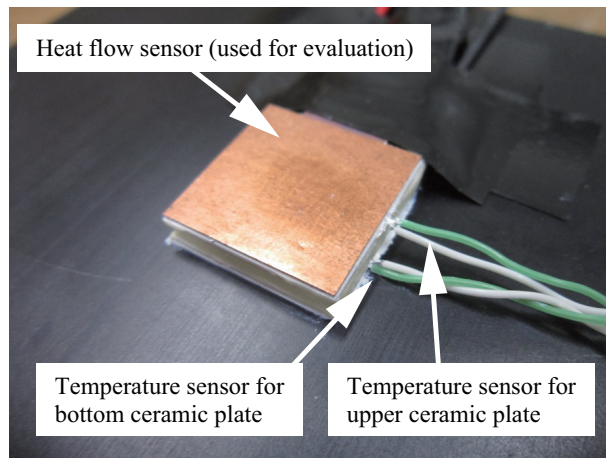


Fig. 6-9: Experimental setup for heat inflow estimation.

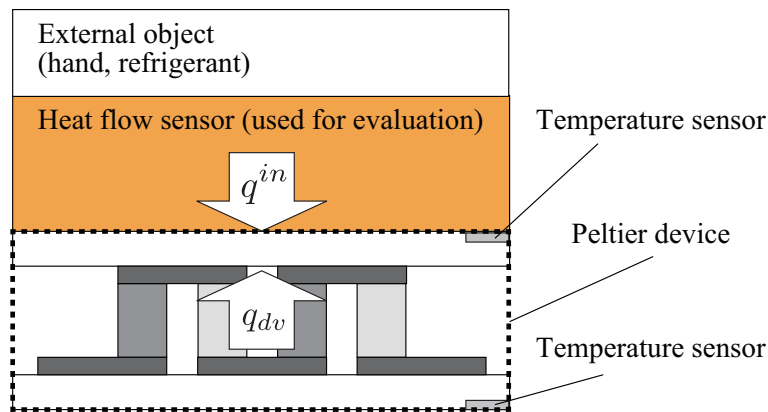


Fig. 6-10: Schematic representation of experimental setup (estimation of heat inflow).

### 6.6.1 Overview of Experiments (Heat Inflow Estimation)

Fig. 6-9 shows the setup used for experiments of heat inflow estimation. The heat-sink is used as the basement, and Peltier device is mounted on it. The temperature sensors are embedded in the upper and bottom sides of ceramic plates. The measured temperatures are used as the alternative of  $T_c$  and  $T_h$ , and used for the calculation of  $q_{dvn}$  in the observer. Because the size of the sensor is small, thermal capacitance of the temperature sensor is ignored. This is expressed schematically in Fig. 6-10. The heat flow sensor is mounted on the Peltier device, in order to evaluate the constructed observer. Then, the external objects are put on the thermal sensor in order to apply the certain thermal load.

In this study, two heat flow sensors are firstly mounted on the Peltier device as shown in Fig. 6-11. Then, the modification of the output of heat flow sensor is experimented before the experiments of esti-

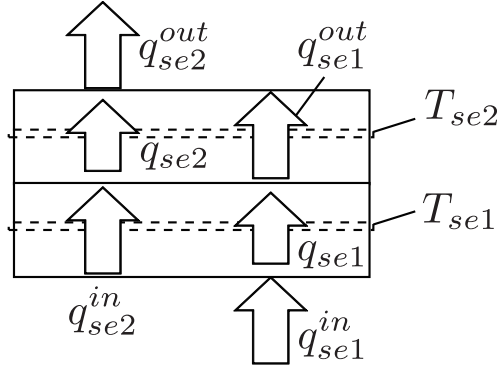


Fig. 6-11: Schematic representation of experimental setup (modification of output of heat flow sensor).

Table 6.1: Parameter values used for identification.

Variables	Value	Unit
Thermal capacity of electrode, $C_{eln}$	0.322	J/K
Thermal capacity of plate, $C_{crn}$	0.925	J/K
Thermal resistance of device, $R_{dvn}$	6.5	K/W
Seebeck coefficient, $\alpha_{sn}$	0.027	V/K
Electrical resistance, $R_{en}$	1.95	$\Omega$
Cut-off frequency of observer, $g_{hiob}$	6.28	rad/s
Thermal contact resistance, $R_{conn}$	0.607	K/W
Thermal capacitance of sensor, $C_{sen}$	0.54	J/K

mation by the observer. In the experiments, without external object, sinusoidal electric current with the frequency 0.1 Hz is applied. In addition to that, contact with aluminum block without electric current is experimented. Supposing that there exists little thermal resistance between two thermal sensors, estimated heat flows  $q_{se2}^{in}$  and  $q_{se1}^{out}$  should become same. Moreover, when there is no external object, heat outflow  $q_{se2}^{out}$  should be 0. These are the evaluation points of the modification.

Next, after the availability of output modification of the thermal sensor is confirmed, evaluation of heat inflow observer is conducted. In the experiments, several cases (step and sinusoidal current, contact of hand) are prepared. Then, the heat inflow information obtained by the thermal sensor  $\hat{q}_{se}^{out}$  is compared with that estimated by the observer  $\hat{q}^{in}$ .

Lastly, the observer is used for the feedback of information and the observer-based control of heat inflow is conducted. In the experiment, aluminum block is mounted as the thermal load, and heat inflow of the thermal system is controlled. The step signal is given as the command, and the responses of the proposed observer with the modified output of heat flow sensor are compared. The parameter values used for the experiments are shown in Table 6.1. Here, the nominal value of  $R_{conn}$  is set based on the

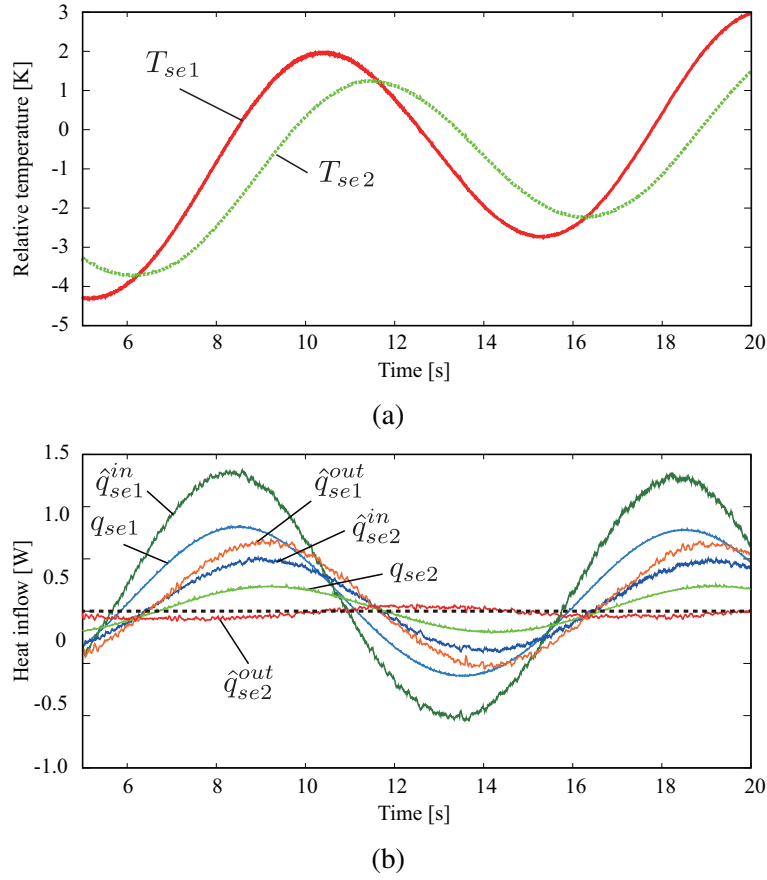


Fig. 6-12: Experimental results (0.1 Hz). (a) Temperature responses. (b) Heat flow responses.

method explained in Section 6.5.

### 6.6.2 Results of Experiments (Output Modification of Heat Flow Sensor)

Fig. 6-12 shows experimental results of the case in which sinusoidal currents were applied. As described in previous section, ideal states for this experiment are  $q_{se2}^{in} = q_{se1}^{out}$  and  $q_{se2}^{out} = 0.0$ . Seeing the results, the proposed observer is less affected by temperature variation, whereas the thermal sensor outputs are relatively deviated from ideal state. There are slight difference between  $q_{se2}^{in}$  and  $q_{se1}^{out}$ . However, this is thought to be caused by the actual existence of thermal resistance between two thermal sensors.

In the case that aluminum block contacts with upper sensor, the results are shown in Fig. 6-13. In this experiment, since the sensor contacts with external object, only  $q_{se2}^{in} = q_{se1}^{out}$  can be used for evaluation. Even in this case, modified outputs are better than the thermal sensor outputs especially in transient state. Though the modified output and output of sensor correspond in steady state, the better performance in

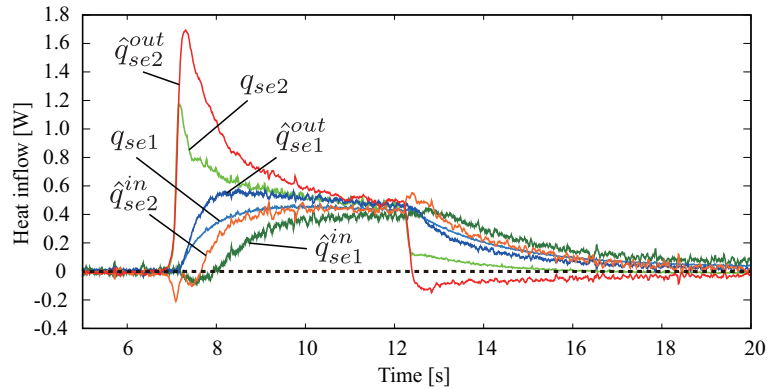


Fig. 6-13: Heat flow responses (contact).

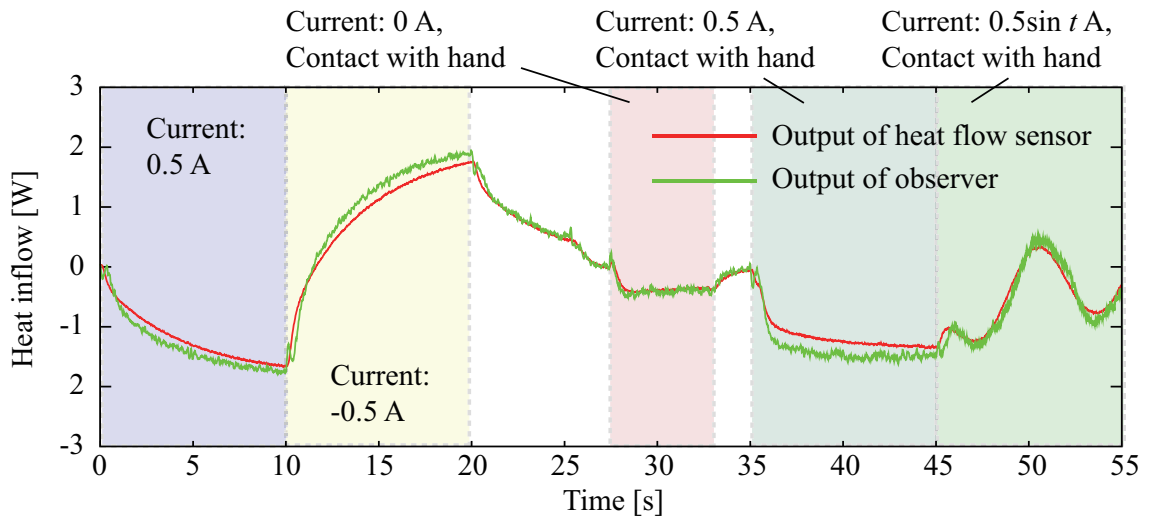


Fig. 6-14: Estimation results of heat inflow.

transient state can contribute especially for the application such as thermal display, in which transient state becomes important.

Based on the results, this research employs the modified output for evaluating the constructed observer.

### 6.6.3 Results of Experiments (Estimation of Heat Inflow)

Next, the estimation of heat inflow by the observer is conducted. The result of heat inflow estimation is shown in Fig. 6-14. Here, several conditions such as application of electrical current and contact with hand are tested sequentially. From the responses, it is able to say that the estimated value well tracks

Table 6.2: Measured gains from electrical current to surface temperature.

Frequency [rad/s]	1.0	3.0	5.0	10.0
Gain (with sensor) [dB]	10.8	-1.0	-6.8	-14.4
Gain (without sensor) [dB]	13.8	3.0	-3.5	-12.0

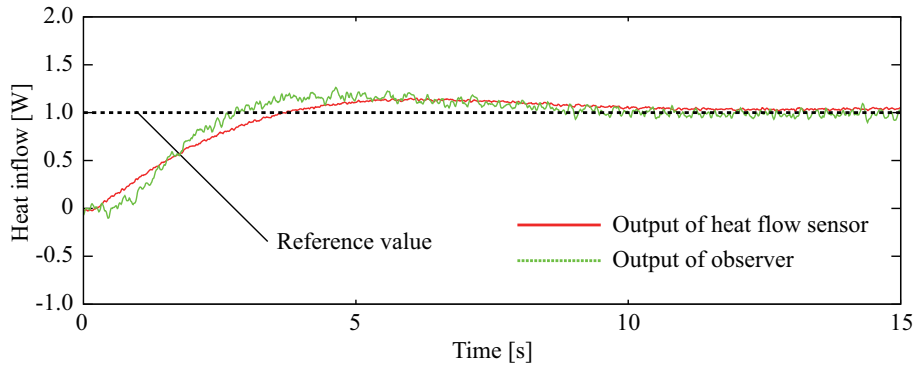


Fig. 6-15: Results of heat inflow control (reference: 1.0 W).

to the output of heat flow sensor. The experimental results shown in Fig. 6-14 indicates the capacity of the proposed observer for estimating heat inflow without using heat flow sensor. This will be advantage for thermal display, since the total thermal capacitance can be decreased and bandwidth of the system is expected to be improved. The Table 6.2 shows the frequency responses of thermal system. Here, the cases of Peltier device with the sensor and without sensor are experimented, and the ratio between the applied sinusoidal electrical current and the sinusoidal response of surface temperature is measured as the gain. From Table 6.2, the gain performance is improved by 2.0 ~ 4.0 dB. This means that the device can change its temperature more with the same amount of electrical current. The increased margin can be utilized for enhancing the bandwidth of control system.

#### 6.6.4 Results of Experiments (Observer-based Control of Heat Inflow)

Lastly, the observer-based control of heat inflow is experimented. As the commands of control, 1.0 W is applied. Then, the estimated signal is fed back to the PI controller. The experimental result of the control is shown in Fig. 6-15. As well as the experiments of the estimation, the output of the observer and that of heat flow sensor correspond well. In the steady state, the responses converge to the reference value, and this indicate that the heat inflow can be controlled without using the heat flow sensor. From the experimental results, it is confirmed that the proposed observer works well for estimating the amount

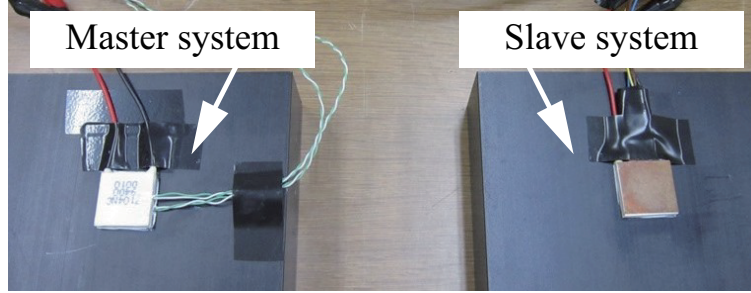


Fig. 6-16: Experimental setup for observer-based thermal bilateral control.

Table 6.3: Parameter values for bilateral control (observer-based thermal bilateral control).

Variables	Value	Unit
Gain for across-variable control, $C_e$	0.5	-
Gain for through-variable control, $C_i$	1.0	-
Nominal value of capacitive element, $C_{dvn}$	2.0 (with the heat flow sensor), 1.5 (with the observer)	J/K
Cut-off frequency of DOB, $g_{dis}$	2.0	rad/s

of heat inflow, and it is expected that the bandwidth of the thermal system is recovered by omitting the heat flow sensor. This feature can contribute for the improvement of the total response characteristics of haptic communication.

## 6.7 Experiments of Observer-based Thermal Bilateral Control

The use of the proposed observer improves the bandwidth of the system, and it is expected to enhance the performance of the bilateral control. In this section, the effectiveness of the observer is tested by the thermal bilateral control.

### 6.7.1 Overview of Experiments (Observer-based Thermal Bilateral Control)

The experimental setup for the thermal bilateral control is shown in Fig. 6-16. In the setup, the heat flow sensor at the master side is omitted; the thermal bilateral control is conducted between the system with the observer and the system with the heat flow sensor. On the master system, an aluminum block is mounted as the external environment. Then, the cooled aluminum plate is put on the slave system, and the transmission of the thermal power is conducted. As the comparative system, normal bilateral

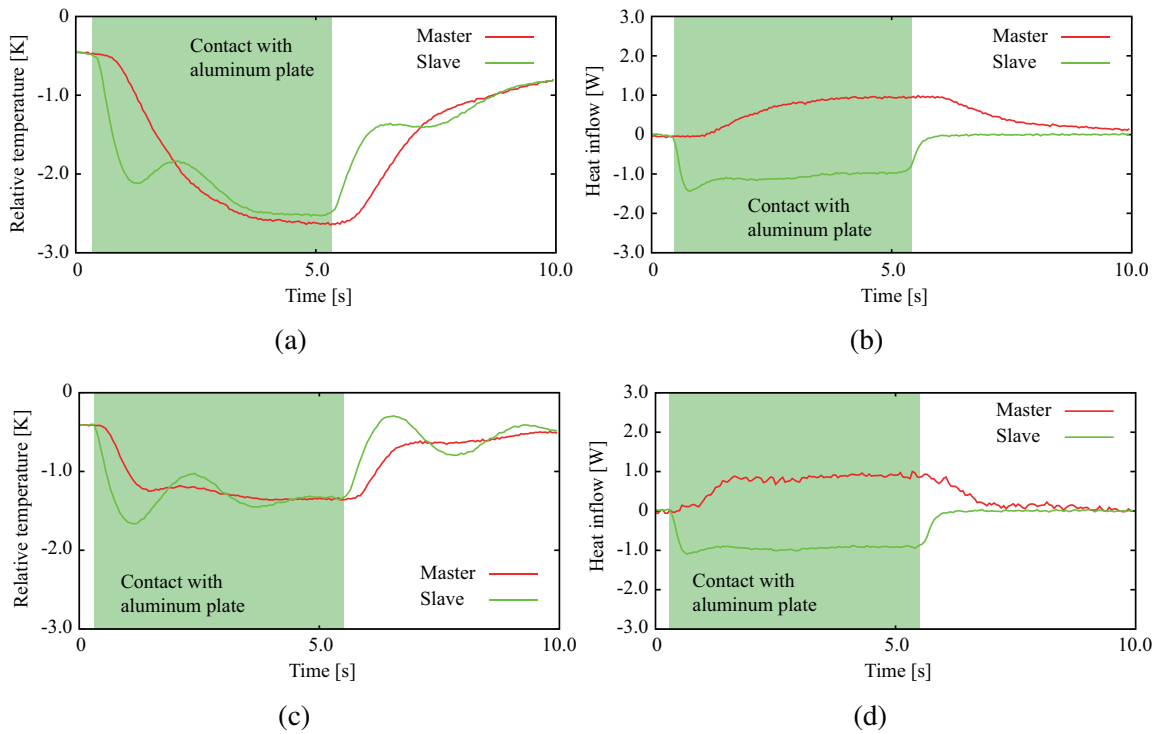


Fig. 6-17: Experimental results of thermal bilateral control (use of heat inflow observer). (a) Temperature responses (the case without using the observer). (b) Heat inflow responses (the case without using the observer). (c) Temperature responses (the case with using the observer). (d) Heat inflow observer (the case with using the observer).

control in which the both master and the slave systems utilize the heat flow sensors is conducted. The effectiveness of using the observer is discussed by comparing the responses of the control systems. The parameters used for the experiment are shown in Table 6.3. Since the system with the observer does not employ the heat flow sensor, whose thermal capacitance is around  $0.5 \text{ J/K}$ , the nominal value of the capacitive element of the device is subtracted in the experiment of the system.

### 6.7.2 Results of Experiments (Observer-based Thermal Bilateral Control)

The experimental results are shown in Fig. 6-17. In the experiments, aluminum plate is contacted for around 5 seconds. When the both master and slave systems use the heat flow sensors, the results become Figs. 6-17(a) and 6-17(b). At least in steady state, the temperatures synchronize and inversed heat inflow is generated at the master system; the transmission of thermal power is conducted. The lags in tracking are thought to be caused by the limited bandwidth of the thermal devices. For improving the performance of the thermal bilateral control, reducing the thermal capacitance of the system is required.



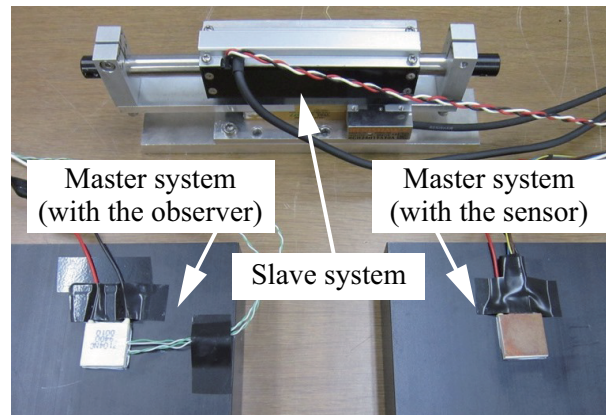


Fig. 6-18: Experimental setup for mixed rendering of mechanical and thermal sensations.

Figs. 6-17(c) and 6-17(d) show the results of the bilateral control in which the heat flow sensor is omitted at the master system. Although the small oscillations are observed, it is shown that the tracking speed of heat inflow becomes faster than the case without using the observer. Including the allocating configurations of temperature sensors for ceramic plates should be considered as the future work, the reduction of the lags in tracking indicate the effectiveness of using the proposed observer.

## 6.8 Experiments of Mixed Rendering of Mechanical and Thermal Sensations

Following to the observer-based thermal bilateral control, the effectiveness of the observer is tested by the haptic communication with mixed rendering of mechanical and thermal sensations in this section.

### 6.8.1 Overview of Experiments (Mixed Rendering of Mechanical and Thermal Sensations)

The experimental setup for the mixed rendering of the mechanical and thermal sensation is shown in Fig. 6-18. In the system, thermal device is employed as the master system, whereas the electrical motor is utilized as the slave system. Since the bilateral control system is generalized into across and through variables, it is able to realize the mixed rendering of different kinds of physical interactions under the framework of the generalized physical power. The operation example of the developed system is shown in Fig. 6-19; the thermal power injected by human finger at master side is transformed into mechanical power, and it enables the mechanical interaction at the slave side. In the system, general AVF-based

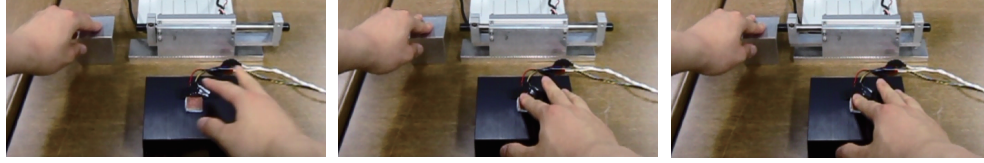


Fig. 6-19: Operation example of the mixed rendering system of mechanical and thermal sensations.

Table 6.4: Parameter values for bilateral control (mixed rendering of mechanical and thermal sensations).

Variables	Value	Unit
Gain for across-variable control, $C_e$	0.5	-
Gain for through-variable control, $C_i$	1.0	-
Nominal value of capacitive element, $C_{dvn}$	0.295 (motor), 2.0 (Peltier device with the heat flow sensor), 1.5 (Peltier device with the observer)	kg, J/K
Cut-off frequency of DOB, $g_{dis}$	10.0 (motor), 2.0 (Peltier device)	rad/s

4ch controller, which is introduced in the Chapter 3, is implemented. Then, across variables (temperature and velocity) are regulated to synchronize, whereas the through variables (heat inflow and force) are controlled so that the summation of the variables becomes zero. As for the master side, two kinds of systems are prepared: the thermal system with the heat flow sensor, and that with the proposed observer. In the experiments, slave side is mechanically fixed so that it does not move, and heated aluminum block as the external environment is mounted on the slave system. By comparing the responses of the cases with the heat flow sensor and that with the observer, the validity of using the proposed observer is discussed. The parameter values used for the experiments are shown in Table 6.4.

### 6.8.2 Results of Experiments (Mixed Rendering of Mechanical and Thermal Sensations)

The experimental results of the mixed rendering of mechanical and thermal sensations are shown in Fig. 6-20. Figs. 6-20(a) and (c) show the responses of the bilateral control with the electrical motor and the thermal system with the heat flow sensor. In the results, vibrational responses after contact and release of the block are observed. This is thought to be caused by the difference of the bandwidth between the electrical motor and the thermal system, as explained in the Chapter 5. The use of the heat flow sensor causes the lag in changing the surface temperature of the thermal display, and the overshoot in tracking is consequently induced.

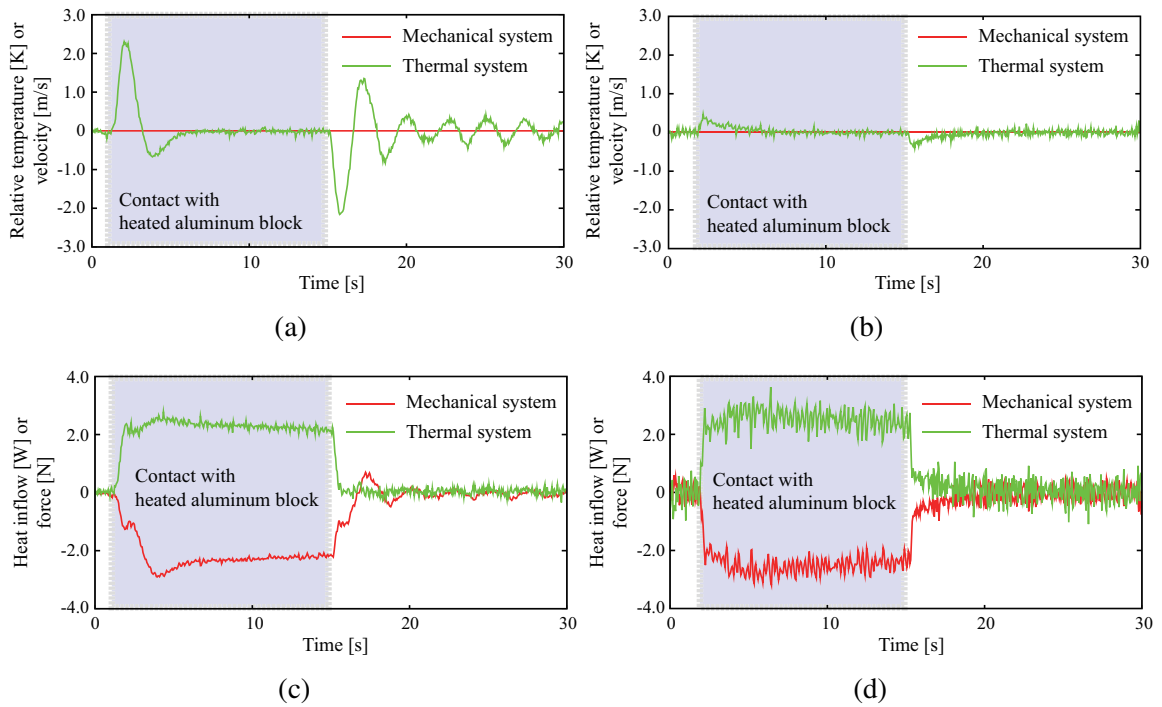


Fig. 6-20: Experimental results of mixed rendering of mechanical and thermal sensations. (a) Responses of across variables (with the heat flow sensor). (b) Responses of across variables (with the observer). (c) Responses of through variables (with the heat flow sensor). (d) Responses of through variables (with the observer).

The experimental results of the system with the proposed observer are shown in Figs. 6-20(b) and (d). In this case, the vibrational responses are much decreased, and more stable haptic communication is realized. The utilization of the heat inflow observer omits the heat flow sensor, and the total thermal capacitance of the thermal system can be reduced. Since it takes less time for the facilitated heat flow by the device to reach to the surface part of the display, the deviation of the across variable (temperature) is able to be reduced. As for the control of through variables, the swing back of the responses is suppressed. From these results, the validity of using the proposed observer is confirmed.

In the case of using the observer, the noises in the responses become larger than the case of using the heat flow sensor. This is due to the differentiation of the temperature response in the observer; the noise in measured temperature is amplified in the derivation. Therefore, employing the methods for filtering the noises is thought to be recommended in the practical implementation of the observer. However, proposed observer at least enables the vibration suppression caused from the limited bandwidth of the thermal system. In this sense, the observer is able to enhance the performance of the haptic communication.

## 6.9 Summary of Chapter 6

In realizing the mixed rendering of mechanical and thermal sensations, as well as the thermal bilateral control, the narrow control bandwidth of thermal device becomes problem for the haptic communication; as described in Chapter 5, the narrow bandwidth induces the interference term and becomes the bottleneck for the bilateral control. In this chapter, for improving the bandwidth of thermal system, heat inflow observer that realizes the estimation of heat flowing into thermal system without using the heat flow sensor was proposed. The heat flow sensor generally has larger thermal capacitance than single temperature sensor, and omitting the heat flow sensor leads to the bandwidth improvement of the system. For addressing this, the observer-based handling of heat inflow was explained in this chapter. The proposed observer was constructed on the basis of distributed parameter system of the device. Then, the system was approximated with the consideration on the poles and zeros of transfer functions. In addition to that, this study proposed the output modification of heat flow sensor. This enabled the robust sensing of heat inflow against the temperature change of the sensor itself. In experiments, the modified output and observer were compared in heat inflow estimation and control. Moreover, the observer-based thermal bilateral control and mixed rendering of mechanical and thermal sensations are demonstrated, for checking the effectiveness of using the proposed observer. From the experimental results, it was confirmed that the bandwidth improvement of the thermal display enhanced the performance of haptic communication. The experiments of the mixed rendering were not only conducted for testing the proposed observer but also for demonstrating the communication of different kinds of physical powers. The obtained results indicate the possibilities of novel types of haptic applications, which can only be realized by considering the generalized physical powers.

## Chapter 7

# Conclusions

---

This dissertation proposed the generalized framework of bilateral control for the remote reproduction of the physical power interaction. The development of the technologies so far enabled humans to transmit the audiovisual information. Following this, the academic field called real-world haptics aims to realize the remote transmission and rendering of tactile information. In the field, bilateral control is considered as the fundamental technology to handle the kinesthetic sensation, which is one of the elements of haptic sensation. The control system employs master and slave systems, in order to reproduce the law of action and reaction artificially between the remote places. Many kinds of control schemes have been invented for the kinesthetic bilateral control, and recently the acceleration-based bilateral control was proposed as the strong candidate for the bilateral control. On the other hand, the control of thermal actuators is also researched for rendering the thermal sensation that is also the essential element of haptic sensation. By realizing the recorded or calculated responses of temperature and heat flow, the thermal contact with materials can be reproduced for the operators. However, although the researches have been conducted on the rendering of kinesthetic and thermal sensations, the framework for bilateral transmission of haptic power has not been established. This point is strongly related to the motivation of this research.

First, in Chapter 2, the robust control of across variable flow (AVF) was proposed. The different kinds of physical systems can be treated in unified way by using the across and through variables. This dissertation focused on the acceleration control which is one of the fundamental control technologies in the field of motion control, and constructed its generalized form. The acceleration corresponds to the changing rate of across variable in unified physical systems. Therefore, the control system was constructed so that the given AVF reference is realized robustly against the disturbance through variables. In this chapter,

the concept of generalized control conductance was also explained. This is the extended form of control stiffness in the field of motion control, and the generalized control system should cover the wide range of the index. The realization of the robust AVF controller makes the controlled device to have single and normalized capacitive element, and it can widen the realizability of the index. In experiments, electrical motor and Peltier device were used in order to verify the concept of the proposed system. Although the control bandwidths of the motor and the thermal actuator are different, both systems showed the similar tendencies and it was confirmed that the AVF controller contributes for widening the range of the index values. Not only the constructed system is essential for the haptic communication, the concept of the system is thought to be important in general control engineering.

The tactile sensation that always involves the contact with external environments can be comprehended as the stimulation phenomena based on the physical power interaction between the human and external materials. Based on this, this dissertation proposed the concept of generalized bilateral control in Chapter 3. The product of across and through variable has the unit of power. Therefore, by realizing the synchronization of across variables and reproducing the inversed through variable each other between master and slave systems, the generalized bilateral control system becomes capable of transmitting the injected power to the remote side. In this dissertation, the acceleration-based 4ch bilateral control system was described in a unified manner, and AVF-based 4ch bilateral control system was constructed. Then, the performance and characteristics were analyzed using the generalized intermediate impedances, bond graphs and pole movements of control systems. The generalized intermediate impedances were derived from hybrid parameters of bilateral control. The impedances make the evaluations on losses and leakages in power transmission easier, and it turned out that the AVF-based 4ch bilateral control could realize the best characteristics of the impedances among the several control schemes. Moreover, the system was compared with the reflection-based bilateral control scheme using the bond graphs. The flows of power were described by using the graphs, and it was shown that the AVF-based 4ch system has superiority over the reflection-based one by the analyses. The experiments were conducted for both kinesthetic and thermal bilateral control, and the superiority of the AVF-based 4ch bilateral control scheme has been confirmed for both kinds of experiments. The reflection-based scheme yielded vibrational responses in a contact operation, whereas the constructed system could perform the stable contact. The proposed framework is considered to be the basis for the haptic communication systems.

The contents in Chapters 2 and 3 put a high value on the conceptive ideas in generalized bilateral control. On the other hand, the Chapters 4, 5 and 6 focused on the problems that arise in practical appli-

cation of haptic technologies. In Chapter 4, the communication delays between master and slave systems were treated. The delays in transmitting the information on across and through variables can easily induce the unstable operation. For addressing the problem, this dissertation firstly increased the stability margin by employing the phase-lag compensator. The phase-lag compensator can produce another lag of the information; however, it was explained that the decrease of the amplitude of the signal was able to contribute for the enhancement of the stability. This point was discussed by the power flows in bond graphs of bilateral control systems. Utilizing the system with the phase-lag compensator as the basis, this research proposed the compensator for through variable controller. The proposed compensator was derived on the basis of the hybrid parameters, and it can enhance the performance of the free operation of bilateral control. Then, the adaptive algorithm for discriminating the free and contact operation was proposed, and the gain in the compensator was set to be variable according to the state of the haptic communication. The performance of the proposed system was tested by the kinesthetic bilateral control, and the experimental results verified the validity of the compensator. In addition to that, the system was compared with the communication disturbance observer-based scheme from the perspective of hybrid parameters, and the parameters of respective system were measured. Among the systems including the scheme with only the phase-lag compensator, the proposed system achieved the most flat gain characteristics of hybrid parameters. The flatness means that the haptic communication can be conducted with less overshoots, and the applicability of the proposed system was experimentally confirmed.

Chapter 5 focused on the imperfect performance of the haptic device. In practical application, there exist possibilities that master and slave systems employ the devices with different control bandwidths. Firstly in this chapter, it was shown that the lack of the performance of one system could induces the degradation of the total performance of haptic communication. For the explanation, the modal spaces of bilateral control system were considered, and the interference between the across and through variable controls were revealed. In order to compensate for the interference and recover the deteriorated performance, this dissertation constructed the disturbance observer in the common modal space of the system. By utilizing the observer, the information on the amount of the interference became available. Since one of the devices has inferior characteristics, the applied compensation input cannot be realized at one system. In this chapter, it was shown that the direct use of the compensation value caused the another interference term. For avoiding this, this dissertation proposed the processing of the compensation value so as not to produce the interference factor. Although the compensation is again limited by the bandwidth of the device, the proposed method was theoretically proved to decrease the disturbance factor for modal

space control. The experimental results of bilateral control verified the effectiveness of the proposed system. Without using the compensation value, the vibration occurred in the bilateral control. On the other hand, the proposed system achieved less oscillation in the haptic communication. The results of experiments showed the validity of the proposed compensation method.

In Chapter 6, the thermal haptic device was focused. As described in the Chapter 5, the narrow bandwidth of the device causes the appearance of interference terms. The response characteristics of the haptic device are crucial for haptic communication, and the heat inflow observer was proposed in order to omit the heat flow sensor and enhance the bandwidth of the thermal system. The propagation of thermal energies is able to be treated by the distributed parameter systems. Therefore, this dissertation firstly constructed the distributed parameter system of the Peltier device using thermal equations. Then, the transfer function of the system was derived by Laplace transformation. The heat inflow observer was constructed using the modeled transfer functions. Since the model has infinite number of poles and zeros, the approximation considering the location of roots was described. For evaluation of the constructed observer, the output of heat flow sensor was employed. However, since the sensor itself has the thermal capacitance and the output is effected in transient state, the modification of the sensor output was proposed. Moreover, the simple identification method of thermal contact resistance between the electrode and ceramic plate was explained. In the experiments, firstly the output modification of heat flow sensor was demonstrated. The deviation of the outputs of doubled-over heat flow sensors was decreased by the modification, thus the validity of the constructed model was confirmed. Then, the output of the heat inflow observer was compared with the modified output next. Moreover, the observer-based thermal bilateral control and mixed rendering of mechanical and thermal sensations were experimented to check the effectiveness of using the proposed observer. The latter experiment was not only conducted for testing the observer but also for demonstrating the reproduction of generalized bilateral power interaction, and it was shown that the interaction between the different kinds of physical powers became possible under the concept of generalized physical powers.

The unification of the remote reproduction of bilateral power interactions is thought to generate the advancement in the field of communication industry. So far, the invention of telephone and television enabled the communication of audiovisual information and altered the lifestyles of human society. As that the transmission technologies of kinesthetic sensation have been expected to contribute for the communication industries, the mutual control of thermal devices can enhance the modality of remote communications. The richness of the communication is increased by this means, and the change in ways of



communication is expected like a handshake that involves mechanical and thermal interactions between distant places. As the another kinds of applications, the scaling of the haptic power can be treated. The magnification and shrinkage of transmitted power can be realized by adjusting the control objectives of across and through variables, and these enable the increase of small power interaction at the remote side so that it can be noticed at the operator side. For example, the tele-manipulation with sensing the magnified thermal sensation can be made possible. The change of influence ratio between the operator and the environment in bilateral control can extend the ability of humans, in a sense that the humans can interact evenly with micro/macro environments.

One of the specific features provided by the content of this dissertation is that different kinds of physical powers can be rendered. The experiments of mixed rendering of mechanical and thermal sensations, which are shown in the Chapter 6, represent the rendering of generalized physical powers that is the important theme in this dissertation. Basically, the thermal contact of hand is passive phenomena since the human cannot adjust the generation of heat flow in the hand. On the other hand, the human can apply the mechanical force arbitrarily. By the mixed rendering, the active thermal palpation system in which the operator can feel the change of thermal properties of body as the mechanical power is thought to be realized. Not only the systems for the pure reproduction of respective physical power interactions, but also the novel types of haptic communication systems are expected to be invented, under the framework of generalized physical power.

As the future work of this study, the integration of the information on elemental sensations should be considered. This dissertation focused on the reproduction of the elements of haptic sensation. However, in actual, the elements can interfere each other; for example, the thermal contact resistance between the thermal device and the external environment changes according to the gaps at the contacting area, that can be influenced by the mechanical pressing force. Although the thermal power is accurately transmitted by the thermal bilateral control, the different configurations between the direct contact with pressing force and mounting the remote object on the thermal display can induce the different thermal effusivities. When the effusivities are not same, the thermal sensations can consequently be different. Since the thermal contact resistance can vary according to the condition of surface conditions, the adjustment of control system based on the surface image of materials may be needed. As represented by the example, the effective combination of the haptic technologies and other kinds of information for the further enhancement of communication quality should be considered also as the future work. In addition to this, the multi-degree of freedom systems that can involve the interferences between the different axes of power

transmission should be handled. In this topic, consideration on the spatial propagation of haptic power from actuators or devices to the controlled area is essential. Although the more sophistication and further development of the theories are needed, the conceptual idea of generalized bilateral control systems as well as the treatment of problems that can appear in practical applications is thought to play important roles as one of the fundamental technologies for the mutual haptic communication between remote places. In that sense, the contents described in this dissertation are expected to provide the progresses in technologies of real-world haptics.

# References

- [1] R. C. Goertz : “Master-Slave Manipulator,” *Argonne National Laboratory*, June, 1949.
- [2] P. F. Hokayem, M. W. Spong : “Bilateral Teleoperation: An Historical Survey,” *Automatica*, Vol. 42, No. 12, pp. 2035–2057, December, 2006.
- [3] A. E. Saddik : “The Potential of Haptics Technologies,” *IEEE Instrumentation & Measurement Magazine*, Vol. 10, No. 1, pp. 10–17, February, 2007.
- [4] T. Slama, A. Trevisani, D. Aubry, R. Oboe, F. Kratz : “Experimental Analysis of an Internet-Based Bilateral Teleoperation System With Motion and Force Scaling Using a Model Predictive Controller,” *IEEE Transactions on Industrial Electronics*, Vol. 55, No. 9, pp. 3290–3299, September, 2008.
- [5] J. H. Cho, H. I. Son, D. G. Lee, T. Bhattacharjee, D. Y. Lee : “Gain-Scheduling Control of Teleoperation Systems Interacting with Soft Tissues,” *IEEE Transactions on Industrial Electronics*, Vol. 60, No. 3, pp. 946–957, March, 2013.
- [6] S. Munir, W. J. Book : “Internet-Based Teleoperation Using Wave Variables with Prediction,” *IEEE/ASME Transactions on Mechatronics*, Vol. 7, No. 2, pp. 124–133, June, 2002.
- [7] A. Lasnier, T. Murakami : “Workspace Based Force Sensorless Bilateral Control with Multi-Degree-of-Freedom Motion Systems,” *IEEE International Workshop on Advanced Motion Control*, pp. 583–588, March, 2010.
- [8] K. H. Zaad, S. E. Salcudean : “Analysis and Evaluation of Stability and Performance Robustness for Teleoperation Control Architectures,” *IEEE International Conference on Robotics and Automation 2000*, Vol. 4, pp. 3107–3113, April, 2000.
- [9] G. J. Raju, G. C. Verghese, T. B. Sheridan : “Design Issues in 2-port Network Models of Bilateral Remote Manipulation,” *IEEE International Conference on Robotics and Automation 1989*, Vol. 4, pp. 1316–1321, May, 1989.

## References

---

- [10] H. Kazerooni, T. I. Tsay, K. Hollerbach : “A Controller Design Framework for Telerobotic Systems,” *IEEE Transactions on Control Systems Technology*, Vol. 1, No. 1, pp. 50–62, March, 1993.
- [11] A. Eusebi, C. Melchiorri : “Force Reflecting Telemanipulators with Time-Delay: Stability Analysis and Control Design,” *IEEE Transactions on Robotics and Automation*, Vol. 14, No. 4, pp. 635–640, August, 1998.
- [12] R. J. Anderson, M. W. Spong : “Asymptotic Stability for Force Reflecting Teleoperations with Time Delay,” *IEEE International Conference on Robotics and Automation*, pp. 1618–1625, May, 1989.
- [13] Z. Zhang, D. Zhao, T. Chen : “Master-Slave Manipulators Bilateral Control System with Force Tele-presence,” *IEEE International Conference on Robotics and Biomimetics*, pp. 307–311, December, 2007.
- [14] W. S. Kim : “Developments of New Force Reflecting Control Schemes and an Application to a Teleoperation Training Simulator,” *IEEE International Conference on Robotics and Automation*, pp. 1412–1419, May, 1992.
- [15] B. Hannaford, R. Anderson : “Experimental and Simulation of Hard Contact in Force Reflecting Teleoperation,” *IEEE International Conference on Robotics and Automation*, pp. 584–589, April, 1988.
- [16] A. Caitt, G. Cannata, G. Casalino, S. Reto : “The Local Force Control Loop Approach in Bilateral Control of Master-Slave Systems,” *Proceedings of the 35th Conference on Decision and Control*, pp. 747–752, December, 1996.
- [17] K. Kaneko, H. Tokashiki, K. Tanie, K. Komoriya : “Macro-Micro Bilateral Teleoperation based on Operational Force Feedforward -Operational Force Feedforward Bilateral Teleoperation and its Dexterity-,” *IEEE/RSJ International Conference on Intelligent Robots and Systems 1998*, Vol. 3, pp. 1761–1769, October, 1998.
- [18] H. I. Son, T. Bhattacharjee, H. Hashimoto : “Effect of Impedance-Shaping on Perception of Soft Tissues in Macro-Micro Teleoperation,” *IEEE Transactions on Industrial Electronics*, Vol. 59, No. 8, pp. 3273–3285, August, 2012.
- [19] S. Susa, T. Shimono, T. Takei, K. Atsuta, N. Shimohima, S. Ozawa, Y. Morikawa, K. Ohnishi : “Transmission of Force Sensation by Micro-Macro Bilateral Control with Scaling of Control gains,” *10th IEEE International Conference on Advanced Motion Control, AMC 2008*, pp. 532–537, March, 2008.

## References

---

- [20] D. A. Lawrence : “Stability and Transparency in Bilateral Teleoperation,” *IEEE Transactions on Robotics and Automation*, Vol. 9, No. 5, pp. 624–637, October, 1993.
- [21] B. Hannaford : “A Design Framework for Teleoperators with Kinesthetic Feedback,” *IEEE Transactions on Robotics and Automation*, Vol. 5, No. 4, pp. 426–434, August, 1989.
- [22] E. Nærum, O. J. Elle, B. Hannaford : “The Effect of Interaction Force Estimation on Performance in Bilateral Teleoperation,” *IEEE Transactions on Haptics*, Vol. 5, No. 2, pp. 160–171, April-June, 2012.
- [23] D. Yashiro, K. Ohnishi : “Performance Analysis of Bilateral Control System with Communication Bandwidth Constraint,” *IEEE Transactions on Industrial Electronics*, Vol. 58, No. 2, pp. 436–443, February, 2011.
- [24] A. Sano, H. Fujimoto, M. Tanaka : “Gain-Scheduled Compensation for Time Delay of Bilateral Teleoperation Systems,” *IEEE International Conference on Robotics and Automation*, Vol. 3, pp. 1916–1923, May, 1998.
- [25] G. M. H. Leung, B. A. Francis, J. Apkarian : “Bilateral Controller for Teleoperators with Time Delay via  $\mu$ -Synthesis,” *IEEE Transactions on Robotics and Automation*, Vol. 11, No. 1, pp. 105–116, February, 1995.
- [26] G. Niemeyer, J. J. E. Slotine : “Stable Adaptive Teleoperation,” *IEEE Journal of Oceanic Engineering*, Vol. 16, No. 1, pp. 152–162, January, 1991.
- [27] A. Aziminejad, M. Tavakoli, R. V. Patel, M. Moallem : “Transparent Time-Delayed Bilateral Teleoperation Using Wave Variables,” *IEEE Transactions on Control Systems Technology*, Vol. 16, No. 3, pp. 548–555, May, 2008.
- [28] B. Yalcin, K. Ohnishi : “Stable Adaptive Transparent Time-Delayed Teleoperation by Direct Acceleration Waves,” *IEEE Transactions on Industrial Electronics*, Vol. 57, No. 9, pp. 3228–3238, September, 2010.
- [29] R. J. Anderson, M. W. Spong : “Bilateral Control of Teleoperators with Time Delay,” *IEEE Transactions on Automatic Control*, Vol. 34, No. 5, pp. 494–501, May, 1989.
- [30] L. Bate, C. D. Cook, Z. Li : “Reducing Wave-Based Teleoperator Reflections for Unknown Environments,” *IEEE Transactions on Industrial Electronics*, Vol. 58, No. 2, pp. 392–397, February, 2011.

## References

---

- [31] M. Franken, S. Stramigioli, S. Misra, C. Secchi, A. Macchelli : “Bilateral Telemanipulation with Time Delays: A Two-Layer Approach Combining Passivity and Transparency,” *IEEE Transactions on Robotics*, Vol. 27, No. 4, pp. 741–755, August, 2011.
- [32] A. F. Villaverde, A. B. Blas, J. Carrasco, A. B. Torrico : “Reset Control for Passive Bilateral Teleoperation,” *IEEE Transactions on Industrial Electronics*, Vol. 58, No. 7, pp. 3037–3045, July, 2011.
- [33] M. Shibata, T. Murakami, K. Ohnishi : “A Unified Approach to Position and Force Control by Fuzzy Logic,” *IEEE Transactions on Industrial Electronics*, Vol. 43, No. 1, pp. 81–87, February, 1996.
- [34] S. Tachi, T. Sasaki : “Impedance Controlled Master Slave Manipulation System Part I:Basic Concept and Application to the System with Time Delay,” *Journal of the Robotics Society of Japan*, Vol. 8, No. 3, pp. 241–252, March, 1990.
- [35] K. Ohnishi, M. Shibata, T. Murakami : “Motion Control for Advanced Mechatronics,” *IEEE/ASME Transactions on Mechatronics*, Vol. 1, No. 1, pp. 56–67, March, 1996.
- [36] T. Murakami, F. Yu, K. Ohnishi : “Torque Sensorless Control in Multidegree-of-freedom Manipulator,” *IEEE Transactions on Industrial Electronics*, Vol. 40, No. 2, pp. 259–265, April, 1993.
- [37] C. Smith, M. Tomizuka : “Shock Rejection for Repetitive Control using a Disturbance Observer,” *Proceedings of the 36th Conference on Decision and Control*, pp. 2503–2504, December, 1996.
- [38] H. Kobayashi, S. Katsura, K. Ohnishi : “An Analysis of Parameter Variations of Disturbance Observer for Motion Control,” *IEEE Transactions on Industrial Electronics*, Vol. 54, No. 6, pp. 3413–3421, December, 2007.
- [39] S. Katsura, K. Irie, K. Ohishi : “Wideband Force Control by Position-Acceleration Integrated Disturbance Observer,” *IEEE Transactions on Industrial Electronics*, Vol. 55, No. 4, pp. 1699–1706, April, 2008.
- [40] A. Sabanovic, K. Ohnishi : “Motion Control Systems,” *Wiley IEEE Press*, 2011.
- [41] A. Sabanovic : “SMC Framework in Motion Control Systems,” *International Journal of Adaptive Control and Signal Processing*, Vol. 21, pp. 731–744, May, 2007.
- [42] M. H. Raibert, J. J. Craig : “Hybrid Position/Force Control of Robot Manipulators,” *Journal of Dynamic Systems, Measurement and Control*, Vol. 102, No. 2, pp. 126–133, June, 1981.

## References

---

- [43] S. Sakaino, T. Sato, K. Ohnishi : “Multi-DOF Micro-Macro Bilateral Controller Using Oblique Coordinate Control,” *IEEE Transactions on Industrial Informatics*, Vol. 7, No. 3, pp. 446–454, August, 2011.
- [44] Y. Matsumoto, S. Katsura, K. Ohnishi : “An Analysis and Design of Bilateral Control Based on Disturbance Observer,” *2003 IEEE International Conference on Industrial Technology*, pp. 802–807, December, 2003.
- [45] W. Iida, K. Ohnishi : “Reproducibility and Operationality in Bilateral Teleoperation,” *The 8th IEEE International Workshop on Advanced Motion Control, AMC '04*, pp. 217–222, March, 2004.
- [46] K. Ohnishi, S. Katsura, T. Shimono : “Motion Control for Real-World Haptics,” *IEEE Industrial Electronics Magazine*, Vol. 4, No. 2, pp. 16–19, June, 2010.
- [47] S. Shimono, K. Ohnishi : “Reproduction of Real World Force Sensation by Micro-Macro Bilateral Control with Respect to Standardized Modal Space,” *The 33rd Annual Conference of IEEE Industrial Electronics Society, IECON 2007*, pp. 374–379, November, 2007.
- [48] S. Susa, K. Natori, K. Ohnishi : “Three Channel Micro-Macro Bilateral Control System with Scaling of Control Gains,” *The 34th Annual Conference of IEEE Industrial Electronics Society, IECON 2008*, pp. 2598–2603, November, 2008.
- [49] S. Katsura, K. Ohnishi : “A Realization of Haptic Training System by Multilateral Control,” *IEEE Transactions on Industrial Electronics*, Vol. 53, No. 6, pp. 1935–1942, December, 2006.
- [50] B. Khademian, K. H. Zaad : “Dual-User Teleoperation Systems: New Multilateral Shared Control Architecture and Kinesthetic Performance Measures,” *IEEE Transactions on Mechatronics*, Vol. 17, No. 5, pp. 895–906, October, 2012.
- [51] M. Shahbazi, H. A. Talebi, S. F. Atashzar, F. Towhidkhan, R. V. Patel, S. Shojaei : “A Novel Shared Structure for Dual User Systems with Unknown Time-Delay Utilizing Adaptive Impedance Control,” *IEEE International Conference on Robotics and Automation 2011, ICRA '11*, pp. 2124–2129, May, 2011.
- [52] B. Khademian, K. H. Zaad : “A Framework for Unconditional Stability Analysis of Multi-master/Multislave Teleoperation Systems,” *IEEE Transactions on Robotics*, Vol. 29, No. 3, pp. 684–694, June, 2013.
- [53] Y. Yokokura, S. Katsura, K. Ohishi: “Stability Analysis and Experimental Validation of a Motion-Copying System,” *IEEE Transactions on Industrial Electronics*, Vol. 56, No. 10, pp. 3906–3913, October, 2009.

---

## References

---

- [54] N. Tsunashima, S. Katsura : “Spatiotemporal Coupler: Strage and Reproduction of Human Finger Motions,” *IEEE Transactions on Industrial Electronics*, Vol. 59, No. 2, pp. 1074–1085, February, 2012.
- [55] K. Natori, T. Tsuji, K. Ohnishi, A. Hace, K. Jezernik : “Time-Delay Compensation by Communication Disturbance Observer for Bilateral Teleoperation Under Time-varying Delay,” *IEEE Transactions on Industrial Electronics*, Vol. 57, No. 3, pp. 1050–1062, March, 2010.
- [56] K. Natori, R. Kubo, K. Ohnishi : “Effects of Controller Parameters on Transparency of Time Delayed Bilateral Teleoperation Systems with Communication Disturbance Observer,” *IEEE International Symposium on Industrial Electronics 2008, ISIE 2008*, pp. 1287–1292, June, 2008.
- [57] A. Suzuki, K. Ohnishi : “Frequency-Domain Damping Design for Time-Delayed Bilateral Teleoperation System Based on Modal Space Analysis,” *IEEE Transactions on Industrial Electronics*, Vol. 60, No. 1, pp. 177–190, January, 2013.
- [58] O. Saglam, E. A. Baran, A. O. Nergiz, A. Savanovic : “Model Following Control with Discrete Time SMC for Time- Delayed Bilateral Control Systems,” *IEEE International Conference on Mechatronics*, pp. 997–1002, April, 2011.
- [59] A. Yamamoto, H. Yamamoto, T. Higuchi : “Thermal Tactile Presentation with On-Site Parameter Identification of Finger,” *Proceeding of the IEEE International Symposium on Industrial Electronics, ISIE’05–CROATIA*, pp. 1365-1370, June, 2005.
- [60] H. Morimitsu, S. Katsura : “Heat Inflow Control of Peltier Device Based on Heat Inflow Observer,” *SICE Annual Conference 2010, SICE 2010–TAIPEI*, pp. 996–1001, August, 2010.
- [61] H. Yano, I. Hayashi, H. Iwata : “1DOF Sensor and Display System of Haptic and Temperature Sensation,” *2008 Symposium on Haptic Interfaces for Virtual Environments and Teleoperator Systems*, pp. 369–370, March, 2008.
- [62] S. Akiyama, K. Sato, Y. Makino, T. Maeno : “Presentation of Thermal Sensation through Preliminary Adjustment of Adapting Skin Temperature,” *IEEE Haptics Symposium 2012, HAPTICS’12*, pp. 355–358, March, 2012.
- [63] L. A. Jones, H. N. Ho : “Warm or Cool, Large or Small? The Challenge of Thermal Display,” *IEEE Transactions on Haptics*, Vol. 1, No. 1, pp. 53–70, June, 2008.
- [64] A. Yamamoto, S. Nagasawa, H. Yamamoto and T. Higuchi : “Electrostatic Tactile Display with Thin Film Slider and Its Application to Tactile Telepresentation Systems,” *IEEE Transactions on Visualization and Computer Graphics*, Vol. 12, No. 2, pp. 168–177, March/April, 2006.



## References

---

- [65] A. F. Ioffe : “Semiconductor Thermoelements and Thermoelectric Cooling,” *Infosearch*, London, 1957.
- [66] M. Chen : “Reconfiguration of Sustainable Thermoelectric Generation Using Wireless Sensor Network,” *IEEE Transactions on Industrial Electronics*, Vol. 61, No. 6, pp. 2776–2783, June, 2014.
- [67] L. U. Odhner, H. H. Asada : “Sensorless Temperature Estimation and Control of Shape Memory Alloy Actuators Using Thermoelectric Devices,” *IEEE/ASME Transactions on Mechatronics*, Vol. 11, No. 2, pp. 139–144, April, 2006.
- [68] F. Felgner, L. Exel, M. Nesarajah, G. Frey : “Component-Oriented Modeling of Thermoelectric Devices for Energy System Design,” *IEEE Transactions on Industrial Electronics*, Vol. 61, No. 3, pp. 1301–1310, March, 2014.
- [69] J. Jiang, G. V. Kaigala, C. J. Backhouse, H. J. Marquez : “Modeling and Controller Design of a Nonlinear Time-Varying Thermal Device in a Microfluidic Platform,” *Proceedings of the 2006 American Control Conference*, pp. 5330–5335, June, 2006.
- [70] G. J. Monkman, P. M. Taylor : “Thermal Tactile Sensing,” *IEEE Transactions on Robotics and Automation*, Vol. 9, No. 3, pp. 313–318, June, 1993.
- [71] S. Ino, S. Shimizu, T. Odagawa, M. Sato, M. Takahashi, T. Izumi, T. Ifukube : “A Tactile Display for Presenting Quality of Materials by Changing the Temperature of Skin Surface,” *IEEE International Workshop on Robot and Human Communication*, pp. 220–224, November, 1993.
- [72] M. B. Khoudja, M. Hafez, J. M. Alexandre, J. Benachour, A. Kheddar : “Thermal Feedback Model for Virtual Reality,” *International Symposium on Micromechatronics and Human Science*, pp. 153–158, October, 2003.
- [73] M. Guiatni, A. Benallegue, A. Kheddar : “Learning-Based Thermal Rendering in Telepresence,” *Lecture Notes in Computer Science*, Vol. 5024, pp. 820–825, June, 2008.
- [74] M. Guitani, A. Kheddar : “Theoretical and Experimental Study of a Heat Transfer Model for Thermal Feedback in Virtual Environments,” *IEEE/RSJ International Conference on Intelligent Robots and Systems*, pp. 2996–3001, September, 2008.
- [75] G. H. Yang, T. H. Yang, S. C. Kim, D. S. Kwon, S. C. Kang : “Compact Tactile Display for Fingertips with Multiple Vibrotactile Actuator and Thermoelectric Module,” *2007 IEEE International Conference on Robotics and Automation*, pp. 491–496, April, 2007.

---

## References

---

- [76] S. M. Cho, S. Y. Kim : “Shake It: A Portable Haptic Mouse and Shaking Application,” *2009 ICROS-SICE International Joint Conference*, pp. 3788–3791, August, 2009.
- [77] M. Guiatni, V. Riboulet, C. Duriez, A. Kheddar, S. Cotin : “A Combined Force and Thermal Feedback Interface for Minimally Invasive Procedures Simulation,” *IEEE Transactions on Mechatronics*, Vol. 18, No. 3, pp. 1170–1181, June, 2013.
- [78] S. Gallo, L. S. Carreras, G. Rognini, M. Hara, A. Yamamoto, T. Higuchi : “Towards Multimodal Haptics for Teleoperation: Design of a Tactile Thermal Display,” *The 12th IEEE International Workshop on Advanced Motion Control, AMC 2012*, pp. 1–5, March, 2012.
- [79] M. Deng, A. Inoue, Y. Tahara : “Experimental Study on Operator Based Nonlinear Temperature Control of an Aluminum Plate Actuated by a Peltier Device,” *SICE Annual Conference 2008*, pp. 1405–1408, August, 2008.
- [80] H. Morimitsu, S. Katsura : “A Method to Control a Peltier Device Based on Heat Disturbance Observer,” *The 36th Annual Conference of the IEEE Industrial Electronics Society, IECON '10-PHOENIX*, pp. 1222–1227, November, 2010.
- [81] S. Yaemprayoon, C. Mitsuntisuk, K. Ohishi, J. Srinoncha : “Novel Method to Control Temperature on Aluminum Side Using Customized Proportional Controller Based on Disturbance Observer,” *International Journal of Information and Electronics Engineering*, Vol. 2, No. 2, pp. 112–118, March, 2012.
- [82] M. Guitani, A. Drif, A. Kheddar : “Thermoelectric Modules: Recursive non-linear ARMA modeling, Identification and Robust Control,” *The 33rd Annual Conference of IEEE Industrial Electronics Society, IECON 2007*, pp. 568–573, November, 2007.
- [83] C. L. Fernando, M. Furukawa, T. Kurogi, S. Kamuro, K. Sato, K. Minamizawa, S. Tachi : “Design of TELESAR V for Transferring Bodily Consciousness in Telexistence,” *2012 IEEE/RSJ International Conference on Intelligent Robots and Systems*, pp. 5112–5118, October, 2012.
- [84] D. G. Caldwell, A. Wardle, O. Kocak, M. Goodwin : “Telepresence Feedback and Input Systems for a Twin Armed Mobile Robot,” *IEEE Robotics and Automation Magazine*, Vol. 3, No. 3, pp. 29-38, September, 1996.
- [85] H. Morimitsu, S. Katsura : “Thermal Bilateral Control for Reproduction of Thermal Contact between Remote Places,” *IEEE Haptics Symposium 2012, HAPTICS'12*, pp. 65–70, March, 2012.
- [86] A. Drif, J. Citérin, A. Kheddar : “Thermal Bilateral Coupling in Teleoperators,” *IEEE/RSJ International Conference on Intelligent Robots and Systems*, pp. 1301–1306, August, 2005.

---

## References

---

- [87] M. Guiatni, A. Kheddar : “Modeling Identification and Control of Peltier Thermoelectric Modules for Telepresence,” *Journal of Dynamic Systems, Measurement, and Control*, Vol. 133, No. 3, pp. 31010, May, 2011.
- [88] H. Morimitsu, S. Katsura : “Thermal Bilateral Control with Scaled Thermal Information Using Peltier Device,” *2011 IEEE/SICE International Symposium on System Integration, SII2011*, pp. 521–526, December, 2011.
- [89] P. J. Gawthrop, G. P. Bevan : “Bond-Graph Modeling,” *IEEE Control Systems Magazine*, Vol. 27, No. 2, pp. 24–45, April, 2007.
- [90] S. Junco: “Stability Analysis and Stabilizing Control Synthesis via Lyapunov’s Second Method Directly on Bond Graphs of Nonlinear Systems,” *The 19th Annual Conference of the IEEE Industrial Electronics Society, IECON '93*, Vol. 3, pp. 2065–2069, November, 1993.
- [91] H. S. Park, P. H. Chang : “Causality Analysis Using Bond-graph and Its Significance in Bilateral Teleoperation,” *2002 IEEE/RSJ International Conference on Intelligent Robots and Systems*, pp. 2991–2998, October, 2002.
- [92] H. M. Paynter : “Analysis and Design of Engineering Systems,” *The M. I. T. Press*, 1961.
- [93] F. A. Firestone : “A New Analogy Between Mechanical and Electrical Systems,” *The Journal of the Acoustical Society of America*, Vol. 4, pp. 249-267, January, 1933.
- [94] J. U. Thoma : “Entropy and Mass Flow for Energy Conversion,” *Journal of the Franklin Institute*, Vol. 299, No. 2, pp. 89–96, February, 1975.
- [95] P. J. Gawthrop : “Physical Model-based Control: A Bond Graph Approach,” *Journal of the Franklin Institute*, Vol. 332, No. 3, pp. 285–305, May, 1995.
- [96] H. Morimitsu, S. Katsura, M. Tomizuka : “Design of Force Compensator with Variable Gain for Bilateral Control System under Time Delay ,” *IEEE International Symposium on Industrial Electronics, ISIE'13-Taipei*, pp. 1–6, March, 2013.
- [97] H. Morimitsu, S. Katsura : “Performance Enhancement of Bilateral Control with Different Control Performances,” *The 39th Annual Conference of the IEEE Industrial Electronics Society, IECON 2013*, pp. 6138–6143, November, 2013.
- [98] H. Morimitsu, E. Saito, S. Katsura : “An Approach for Heat Flux Sensor-less Heat Inflow Estimation Based on Distributed Parameter System of Peltier Device,” *The 37th Annual Conference of the IEEE Industrial Electronics Society, IECON 2011*, pp. 4214–4219, November, 2011.

## References

---

- [99] N. Abe, A. Kojima : “Control of Time Delayed and Distributed Parameter Systems,” *Coronasha*, 2007. (in Japanese)
- [100] J. Thoma, B. O. Bouamama : “Modeling and Simulation in Thermal and Chemical Engineering, A Bond Graph Approach,” *Springer*, 2000.
- [101] Simon Lineykin, Shmuel Ben-Yaakov : “Modeling and Analysis of Thermoelectric Modules,” *IEEE Transactions on Industry Applications*, Vol. 43, No. 2, March/April, pp. 505–512, 2007.
- [102] H. Morimitsu, S. Katsura : “Heat Inflow Control of Peltier Device Based on Heat Inflow Observer,” *SICE Annual Conference 2010, SICE2010*, pp. 996–1001, August, 2010.
- [103] H. Morimitsu, S. Katsura : “Two-Degree-of-Freedom Robust Temperature Control of Peltier Device Based on Heat Disturbance Observer,” *IEE Japan Transactions on Industry Applications*, Vol. 131-D, No. 7, pp. 967–973, July, 2011. (in Japanese)
- [104] N. Iiyama, K. Natori, R. Kubo, K. Ohnishi, H. Furukawa, K. Miura, M. Takahata : “A Bilateral Controller Design Method Using Delay Compensators,” *International Conference on Industrial Technology 2006, ICIT 2006*, pp. 836–841, December, 2006.
- [105] D. Tian, D. Yashiro, K. Ohnishi : “Wireless Haptic Communication under Varying Delay by Switching-Channel Bilateral Control with Energy Monitor,” *IEEE/ASME Transactions on Mechatronics*, Vol. 17, No. 3, pp. 488–498, June, 2012.
- [106] N. Motoi, R. Kubo, T. Shimono, K. Ohnishi : “Bilateral Control with Different Inertia Based on Modal Decomposition,” *The 11th IEEE International Workshop on Advanced Motion Control, AMC '11*, pp. 697–702, March, 2010.

# List of Achievements

## Journals

- [1] Hidetaka Morimitsu and Seiichiro Katsura, “Two-Degree-of-Freedom Robust Temperature Control of Peltier Device Based on Heat Disturbance Observer,” *IEE Japan Transactions on Industry Applications*, Vol. 131-D, No. 7, pp. 967–973, July, 2011. (in Japanese)
- [2] Hidetaka Morimitsu and Seiichiro Katsura, “Thermal Conductance Control of Peltier Device Based on Heat Disturbance Observer,” *IEE Japan Transactions on Industry Applications*, Vol. 132-D, No. 3, pp. 333–339, March, 2012. (in Japanese)

## International Conference (As a first author)

- [1] Hidetaka Morimitsu and Seiichiro Katsura, “Thermal Bilateral Control without Heat Flux Sensor,” *International Symposium on Application of Biomechanical Control Systems to Precision Engineering, ISAB2010-FUKUSHIMA*, pp. 223–224, July, 2010 (poster session).
- [2] Hidetaka Morimitsu and Seiichiro Katsura, “Heat Inflow Control of Peltier Device Based on Heat Inflow Observer,” *SICE Annual Conference 2010, SICE2010-TAIPEI*, pp.996–1001, August, 2010.
- [3] Hidetaka Morimitsu and Seiichiro Katsura, “A Method to Control a Peltier Device Based on Heat Disturbance Observer,” *The 36th Annual Conference of the IEEE Industrial Electronics Society, IEEE IECON 2010-PHOENIX*, pp. 1222–1227, November, 2010.
- [4] Hidetaka Morimitsu and Seiichiro Katsura, “Construction of Heat Inflow Control System Based on Disturbance Heat Flow Estimation,” *The 8th France-Japan and 6th Europe-Asia Congress on Mechatronics, MECHATRONICS2010-YOKOHAMA*, pp. 591–596, November, 2010.
- [5] Hidetaka Morimitsu and Seiichiro Katsura, “Frequency Response Analysis of Observer-Based Thermal Control System of Peltier Device,” *4th International Conference on Human System Interaction, HSI2011-YOKOHAMA*, pp. 250–255, May, 2011.

- [6] Hidetaka Morimitsu and Seiichiro Katsura, “Experimental Evaluation of Disturbance Observer-Based Heat Inflow Estimation Method,” *SICE Annual Conference 2011, SICE2011-TOKYO*, pp. 1069-1074, September, 2011.
- [7] Hidetaka Morimitsu, Eiichi Saito and Seiichiro Katsura, “An Approach for Heat Flux Sensorless Heat Inflow Estimation Based on Distributed Parameter System of Peltier Device,” *The 37th Annual Conference of the IEEE Industrial Electronics Society, IEEE IECON 2011-MELBOURNE*, pp. 4214-4219, November, 2011.
- [8] Hidetaka Morimitsu and Seiichiro Katsura, “Thermal Bilateral Control with Scaled Thermal Information Using Peltier Device,” *2011 IEEE/SICE International Symposium on System Integration, SII2011-KYOTO*, pp. 521–526, December, 2011.
- [9] Hidetaka Morimitsu and Seiichiro Katsura, “Thermal Bilateral Control for Reproduction of Thermal Contact between Remote Places,” *Proceedings of the IEEE Haptics Symposium 2012, VANCOUVER*, pp. 65–70, March, 2012.
- [10] Hidetaka Morimitsu and Seiichiro Katsura, “Design of Temperature Control System toward Thermal Display with Fast and Precise Response ,” *The 38th Annual Conference of the IEEE Industrial Electronics Society, IEEE IECON 2012-VANCOUVER*, pp. 2573–2578, October, 2012.
- [11] Hidetaka Morimitsu and Seiichiro Katsura, “A Design of Four-Channel Bilateral Control System under Time Delay based on Hybrid Parameters,” *2013 IEEE International Conference on Mechatronics, ICM 2013-VICENZA*, pp. 874–879, February, 2013.
- [12] Hidetaka Morimitsu, Seiichiro Katsura and Masayoshi Tomizuka, “Design of Force Compensator with Variable Gain for Bilateral Control System under Time Delay,” *Proceedings of the IEEE International Symposium on Industrial Electronics, ISIE 2013-TAIPEI*, pp. 1–6, May, 2013.
- [13] Hidetaka Morimitsu and Seiichiro Katsura, “Performance Enhancement of Bilateral Control with Different Control Performances,” *The 39th Annual Conference of the IEEE Industrial Electronics Society, IEEE IECON 2013-VIENNA*, pp. 6138–6143, November, 2013.
- [14] Hidetaka Morimitsu and Seiichiro Katsura, “Filter Design of Multilateral Control under Time Delay for Tele-teaching by Hand,” *Proceedings of the 13th IEEE International Workshop on Advanced Motion Control, AMC 2014-YOKOHAMA*, pp. 98–103, March, 2014.
- [15] Hidetaka Morimitsu, Seiichiro Katsura and Kouhei Ohnishi, “Performance Enhancement of Bilateral Control under Time Delay Using Nonlinear Filter,” *Proceedings of the 13th IEEE International Workshop on Advanced Motion Control, AMC 2014-YOKOHAMA*, pp. 735–740, March, 2014.

### **International Conferences (As a Co-author)**

- [1] Noboru Tsunashima, Hidetaka Morimitsu, and Seiichiro Katsura, “Reproduction of 2-DOF Motion Adapting to Environmental Angle Change,” *Proceedings of the 13th IEEE International Workshop on Advanced Motion Control, AMC 2014-YOKOHAMA*, pp. 729-734, March 14–16, 2014.
- [2] Dođancan Kebude, Hidetaka Morimitsu, Seiichiro Katsura, and Asif Sabanovic, “Multilateral Control-Based Motion Copying System for Haptic Training,” *Proceedings of the IEEE International Symposium on Industrial Electronics, ISIE 2014-ISTANBUL*, pp. 2246–2251, June 1–4, 2014.

### **Domestic Conference (As a first author)**

- [1] Hidetaka Morimitsu and Seiichiro Katsura, “Robust Thermal Control of Peltier Device for Realization of a Communication of Thermal Sensation,” *IEEJ, The papers of Technical Meeting on Industrial Instrumentation and Control, IIC10*, Vol. 12, pp. 13–18, March, 2010. (in Japanese)
- [2] Hidetaka Morimitsu and Seiichiro Katsura, “Estimation of Heat Inflow in Peltier Device without a Heat Flux Sensor,” *Proceedings of the 2010 Annual Meeting of the Institute of Electrical Engineers of Japan*, pp. 286–287, March, 2010. (in Japanese)
- [3] Hidetaka Morimitsu and Seiichiro Katsura, “Robust Thermal Control of Peltier Device Based on Heat Disturbance Observer,” *Mechanical Engineering Congress 2010, MECJ 2010-NAGOYA*, pp. 267–268, September, 2010. (in Japanese)
- [4] Hidetaka Morimitsu and Seiichiro Katsura, “Thermal Conductance Control of Peltier Device Based on Heat Disturbance Observer,” *IEEJ, The papers of Technical Meeting on Industrial Instrumentation and Control, IIC11*, Vol. 11, pp. 107–112, March, 2011. (in Japanese)
- [5] Hidetaka Morimitsu and Seiichiro Katsura, “Bandwidth Investigation of Heat Disturbance Observer-Based Temperature Control of Peltier Device,” *Proceedings of the 2011 Annual Meeting of the Institute of Electrical Engineers of Japan*, pp. 290–291, March, 2011. (in Japanese)
- [6] Hidetaka Morimitsu and Seiichiro Katsura, “Thermal Impedance Control of Peltier Device Based on Disturbance Heat Flow Estimation,” *Japan Joint Automatic Control Conference, JACC 2011*, pp. 419–424, November, 2011. (in Japanese)
- [7] Hidetaka Morimitsu, Eiichi Saito and Seiichiro Katsura, “Construction of Bilateral Control System with Transformation of Thermal-Mechanical Information,” *IEEJ, The papers of Technical Meeting on Industrial Instrumentation and Control, IIC11*, Vol. 2, pp. 61–66, March, 2012. (in Japanese)

- [8] Hidetaka Morimitsu and Seiichiro Katsura, “Construction of Thermal Multilateral Control System Based on Quarry Matrix,” *Proceedings of the 2013 Annual Meeting of the Institute of Electrical Engineers of Japan*, Vol. 4, pp. 386–387, March, 2013. (in Japanese)
- [9] Hidetaka Morimitsu, Eri Fujii, Yusuke Kawamura and Seiichiro Katsura, “Discussions on Synchronization Performance of Kinesthetic and Thermal Sensation in Multimodal Information Rendering,” *Proceedings of the 2014 Annual Meeting of the Institute of Electrical Engineers of Japan*, pp. 57–62, March, 2014. (in Japanese)

### **Domestic Conference (As a co-author)**

- [1] Nozomi Suzuki, Takahiro Kosugi, Hidetaka Morimitsu, Yuki Yokokura and Seiichiro Katsura, “Performance evaluation of communication protocol for haptic communication,” *IEEJ, The papers of Technical Meeting on Industrial Instrumentation and Control, IIC11*, Vol. 2, pp. 59–65, March, 2011. (in Japanese)
- [2] Nozomi Suzuki, Takahiro Kosugi, Hidetaka Morimitsu, Yuki Yokokura and Seiichiro Katsura, “Experimental Validation of Sequential Control in Haptic Communication via Network,” *Proceedings of the 2011 Annual Meeting of the Institute of Electrical Engineers of Japan*, pp. 336–337, March, 2011. (in Japanese)

### **Awards**

- [1] August 21st, 2010  
“SICE 2010 Annual Conference International Award Finalists”  
SICE Annual Conference 2010, SICE2010-TAIPEI
- [2] May 21st, 2011  
“4th International Conference on Human System Interaction Best Presentation Award”  
4th International Conference on Human System Interaction, HSI2011-YOKOHAMA
- [3] January 12th, 2012  
“2011 Excellent Presentation Award from the IEEJ Technical Meeting on Industrial Instrumentation and Control”  
The Institute of Electrical Engineers of Japan
- [4] March 31st, 2012  
“2011 IEEJ Excellent Presentation Award”  
The Institute of Electrical Engineers of Japan



- [5] March 19th, 2014  
“2013 IEEJ Excellent Presentation Award”  
The Institute of Electrical Engineers of Japan

## **Career**

- [1] October, 2011~March, 2012  
GCOE RA  
Keio University Graduate School  
The Global COE Program
- [2] April, 2012~  
Research Fellow (DC1)  
The Japan Society for the Promotion of Science

## **Patent Applications**

- [1] Hidetaka Morimitsu and Seiichiro Katsura  
“Transmission System of Thermal Sensation”  
Serial Number: 2014-3402  
Application Date: June 25th, 2012  
Applications: Keio University.